NOTICE

The quality of this microform is heavily dependent upon the quality of the original thesis submitted for microfilming. Every effort has been made to ensure the highest quality of reproduction possible.

If pages are missing, contact the university which granted the degree.

Some pages may have indistinct print especially if the original pages were typed with a poor typewriter ribbon or if the university sent us an inferior photocopy.

Reproduction in full or in part of this microform is governed by the Canadian Copyright Act, R.S.C. 1970, c. C-30, and subsequent amendments.

AVIS

La qualité de cette microforme dépend grandement de la qualité de la thèse soumise au microfilmage. Nous avons tout fait pour assurer une qualité supérieure de reproduction.

S'il manque des pages, veuillez communiquer avec l'université qui a conféré le grade.

La qualité d'impression de certaines pages peut laisser à désirer, surtout si les pages originales ont été dactylographiées à l'aide d'un ruban usé ou si l'université nous a fait parvenir une photocopie de qualité inférieure.

La reproduction, même partielle, de cette microforme est soumise à la Loi canadienne sur le droit d'auteur, SRC 1970, c. C-30, et ses amendements subséquents.

Multi-Channel Photonic Networks

By

Emil Savov, B.A.Sc., M.A.Sc.

A dissertation submitted to the
School of Graduate Studies and Research,
University of Ottawa,
in partial fulfillment of the requirements
for the degree of
Doctor of Philosophy (Electrical Engineering)

Ottawa-Carleton Institute for Electrical Engineering

Department of Electrical Engineering
Faculty of Engineering
University of Ottawa

January 1991

ISBN 0-315-68079-2

UNIVERSITÉ D'OTTAWA
UNIVERSITY OF OTTAWA

Abstract

This thesis presents several alternatives for fibre-optic local and metropolitan area networks. The issues considered are mainly related to the physical layer of the networks, i.e., the topology and the optical communications problems.

The following approaches were considered in more detail: photonic switching using spatial light modulators; subcarrier-multiplexing techniques using direct optical detection, and in particular the transmission of 64-QAM signals by optical fibre; and subcarrier-multiplexing techniques combined with coherent optical detection.

The spatial light modulator appears to be one of the most promising means for building a large-size (e.g., 1000×1000) optical space switch. The main constraints are the attenuation of the optical signal and the crosstalk between the channels. Other problems such as fan-in and fan-out are also addressed.

Theoretical and experimental results are presented on the fibre-optic transmission of microwave 64-QAM signals at 90 Mb/s rate. Two important methods of improving the system performance are discussed and demonstrated: laser reflection-induced intensity noise minimization, and error-correction coding using a self-orthogonal convolutional code. The applicability of this transmission technique to the distribution of digital video services is assessed.

The concept of photonic networks which use subcarrier-multiplexing techniques together with coherent optical detection is presented. The different radio and optical modulation formats that can be used are investigated and compared for several system modes of operation. The effects of laser phase noise on the system performance are

also addressed. An 8-port homodyne phase-diversity receiver is analyzed theoretically.

Acknowledgements

I wish to express my sincere gratitude to my academic supervisors Dr. Willem Steenaart and Dr. Mohsen Kavehrad for their scientific guidance and moral support during the course of the program.

The help and advice of all members of my supervisory committee — Dr. A. Javed, Dr. W. McGee, Dr. M. Ney, and Dr. B. Syrett — is greatly appreciated.

I am thankful to Dr. J. Chrostowski and Dr. M. O'Sullivan from the Photonics and Sensors Section of the National Research Council of Canada for the useful discussions and advice provided.

I would like to thank Dr. R. Gross and Dr. R. Olshansky from GTE Laboratories for providing me with a copy of a paper prior to its publication.

Many thanks to all professors, colleagues and friends at the Department of Electrical Engineering, University of Ottawa, for the good academic atmosphere and the encouragement during the period of my studies.

This research was partially supported by the Telecommunications Research Institute of Ontario, Photonic Networks and Systems Thrust, and by a grant from Bell-Northern Research, Canada.

Contents

List of Tables

List of Figures

Chapter 1

Introduction

1.1 Motivation

The information needs of the modern society are increasing faster than ever. Consequently, the transmission capacity required from communication networks is also growing rapidly. There is general agreement in the research and business communities that fibre optics is one of the most promising technologies that can help in providing the required transmission capacity [1]. The total usable bandwidth (i.e., within the low-loss optical spectrum) of a single optical fibre is in the order of 20 THz. The challenge is to find practical ways of accessing this abundant bandwidth, since there are presently no electronic devices with such a large bandwidth.

During the last two decades, significant advances have been made in the field of fibre optic communications, especially in long-haul point-to-point transmission. There are still many problems to be solved in this area, but the main challenge now is to utilize the potential of the optical fibre to its full extent in the local and metropolitan area networks (LANs and MANs). Shortly after the introduction of the optical fibre as a communication medium, many LAN and MAN designers were able to appreciate some of the attractive features of the optical fibre: low transmission loss, light weight, immunity to interference, high-speed transmission capacity, etc. Several experimental

designs of such networks using fibre were implemented. A list is provided in Table 1.1 (after [2]). Judged by traditional network standards, the performance characteristics of these networks are quite impressive. However, they still use only a tiny fraction of the transmission capacity of the optical fibre. The fibre is used essentially as a replacement for the copper wire (or coaxial cable), and the access techniques are directly borrowed from conventional LAN design. The speed of the electronics is still the capacity-limiting factor.

Utilizing the bandwidth of the optical fibre is not a goal in itself, and certainly not the only issue in optical fibre communications. The transmission characteristics of the fibre are in general so much superior than those of the other media, that a radically new way of thinking is possible, and even necessary, in fibre-optic network design. There is a strong trend towards passive architectures, i.e., with no electronic components in the communication path, except at the user-network interface. Such passive architectures are made possible by the low signal attenuation in the fibre which permits extensive splitting and branching of the optical signal. Another direction of thinking is that one can trade bandwidth efficiency for simplified network control. The argument is that the usable bandwidth of the fibre is so large, that one can afford to utilize it inefficiently, provided that this opens new possibilities for network organization. An example of such an approach is the spread-spectrum networking concept which will be discussed in more detail in Chapter 2. Some other possibilities for fibre-optic network design will also be discussed in Chapter 2.

To emphasize again, in this thesis our attention is directed towards ways of exploiting the inherent properties of the fibre, in order to achieve concurrency (multiple independent connections between network users) in the network. The goal of modern fibre-optic network design is to utilize to a maximum the bandwidth of the fibre, to minimize the optical-to-electrical and the electrical-to-optical conversions that create bottlenecks, to simplify the access protocols, and to provide flexibility and multiple concurrent heterogeneous services.

Network	Topology	Access	Bit Rate Mb/s	Span km	No. of Nodes
Fibernet II	active star	CSMA/CD	10	2.5	1000
Codenet	passive star	CSMA/CD	3.4	2.8	1000
Hubnet	star hub	hub access	50	open	65,536
Two-Way Bus	loop-bus	TDMA	100	—	13
D-Net	several	"locomotive"	100	—	—
Loop 6770 (NEC)	active ring	token passing	32	2.0	126
NASA/ITT	passive star	TDMA	100	2.0	16
Hara's PBX	active star	circ.-sw. TDMA	10	—	—
FACOM 2881 (Fujitsu)	active ring	TDMA	4	96	32
FACOM 2883 (Fujitsu)	active ring	TDMA	33	576	54
H-8644 (Hitachi)	active ring	token passing	32	100	50
Loop Network (Hitachi)	active ring	TDMA	32	2.0	—
Loop 6530 (NEC)	active ring	hybrid	32	7	—
Loop 6830 (NEC)	active ring	hybrid	32	12	—
BRANCH 4800 (NEC)	tree	CSMA/CD	10	1.0	—
Prototype (Toshiba)	passive star	CSMA/CD	10	1.5	—
SIGMA (Hitachi)	active ring	TDMA	32	2.0	64
BILNET (Mitsubishi)	passive ring	TDMA	50	—	—

Table 1.1: Comparison of various conventional fibre-optic LANs. The bit error rate is presumably better than 10^{-9} in all cases. CSMA/CD stands for carrier-sensing multiple access with collision detection.

In our work, we analyze the possibilities offered by the optical fibre technology to provide concurrency mainly in the optical LAN and MAN environments. We consider issues related to distribution networks (where the information flow is mostly from one source to many destinations), multiple-access networks (where the information flow is generally the same in all directions), and integrated services networks (where several types of traffic patterns can exist simultaneously). We will concentrate our attention to the physical layer of the networks (topology and transmission problems), making only occasional references to protocol issues.

There are several possible approaches for achieving concurrency in a fibre-optic network. We discuss them briefly in Chapter 2. It is impossible to predict at present which approach will prevail in the future. It depends on the progress of fibre-optic technology in general. However, based on our extensive research, we consider certain approaches more promising than others. We have concentrated our efforts on three (arguably the most promising) of them:

1. Space switching using spatial light modulators
2. Subcarrier multiplexing with direct optical detection, and in particular the transmission of microwave 64-QAM (quadrature amplitude modulation) signals
3. Subcarrier multiplexing with coherent optical detection.

The merits and the implementation difficulties of each approach will be discussed in subsequent chapters of this thesis.

1.2 Contribution

The contributions of this thesis are in the following areas:

1. The investigation of the potential of spatial light modulators (SLMs) for photonic switching in the context of network interconnection devices. We have

discussed the fundamental limitations of this approach, and the problems that must be solved for its successful practical implementation. Our findings were reported in [3].

2. We carried out theoretical and experimental work on fibre-optic transmission of microwave 64-QAM (quadrature amplitude modulation) signals. This was the highest-level fibre-optic QAM transmission experiment at the time of the publication [4,5]. The previous highest level was 16-QAM [6]. We also introduced the notion of effective optical modulation index in multi-level QAM transmission. We show as well the potential of multi-level QAM subcarrier fibre-optic transmission for the distribution of large volumes of data or digital high-definition TV (HDTV).

3. The introduction of the novel concept of a multiple-access photonic network which uses subcarrier-multiplexing techniques in combination with coherent optical detection. We have investigated the topology, the modulation methods (both radio and optical), and several implementation issues. The results were reported in [7].

4. We presented, for the first time, a comparison of optical modulation methods suitable for photonic networks using subcarrier multiplexing and coherent optical detection. Our results were reported in [7,8].

5. We presented a discussion of the effects of laser phase noise on the performance of subcarrier-multiplexed coherent photonic systems. The results were reported in [9].

1.3 Outline of the Thesis

Chapter 2 of the thesis presents an overview of the alternatives for providing concurrency in a photonic network. The advantages and disadvantages of various techniques such as TDMA (Time-Division Multiple Access), SS (Space Switching), CDMA (Code-Division Multiple Access), WDM/FDM (Wavelength/Frequency Division Multiplexing), and SCM (Subcarrier Multiplexing) are discussed. More emphasis will be put on SCM, in order to provide a background for the discussions in Chapter 6.

Chapter 3 gives an introduction to coherent optical communications. Different receiver types are discussed briefly. The advantages of coherent detection over direct detection in terms of sensitivity and spectral resolution are highlighted. The problems of phase noise, polarization fluctuations, and intensity noise are outlined, together with techniques for their solution.

In Chapter 4, we present our work on spatial light modulators as crossbar switching elements for photonic networks. We have investigated the feasibility of such an approach, and provided some guidelines about what is achievable and the areas where technological progress is needed. Some of the specific problems addressed are the power splitting loss, the inter-channel interference due to the finite contrast ratio of the spatial light modulator, the fan-in and fan-out implementation, and some other implementation issues.

Chapter 5 presents theoretical and experimental results on fibre-optic transmission of 64-QAM microwave signals. We discuss the system degradation due to laser intensity noise (intrinsic and reflection-induced), and the one due to laser nonlinearities. The use of a convolutional self-orthogonal error-correction code is shown to improve the system performance significantly.

Chapter 6 introduces the novel concept of photonic networks using both subcarrier multiplexing and coherent optical detection (SCM/CD systems). The topics discussed are topology issues, comparison of optical modulation methods, potential number of users, and various implementation problems.

In Chapter 7, we present a discussion of the impact of laser phase noise on the performance of SCM/CD systems. Different types of optical and radio modulation formats are evaluated in terms of their immunity to phase noise.

In Chapter 8, we give some theoretical results about the performance of an 8-port phase-diversity homodyne receiver for FSK (frequency shift keying) SCM/CD systems which uses delay-and-multiply demodulators. The factors that influence the receiver performance are laser phase noise, optical modulation depth, and frequency deviation.

Chapter 9 summarizes the results of the thesis and gives suggestions for further research in this field.

Chapter 2

Alternatives for Photonic Communication Networks

2.1 Introduction

We may classify photonic networks based on the general principle for achieving concurrency. We need not explicitly consider the topology, or circuit/packet switching issues, although these issues are often intimately related to the method of providing concurrency.

We classify photonic networks in six broad categories:

1. Time-division multiplexing (TDM). The individual channels are assigned separate time slots within a frame.

2. Code-division multiple access (CDMA). The information in each channel is coded using code words that are unique to the particular channel.

3. Wavelength/frequency division multiplexing (WDM/FDM). The individual channels use separate optical wavelengths for transmission.

4. Space switching (SS). The channels are physically separated optical waveguides.

5. Subcarrier multiplexing with direct optical detection (SCM/DD). The individual channels use separate radio frequency channels.

6. Subcarrier multiplexing with coherent optical detection (SCM/CD). Same as SCM/DD, but the optical detection is coherent.

These techniques are discussed in more detail in the subsequent sections of this chapter. It should be mentioned that sometimes the distinction between the different types is blurred, and a combination of two, or more, techniques may be used. For example, some CDMA network architectures require the use of a space switch, and subcarrier multiplexing can be used together with wavelength division multiplexing.

2.2 Time-Division Multiplexing

Synchronous TDM has become the favorite approach for electronic multiplexing. In this approach, every network user is assigned a specific time slot for its transmission within the frame structure of the aggregate signal which is transmitted throughout the network. Therefore, each user terminal is required to operate at the aggregate network speed. In order to increase the total throughput of the network, and consequently the available capacity per user terminal, it is necessary to increase the speed of transmission. Since the user-network interfaces are electronic, there is an obvious bottleneck created by the limited speed of the digital (or even analog) electronics. The achievable switching speed limit for digital electronic components is expected to be about few tens of Gb/s. Therefore, this approach has major limitations for use in ultra-high speed photonic networks [10,11]. The projected transmission speeds (hundreds of Gb/s) will require the use of all-optical components, e.g., multiplexer/demultiplexers, time-slot interchangers, etc. These devices are difficult to build, because photons do not interact with each other, therefore it is impossible to control directly a light beam with another light beam. Usually some intermediate process has to be used, e.g., nonlinear optical effects, or electro-optic effects, etc.

Synchronization (i.e., all-optical clock recovery) will be a very difficult problem to solve. Insert-drop operations would require the user terminals to operate at the aggregate line speed. Even with the use of all-optical components, there will be a limiting point in speed, due to fundamental physical limits [12].

In spite of these limitations, much work has been done in this area [10,11,13]: generation of ultra-short optical pulses, multiplexing and demultiplexing using electro-optic switches, optical tapped delay lines for correlators, etc. TDM could be useful for near-term, lower-speed applications.

2.3 Code-Division Multiple Access

In the literature on photonic networks, CDMA is often referred to as Spread Spectrum. It unifies several possible techniques, the common thing being that each information bit is coded with a specific sequence of shorter pulses [14]. In this respect, it is similar to what is known in radio communications as direct-sequence spread spectrum. The two most widely known approaches are CDMA with self routing and random-carrier CDMA, which are discussed in more detail in the following subsections.

2.3.1 CDMA with Self Routing

This technique, advocated by Prucnal and other researchers [15,16], uses the coding in tandem with optical correlators to decide where each bit of information should be directed. Each signal bit carries the source and destination information coded in a specific way. The actual switching of the optical path requires the use of a space switch.

The disadvantage of such an approach is that, as the number of users increases, the transmission overhead due to coding increases even faster [14]. There is a need to generate extremely narrow optical pulses (femtosecond duration) and multiplex them together. This technique shares the same problems with the synchronous TDMA,

together with the problems of space switching. Therefore, its future as a long-term research direction is unclear.

2.3.2 Random-Carrier CDMA

This approach was described in a recent publication [17]. It uses a combination of coherent detection techniques and CDMA techniques. Its advantage is that it does not require the locking of the laser transmitter sources to any strictly specified wavelength; in fact their individual wavelengths are allowed to drift in a random manner. The control is distributed, which makes the network very robust. The advocates of this approach predict the possibility to implement a network with thousands of users transmitting at 10 Mb/s each, simultaneously.

The challenges that remain are:

- Frequency acquisition
- Optical power level nonuniformity
- Polarization control
- Statistical distribution and temporal evolution of laser frequencies.

2.4 WDM/FDM Approach

As the name suggests, WDM uses transmission on different optical wavelengths, in order to achieve concurrency. The most advantageous topology from power budget point of view is the passive star. The channel selection is done with optical filtering techniques like diffraction gratings, prisms, selective couplers, etc.. The detection is direct. The advantage is the relative simplicity of the transmission/detection methods. The number of channels achieved so far is not very large (few tens), due to the poor selectivity of the optical filters.

Some recent work on Fabry-Perot optical filters by Kaminow et al. [18] suggests that better selectivity can be achieved, providing hundred or more separate optical channels. An experiment with 128-channel transmission has been reported recently [19].

The name FDM is used to denote an approach using very densely spaced optical carriers. This is probably the ultimate photonic network [20] and the only method allowing the possibility to use the full bandwidth of the fibre [20,21]. It presents the following advantages:

- Uses passive star topology (broadband optical amplifiers can be used to offset attenuation)
- Promises a large number of users — up to several thousand
- Great flexibility — each channel can operate at a different rate
- The electronic equipment in each individual channel is not required to work at the aggregate speed
- The control of the network can be distributed
- Very suitable for integrated services networks.

On the other hand, there are many problems to be solved before such a network becomes a reality. FDM requires coherent optical detection (for more information see Chapter 3), which is complex and expensive. This will result in expensive user terminals, unless considerable progress is made in integrated opto-electronics. Narrow-linewidth, frequency-agile lasers will be needed too. The specific difficulties of coherent detection will be discussed in Chapter 3.

A global network problem that still remains unsolved is the frequency referencing of the lasers. There are techniques proposed [22,23], but they are not satisfactory for large network sizes. More will be said on this topic in Chapter 3.

Another consideration to be taken into account is the nonlinearities that occur in the fibre at high power levels, which is the case when the number of users is large. Fortunately, it appears that this will not impose a major limitation on the network performance [24].

2.5 Space Switching

Space switching derives its name from its principle of operation, where the light signal is switched from one input optical fibre to a physically separate output fibre. The major attractiveness of this approach is that once the connection is established, the link can carry a very high rate signal. Several associated technologies have been investigated recently: directional coupler switching matrices; bulk optics; and spatial light modulators.

2.5.1 Directional Coupler Switching Matrices

The directional coupler is an electro-optic device which can couple (or switch) the optical signal from one input optical waveguide into any of two output optical waveguides. It has two input and two output waveguides (and therefore is denoted as a 2×2 switch). When operated in a digital mode, the device can have two states: straight-through, or cross-connect. The switching of the device is controlled by an electrical signal. Note that this device can be operated as a digital intensity modulator (on/off key). By combining several 2×2 devices, it is possible to build larger switching arrays.

Most modern implementations of directional couplers are integrated optics devices. A substantial amount of work has been done on Ti:$LiNbO_3$ (i.e., waveguides formed in a $LiNbO_3$ substrate by diffusion of Ti) directional coupler switches [10,11] during the last several years. Some impressive results have been achieved for applications as modulators and mux/demultiplexers, achieving modulation and switching speeds

in excess of 20 Gb/s. On the other hand, the largest-size optical switching arrays implemented so far are 16 × 16 and this size already approaches the limits of the technology. There are several obstacles in the way of implementing larger array sizes. The first one is the size of the individual couplers used to build the crossbar, which is relatively large (on the order of several mm), whereas the size of the wafer is limited. Other major obstacles are the insertion loss and the crosstalk, which become unacceptable for large array sizes [25].

2.5.2 Bulk Optics

This approach uses bulk optical components. Bulk optics is a term used to make a distinction from integrated optics. For example, a lens, a crystal, an optical fibre, are all bulk optical components.

There are a number of proposed approaches to use acousto-optic deflection [26] and other beam deflection techniques for optical switching, but it is unclear at present how many channels can be achieved. A 4 × 4 switch using acousto-optic Bragg cells has been demonstrated [27]. Another 1 × 16 switching element was reported in [28]. These devises are in a rudimentary stage of development, and it is not clear how many channels they can support. In addition, precisely because the devices are bulky, they can pose severe reliability problems, due to misalignment, vibration, temperature dependence, among many others.

2.5.3 Using Spatial Light Modulators

The spatial light modulator is a two-dimensional array of optical cells (pixels) which can be either transparent, or oblique. Normally (but not always), the state of each cell can be controlled individually. These devices have been used extensively for optical signal processing. In our opinion, they offer one of the few possible alternatives for the design of a large-size space switch.

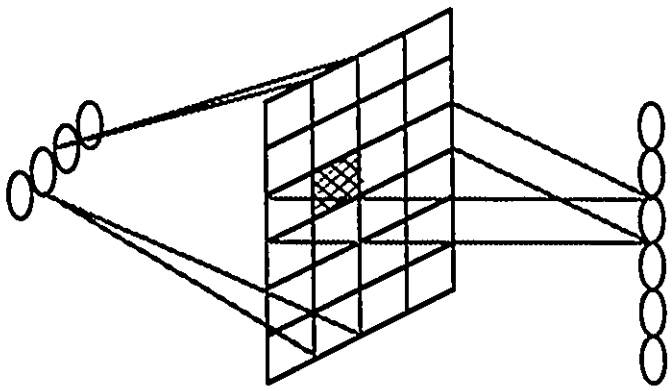

Figure 2.1: Principle of operation of an optical crossbar switch using an SLM.

The idea of using spatial light modulators for optical space switching and interconnection is not new [26,29,30,31]. But, to the best of our knowledge, no evaluation has been done of the ultimate performance capabilities of the SLMs for optical switching.

The principle of operation of an optical switch using an SLM is illustrated in Fig. 2.1. The light from each input channel is spread out to illuminate an entire column of the two-dimensional matrix. On the other side, the light from each row is focused on one of the outputs (could be vice-versa). By making the appropriate cell transparent, a connection can be established between any input-output pair. Moreover, broadcasting capability is inherently obtained, a fact that is of great importance for integrated services networks.

In a recent paper [3], we investigated the feasibility of such an approach. The conclusion of this paper is that a 1000 $\times$ 1000 space switch could be constructed. Many technological problems must be solved before we can talk about a real device. More details on the topic are presented in Chapter 4.

2.6 SCM/DD Networks

The SCM/DD technique uses separate RF (radio frequency) subcarriers for the individual channels. The SCM/DD approach is intended to be a short-term, inexpensive solution to network problems. Several independent channels can be transmitted using only one laser. It employs direct detection, which is a simple and well understood way of optical detection. Broadband microwave equipment is already developed for radio communications, whereas the speed of electronic switches is still limited to a few GHz.

2.6.1 Basics

The basic idea of multi-channel SCM transmission is illustrated in Fig. 2.2. A number of N different information streams $x_i(t)$ $(i = 1, \ldots N)$ are transmitted simultaneously using N separate microwave carriers at frequencies f_i. The modulation of the subcarriers can be digital, or analog. The sum of all microwave carriers is used to modulate the intensity of the light source (light-emitting diode (LED) or laser diode (LD)):

$$P(t) = P_0 \left[1 + \sum_{i=1}^{N} m_i s_i(t)\right] \tag{2.1}$$

where:

P_0 — optical power when the input signal to the laser is zero,

m_i — i-th modulation index,

$s_i(t)$ — i-th modulated subcarrier.

An RMS (root-mean-square) modulation index can be defined as:

$$m_{rms} = \sqrt{\sum_{i=1}^{N} m_i^2} \tag{2.2}$$

Note that the modulation of the optical source is *analog*.

After transmission through the fibre, the optical signal is detected by a photodiode. The individual channels are again separated in frequency and can be demodulated by conventional radio techniques.

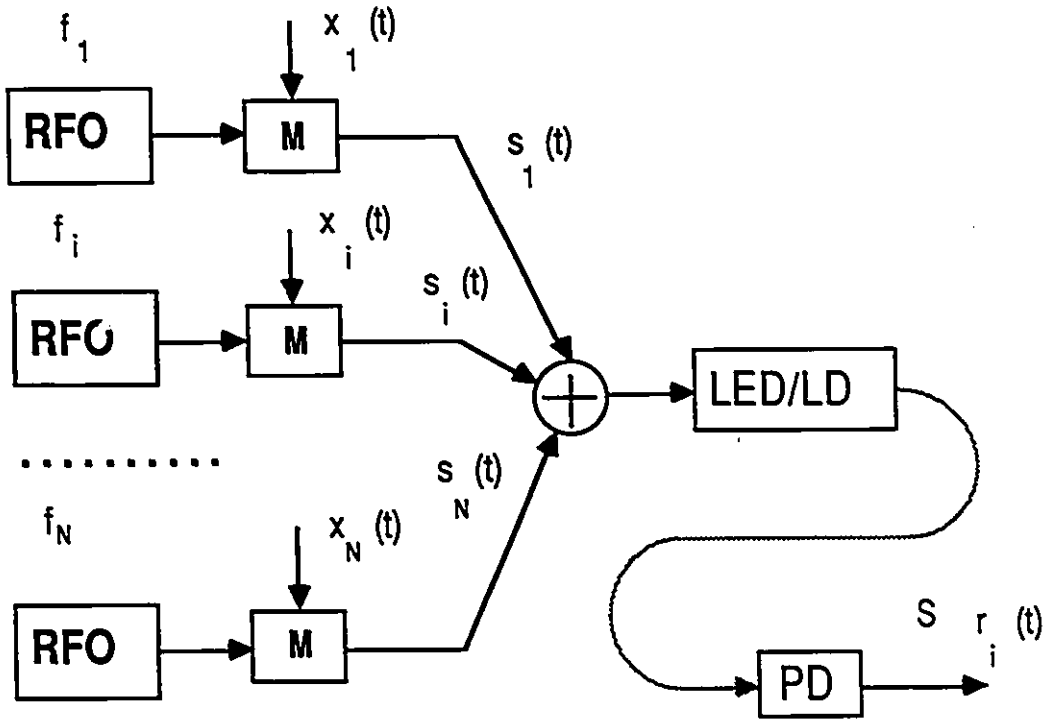

Legend:

RFO — Radio Frequency Oscillator

M — Modulator (RF)

LED/LD — Light-Emitting Diode/Laser Diode

PD — Photo-Diode

——— Electrical signal

——— Optical signal

Figure 2.2: Principle of Subcarrier Multiplexing.

The SCM approach has been successfully used for the distribution of analog video [32], data [33], a mixture of analog and digital channels [34], and for the transmission of microwave signals [35,6].

A major problem in analog optical transmission is the nonlinearity in the relationship between the driving electrical signal and the optical power output [36,37]. Appendix A of the thesis provides information about nonlinear distortion. There is a trade-off between modulation index and nonlinearities. From a power budget point of view, the modulation index should be as large as possible. On the other hand, the nonlinearities impose a lower modulation index, in order to avoid distortion. When m_i is small, the regime of operation is quasi-linear.

Another severe problem in analog transmission is the intensity laser noise. This noise is a result of the statistical nature of the electrical carrier re-combination and the photon-generation process within the gain medium of the laser. We are going to elaborate on this topic in Chapter 5.

A third drawback of SCM transmission is that the total usable bandwidth, when operating on a single optical wavelength, is limited by the bandwidth of the microwave electronics and by the electro-optic conversion processes. This was one of our main motivations to investigate the transmission of 64-QAM signals. This shall be discussed in more detail in Section 2.6.3 of this chapter and in Chapter 5 of the thesis.

2.6.2 Multiple-Access Networks

Darcie [38,39] has proposed a multiple-access photonic network based on subcarrier multiplexing. Fig. 2.3 illustrates the idea. The network is built using a passive star coupler. The star topology is proven to be the most advantageous in terms of power budget for passive networks. Every user receives the optical signals transmitted by all other users of the network, including its own transmission. The desired channel selection is done by tuning the radio frequency (RF) receiver to the appropriate subcarrier frequency. The subcarriers are digitally modulated. The analysis that we

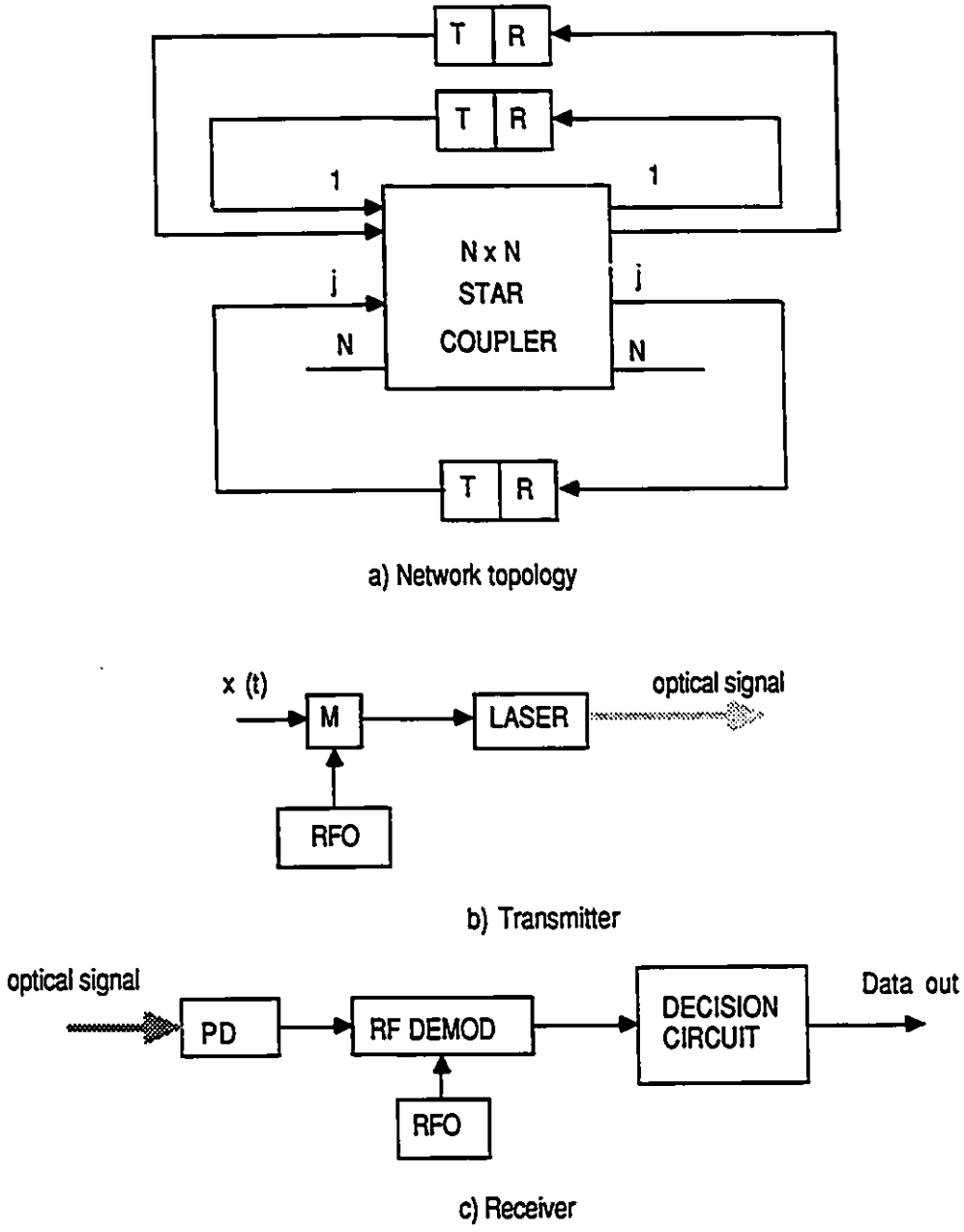

Figure 2.2: Multiple-access network using subcarrier multiplexing and direct detection.

present follows Darcie's work [39].

The intensity-modulated optical signal transmitted by user j can be described by:

$$P_j(t) = P_{DCj}[1 + m_j a_j(t)\cos(\omega_{ij}t + \phi_j(t))] \tag{2.3}$$

where:

P_{DCj} — the average optical intensity of laser j,

ω_{ij} — subcarrier frequency in channel i coming from user j,

$a_j(t)$ — amplitude modulation of the subcarrier,

$\phi_j(t)$ — angle modulation of the subcarrier.

If the star coupler of size $N \times N$ (where $N = 2^n$) is built by using a number of 3-dB couplers, then the power loss is given by:

$$L = n(3 + l_c) + l_f \qquad \text{dB} \tag{2.4}$$

where l_c (in dB) includes the excess loss of the 3-dB couplers and the fibre splice loss, and l_f (in dB) is the fibre propagation loss.

A network user interested in receiving the information transmitted by user j on subcarrier channel i will receive a root-mean-square (RMS) current signal:

$$i_{sij} = \frac{R_0 P_{DCj} m_j}{\sqrt{2}} 10^{-L/10} \tag{2.5}$$

where R_0 is the responsivity of the photo-diode.

When using direct optical detection in a point-to-point transmission, the signal-to-noise ratio (SNR) is limited mainly by the dark current of the photo-diode and by the thermal noise of the receiver electronics. In the case of this particular network, however, the SNR will be limited by the shot noise due to the total received optical power coming from all users, even unwanted ones. This is especially true for a large number of users N transmitting at the same time. The shot-noise process is due to the statistical nature of the photon/electron conversion process.

The total average photo-current at any receiver is:

$$I_t = R_0 10^{-L/10} \sum_{j=1}^{N} P_{DCj} \tag{2.6}$$

Here we assume that all N users are transmitting at the same time, which is the worst-case situation.

The shot noise can be modeled as a zero-mean white Gaussian current noise signal (e.g. [40]), with variance given by:

$$\bar{i}^2_{sh} = 2qI_0B \tag{2.7}$$

where:

q — electron charge,

I_0 — average photo-current,

B — receiver bandwidth.

Thus, the mean-square current noise in our case is:

$$\bar{i}^2_{sh} = 2qI_tB = 2qR_0B10^{-L/10}\sum_{j=1}^{N} P_{DCj} \tag{2.8}$$

From (2.5) and (2.8), we can find the signal-to-shot-noise ratio:

$$SNR_s = \frac{i^2_{sij}}{\bar{i}^2_{sh}} = \frac{R_0(P_{DCj}m_j)^210^{-L/10}}{4qB_jP_t} \tag{2.9}$$

where:

$$P_t = \sum_{j=1}^{N} P_{DCj}$$

Assume that all users have identical P_{DCj}, m_j, and B_j. In this case we can write:

$$NB = \frac{P_{DC}R_0m^210^{-L/10}}{4qSNR_s} \tag{2.10}$$

This equation gives the shot-noise-limited total usable bandwidth NB that is available to the network. All the values on the right-hand side of 2.10 should be known to the system designer. Darcie [39] gives an example using the following values: $R_0 = 0.5$ A/W; $SNR_s = 16$ dB; $m = 0.5$; $P_{DC} = 2$ mW; $l_c = 0.3$ dB; $l_f = 2$ dB. The results obtained are shown in Table 2.1. Compared to the present-day LANs, this network offers impressive performance and could be a near-term approach. However, considering the potential of the fibre-optic technology, this is only a small fraction of

N	Coupler loss (dB)	NB (GHz)	B (MHz)
256	28.4	14.2	55
512	31.7	6.63	13
1,024	35.0	3.10	3.0
2,048	38.3	1.45	0.71

Table 2.1: Number of users and available bandwidth in an SCM/DD network.

the available optical bandwidth. Moreover, the number of users is severely limited by the excess shot noise.

In estimating the number of users and the total bandwidth NB, Darcie assumes narrow-deviation Frequency-Shift Keying (FSK) modulation of the subcarriers. Thus, B is twice the data rate in each channel. There are no guard bands between the channels. The last assumption seems a rather optimistic one to use. In reality, a far greater (e.g., several times) bandwidth than NB may be required from the receiver front end, in order to avoid crosstalk between the channels.

2.6.3 Technological Requirements

From the preceding discussions in this section, it is clear that, in order to accommodate a large number of subcarriers, it is necessary to have wide-band lasers, photodiodes, and electronic devices — amplifiers, mixers etc..

Steady progress is made in the fabrication of laser diodes that can be modulated at high speeds. There are lasers that reportedly have modulation bandwidths larger than 22 GHz [41]. This figure will probably be extended in the future.

External electro-optic modulators can also be used. The bandwidths achieved with traveling-wave modulators exceed 20 GHz [42,43]. There are expectations that new organic electro-optic materials will allow the achievement of 50 GHz bandwidth, or more.

Photodiodes can be fabricated with extremely large bandwidths — up to 100 GHz. Steady progress in GaAs technology will make the use of very wide-band electronic

devices practical [44].

As discussed before, the linearity of the optical modulation is of crucial importance. Good linearity will contribute to both increased usable bandwidth and higher power budget.

The requirements for the laser spectral characteristics are quite relaxed for this kind of network. In fact, it is desirable that the lasers have a short coherence time (i.e., large linewidths), so that they do not beat with each other in a manner similar to coherent detection, thus creating undesirable interference.

2.7 SCM/CD Networks

The concept of the SCM/CD networks is very new. At the time this research began, there were very few publications [45,46], dealing with coherent detection of analog optical signals. Since then, several other results were published by R. Gross and R. Olshansky [47]–[50] which address multi-carrier SCM/CD transmission. The available publications on multiple-access SCM/CD networks are [7,8].

The SCM/CD networks use subcarrier-multiplexing techniques in combination with coherent optical detection at the receiver. The intention is to combine the advantages of both techniques (or, to put it differently, to overcome certain difficulties and shortcomings of the other techniques). The advantages of the SCM/CD approach are as follows:

- Compared to SCM/DD techniques, the receiver sensitivity can be greatly increased
- Can provide multiple channels on a single optical wavelength, thus avoiding the need for frequency agility of the lasers and the frequency registration problem
- Provide a way to overcome the limitations from excess shot noise from unwanted users in multiple-access network configurations

- Will be compatible with future FDM coherent networks.

On the other hand, SCM/CD networks are more complex than SCM/DD networks, because they still have to cope with some of the difficulties associated with coherent optical detection, namely:

- Polarization fluctuations in the fibre
- Laser phase noise.

More information about the difficulties of coherent optical detection will be given in Chapter 3.

In order for the SCM/CD networks to become practical, the advantages must outweigh the difficulties. Our goal in Chapters 6 and 7 this thesis is to address potential problems and to propose possible solutions.

Chapter 3

Background on Coherent Optical Communications

3.1 Principles and Receiver Types

The field of coherent optical communications has received considerable attention since the beginning of the 1980's. This is due to the potential for a large increase in receiver sensitivity and fine spectral resolution. Historically, the idea of coherent optical detection was born almost immediately after the discovery of the laser [51]. However, the enthusiasm did not last very long, because the laser sources were bulky, expensive and not very reliable. The renewed interest is stimulated by the progress made in the production of laser diodes, as well as due to the advantages that coherent detection (CD) offers, compared to direct detection (DD).

At this point, a clarification of our definition for coherent detection is necessary. In conventional communications theory "coherent detection" means that at the receiver there is a local oscillator which is phase-locked to the carrier of the received signal. In optical communications, this is not necessarily so. "Coherent detection" most often means that there is a local laser at the receiver, but it is not always phase-locked to the incoming optical carrier. The term "coherent" refers to the spatial coherence of

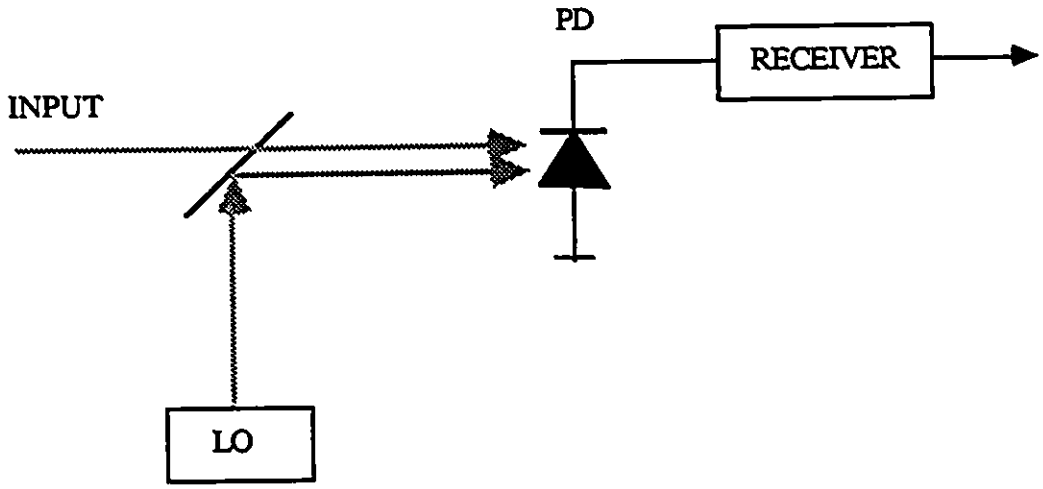

Figure 3.1: Principle of photo-mixing.

the optical signals.

Thus, our definition of coherent optical detection is one that uses a local laser oscillator. To denote the case of phase locking, the term "synchronous detection" will be used throughout this paper.

3.1.1 Photomixing

Photomixing is at the heart of coherent optical detection. Fig. 3.1 illustrates the principle.

The two optical signals — received signal and local oscillator signal — are mixed on the surface of a photo-diode. There must be a good wavefront and polarization matching between the optical signals, in order to achieve efficient mixing.

To a very good approximation, the photo-diode exhibits the characteristics of a square-law device, i.e., its output current is proportional to the square of the incident

electrical field of the optical wave:

$$i \sim E^2$$

Let us define the electrical fields of the signal as:

$$E_s = \sqrt{P_s}\cos(\omega_s t + \phi_s) \tag{3.1}$$

and of the local oscillator (LO) as:

$$E_{LO} = \sqrt{P_{LO}}\cos(\omega_{LO} t + \phi_{LO}). \tag{3.2}$$

Noting that the frequency term $\omega_{LO} + \omega_s$ is in the optical range, and therefore far away from the passband of the photodiode, for the output current of the photo-diode we have:

$$i(t) = R_0\left(P_s + P_{LO} + 2\sqrt{P_s P_{LO}}\cos\left[(\omega_{LO} - \omega_s)t - \phi_s + \phi_{LO}\right]\right) \tag{3.3}$$

where:

R_0 — detector responsivity,

$\omega_s = 2\pi\nu_s$ — the signal angular frequency,

$\omega_{LO} = 2\pi\nu_{LO}$ — the LO angular frequency,

P_s — signal power,

P_{LO} — LO power,

ϕ_s — signal phase,

ϕ_{LO} — LO phase.

Usually $P_{LO} \gg P_s$, therefore P_s can be ignored in (3.3). The information-carrying signal is:

$$i_{inf}(t) = 2R_0\sqrt{P_s P_{LO}}\cos\left[(\omega_{LO} - \omega_s)t - \phi_s + \phi_{LO}\right] \tag{3.4}$$

This latest equation shows that the coherent optical detection retains the phase and the frequency of the signal, relative to the local oscillator. It also shows that the *amplitude*, rather than the power of the signal, is detected. This is not significant for

digital systems, but is of crucial importance in analog systems, as will be demonstrated in subsequent chapters.

The signal $i_{inf}(t)$ is in the electrical frequency region, and from that point on radio communication techniques are applied for its further demodulation.

3.1.2 Receiver Types

Equation (3.4) shows that the coherent detection allows for the use of amplitude modulation/demodulation, as well as angle mod./demod.. This represents one criteria for receiver classification. Another criteria is the difference $\omega_{LO} - \omega_s$. If $\omega_{LO} - \omega_s = \omega_{IF} \neq 0$, then the receiver is called *heterodyne*. If $\omega_{LO} \cong \omega_s$, i.e. $\omega_{IF} \cong 0$, then it is a *homodyne* receiver.

Heterodyne detection requires only frequency locking of the local laser to the optical signal, whereas homodyne detection usually requires phase-locking. To illustrate that, for the homodyne case using (3.4) we can write:

$$i_{inf}(t) = 2R_0\sqrt{P_s(t)P_{LO}}\cos[\phi_{LO} - \phi_s(t)] \tag{3.5}$$

where $P_s(t)$ and $\phi_s(t)$ are now functions of time to indicate possible amplitude or angle modulation. Thus, phase locking of the local laser to the incoming signal is necessary, otherwise a complete signal fading can occur. Optical phase locking is rather difficult, but fortunately enough, a new technique has been introduced recently called *phase diversity*, which avoids the need for any phase-locking. This technique will be discussed later in more detail.

A summary of receiver types is given in Table 3.1 (after [52]).

The advantages of homodyne detection compared to heterodyne are: a) that better sensitivity can be obtained and b) less receiver bandwidth is necessary, since the signal is brought to base-band.

Modulation format	Class of detection	Receiver system	Optical local oscillator	IF/baseband processing	Relative sens. penalty	System linewidth/ bit rate ratio
PSK	Synchronous	Homodyne (Ideal)	Phase locked to suppressed carrier	-	0	0.0006 %
		Homodyne	Carrier PLL (reduced carrier)	-	~ 1 dB	
			Decision-driven PLL (suppressed carrier)	-	~ 1 dB	0.03 %
			Costas PLL (suppressed carrier)	-	~ 1 dB	0.05 %
		Heterodyne	Freq. locked	Phase locked	≥ 3 dB	0.5 %
DPSK	Sync.	Homodyne	Freq. locked	Delay line + multiplier	≥ 4 dB	0.3 %
DPSK	Non-sync.	Heterodyne/ Phase Diversity				
FSK	Non-sync.	Heterodyne/ Phase diversity	Freq. locked	Discriminator	≥ 7 dB	1.8 % - 7.5 %
				Dual filter/ Envelope	≥ 6 dB	2.5 % - 10 %
				Single filter/ Envelope	≥ 9 dB	10 %
ASK	Synchronous	Homodyne	Phase locked	-	~ 3 dB	10 %
	Non-sync.	Heterodyne	Freq. locked	Phase lock	~ 6 dB	
	Non-sync.	Heterodyne/ Phase diversity	Freq. locked	Envelope	≥ 6 dB	

Table 3.1: Characteristics and comparison of coherent optical receivers (after [52]).

3.2 Sensitivity Improvement

In this section, a brief and simplified explanation will be given of the sensitivity advantages that coherent detection offers, compared to direct detection. A complete and comprehensive treatment of the topic is given in [40,51,53].

It can be shown that the sensitivity of direct detection can be very close to the theoretical limit, provided that the optical receiver is ideal, meaning an ideal photodiode with zero dark current, and electronics without any circuit noise. Under these ideal conditions, the signal-to-noise ratio (SNR) is governed only by the shot-noise process. This limit is called *shot-noise limit*, or *quantum limit*, and the ideal SNR is [40]:

$$SNR_{ideal} = \frac{P_s}{2h\nu B_{DD}} \tag{3.6}$$

where:

P_s — received signal power,

h — Planck's constant (=1.38 $\times 10^{-34}$ J.s),

ν — optical frequency,

B_{DD} — receiver bandwidth for direct detection (DD) case. The quantum efficiency η is assumed equal to 1.0. In practice, it usually varies between 0.9 and 1.0.

In practice, the noise contribution of the dark current and the thermal noise cannot be neglected. The SNR in continuous-wave (CW) operation is given by:

$$SNR_{DD} = \frac{\bar{i}_s^2}{\bar{i}^2_{sh} + \bar{i}_d^2 + \bar{i}_c^2} \tag{3.7}$$

where:

$\bar{i}_s^2 = (R_0 P_s)^2$ — MS (mean square) signal current,

$\bar{i}^2_{sh} = 2qR_0 P_s B_{DD}$ — MS shot-noise current,

$\bar{i}_d^2 = 2qI_d B_{DD}$ — shot noise due to dark current,

$\bar{i}_c^2 = 4kTFB_{DD}/R_L$ — MS thermal noise current,

I_d — dark current,

k — Boltzmann's constant,

F — noise figure of the receiver,

T — absolute temperature in K°,

R_L — PD biasing resistor.

The contribution of $\bar{i}_c^2$ is so large that in practice the SNR is often more than 20 dB worse than the quantum limit. The situation is worse at longer wavelengths, i.e. from 1.3 to 1.6 μm, where Ge PD's and III–V compounds must be used. These devices produce large dark currents (compared for example to Si semiconductors).

Now, consider the SNR for coherent detection in CW operation. It is given as:

$$SNR_{CD} = \frac{\bar{i}^2_{inf}}{\bar{i}^2_{sh} + \bar{i}^2_d + \bar{i}^2_c} \tag{3.8}$$

where:

$\bar{i}^2_{inf}$ — MS signal current.

From (3.8) it can be seen that, at least in principle, almost shot-noise limited detection can be achieved if sufficient local oscillator power is available, so that $\bar{i}^2_d$ and $\bar{i}^2_c$ are negligible, compared to $\bar{i}^2_{sh}$. We can also write:

$$\bar{i}^2_{sh} = 2qR_0(P_{LO} + P_s)B_{CD} \approx 2qR_0P_{LO}B_{CD} \tag{3.9}$$

since $P_{LO} \gg P_s$. B_{CD} is the receiver bandwidth. For a heterodyne receiver, from (3.4), (3.8), and (3.9) we have:

$$SNR_{CD} \cong \frac{2R_0^2P_sP_{LO}}{2qR_0P_{LO}B_{CD}} = \frac{R_0P_s}{qB_{CD}} \tag{3.10}$$

Knowing that $R_0 = \eta q/h\nu$, where η is quantum efficiency and is assumed to be 1, we have:

$$SNR_{CD} = \frac{P_s}{h\nu B_{CD}} \tag{3.11}$$

This expression differs from (3.6) by a factor of two, but knowing that $B_{CD} = 2B_{DD}$, it shows that, with sufficient LO power, ideal shot-noise limited detection can be achieved with coherent detection, regardless of the non-ideal receiver components. The heterodyne receiver achieves roughly the same performance as an ideal direct

Modulation/Detection Type	No. of Photons/Bit
ASK heterodyne	72
ASK homodyne	36
FSK heterodyne	36
PSK heterodyne	18
PSK homodyne	9
Direct detection quantum limit	21
practical DD receiver	400-4000

Table 3.2: Theoretical sensitivity of different optical modulation and detection schemes and probability of error 10^{-9}. (after [54])

detection receiver, whereas the homodyne receiver can achieve an additional 3 dB better sensitivity. The necessary power levels are already available from semiconductor laser diodes. There is a practical limit though — not to exceed the current that the PD can handle without damage.

Table 3.2 (after [54]) summarizes the receiver sensitivity results for different modulation formats and detection methods. Analysis of receiver sensitivity and bit-error rate (BER) performance for different receiver types can be found also in [55,56,57,58].

3.3 Spectral Selectivity Improvement

As mentioned in Chapter 2, the coherent detection provides a very good spectral selectivity. This is because the IF signal is in the radio frequency domain, where electrical filtering can be applied. At these much lower frequencies, the filters can have sharp cut-offs. The situation is analogous to heterodyne (super-heterodyne) radio communications.

The good spectral selectivity of coherent detection is particularly attractive for LAN/MAN-related applications, where it can provide a large number of independent channels, thus increasing the total throughput of the network. For the time being, semiconductor lasers with narrow linewidth, combined with wide tuning range, are

not available. But considering the substantial research effort in this direction, the problems will be solved in the not so distant future.

3.4 Problems in Coherent Communications

In this section, we discuss briefly the major problems that designers of coherent optical communications face. The most promising techniques for solving these problems are outlined. Our intention is not to analyze in detail all the issues, but rather to evaluate the practical limitations of coherent optical communications, which will be useful in discussing our proposed network structure.

3.4.1 Phase Noise

In the early experiments with coherent optical communications, laser phase noise was considered as probably the single most important problem. This is still the case for homodyne systems. On the other hand, progress in laser technology (more specifically linewidth reduction), and the use of suitable modulation techniques have largely alleviated this problem in heterodyne systems.

The phase noise is due to the spontaneous emission in the laser gain medium. It causes spectral broadening of the laser emission and random phase fluctuations. The total phase noise power at the intermediate frequency (IF) of the receiver is the sum of the phase noise powers of the signal and of the local oscillator. It is a very difficult task to design a phase-locked loop (PLL) that can track and eliminate the phase noise [59]. Such a PLL is needed for homodyne systems. The loop bandwidth should be wide enough to permit tracking of the phase noise variations, and at the same time narrow enough to filter out the data modulation from the carrier. These are contradictory requirements, and the PLL bandwidth needs careful optimization, and a large ratio of modulation rate to laser linewidth. A simple relationship has been derived between the phase-noise variance, laser linewidth, and PLL bandwidth

[54]:

$$\sigma_\phi^2 = \frac{\Delta\nu_s + \Delta\nu_{LO}}{2B_L} \tag{3.12}$$

where:

σ_ϕ^2 — phase-noise variance,

$\Delta\nu_s$ — signal linewidth,

$\Delta\nu_{LO}$ — LO linewidth,

B_L — loop bandwidth.

B_L can be optimized and varies between 0.1 and 0.35 B (the bit rate) [54]. Equation (3.12) shows that, in order to keep σ_ϕ^2 small, the ratio $\Delta\nu/B_L$ must be kept small. This can be achieved by either making $\Delta\nu$ small, or increasing B_L (which means increasing the speed of transmission).

First, let us consider the laser linewidth $\Delta\nu$. Presently commercially available distributed-feedback (DFB) semiconductor lasers have linewidths between 10 and 50 MHz, occasionally individual samples have linewidths down to 1 MHz. Some experimental devices have sub-megahertz linewidths. Still, these values are too large for most synchronous demodulation formats. Obviously, one research direction is to design laser sources with narrow linewidths.

Another approach is to injection lock the semiconductor laser to a narrow-linewidth optical source, e.g., a gas laser. Encouraging results have been achieved, but it is hardly justified to have a bulky gas laser at every user location. A centralized reference source can be a viable alternative. Problems may occur with the tunability.

A powerful method of achieving a narrow linewidth is by using an external cavity coupled to the laser, as shown in Fig. 3.2. Both laser facets are anti-reflection coated. The linewidth is approximately given by the equation [60]:

$$\Delta\nu = \frac{K}{PL^2} \tag{3.13}$$

where:

K — constant, depends on the laser construction,

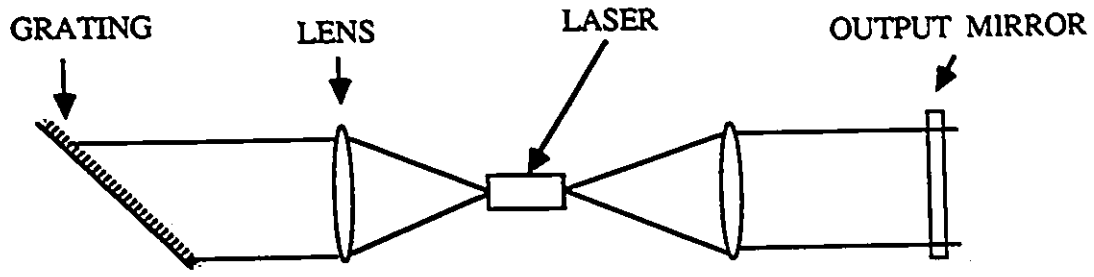

Figure 3.2: External-cavity laser.

P — laser power output,

L — optical cavity length.

Linewidths of 2 to 27 kHz have been achieved with cavities from 25 to 7 cm long.

The cavity shown is somewhat bulky and could be unreliable. But there are more elegant ways of implementation. The "cavity" can be an integrated optic waveguide, or simply a piece of fibre with reflective coating at the end.

External-cavity lasers can achieve very narrow linewidths, but they may suffer from occasional frequency hopping and are difficult to tune. If tunability is not required, then this technique can be very useful.

A very promising laser for coherent communications is the diode-pumped ring laser [61] which has linewidths of just a few kHz.

A more radical approach to avoid the adverse effects of phase noise is to use asynchronous modulation/demodulation techniques [62,63]. The most robust schemes are asynchronous ASK and FSK. They can tolerate linewidths as large as the transmission rate. There is a penalty of about 2 – 3 dB, due to the fact that the IF filter bandwidth is larger than the optimum one (when phase noise is not present) [63].

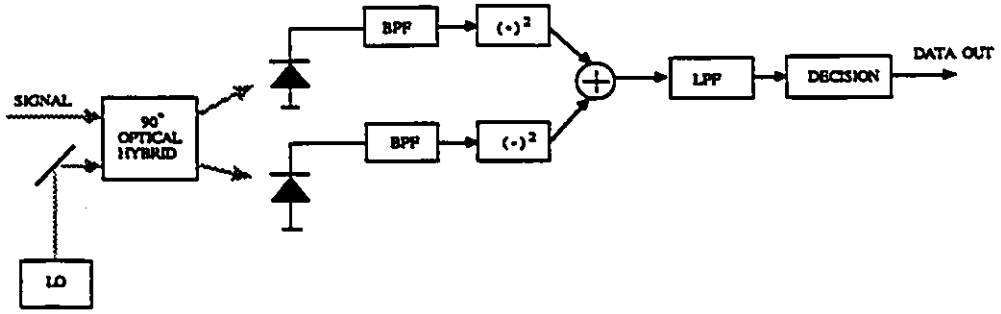

Figure 3.3: Two-branch phase-diversity homodyne ASK receiver.

Until recently, it was thought that homodyne receivers cannot use asynchronous demodulation and always require an optical PLL. Fortunately, a new receiver structure was introduced, called *phase-diversity* receiver [52,64,63,65]. The principle of operation is shown in Fig. 3.3. For simplicity, only a two-branch ASK receiver is shown, although theoretically a multi-branch receiver can be implemented.

The signal and the LO have the same optical frequency. The role of the optical hybrid is to introduce a 90° relative phase shift between the signal and the LO in the two output branches. Assuming identical photo-detectors and using (3.5), we have for the PD currents in branches 1 and 2:

$$i_1 = R_0\sqrt{P_s P_{LO}}\cos(\phi) \tag{3.14}$$

$$i_2 = R_0\sqrt{P_s P_{LO}}\sin(\phi) \tag{3.15}$$

Thus, if ϕ changes, i_1 and i_2 will not fade at the same time. After the squaring and summation operations, the result is:

$$i_\Sigma^2 = R_0^2 P_s P_{LO} \tag{3.16}$$

and is independent of ϕ.

The number of electronic components is doubled, but it is worth the effort, in order to avoid the optical PLL.

There are modifications of the phase-diversity technique that switch the phase of the LO twice during each bit period and average over the whole duration [66].

3.4.2 Polarization Fluctuations

As mentioned earlier in this chapter (Section 3.1.1), the state of polarization (SOP) of the signal and the LO must be aligned, for efficient photo-mixing to take place.

Ordinary optical fibres do not maintain the SOP [40]. Polarization-maintaining fibres have been introduced, but they are still quite expensive and considerably more lossy than ordinary fibres. For the moment, they are used only for very short (few metres) connections. This situation may change in the future.

Polarization control techniques (e.g., fibre squeezers) were used in the earlier experiments with coherent detection [51,56,57]. These techniques may not work in all circumstances.

Another approach is to use *polarization-diversity* receivers [65,67]. The idea is illustrated in Fig. 3.4.

The LO light is split in the two orthogonal SOP's which are mixed separately with the incoming signal. The two mixed signals are detected and demodulated separately, and then added together. The two channels fade in opposite directions, so that the output of the receiver is essentially independent of the SOP of the input signal.

A modification of the polarization-diversity receiver is described in [68]. The authors propose a scheme, where the SOP is switched twice (or more times) during each signal bit, either at the transmitter, or at the receiver (the LO). The decision variables are averaged over the whole duration of the bit. Thus, the polarization diversity is implemented not in space, but in time. This approach has the advantage that it does not require two separate branches, thus simplifying the receiver design.

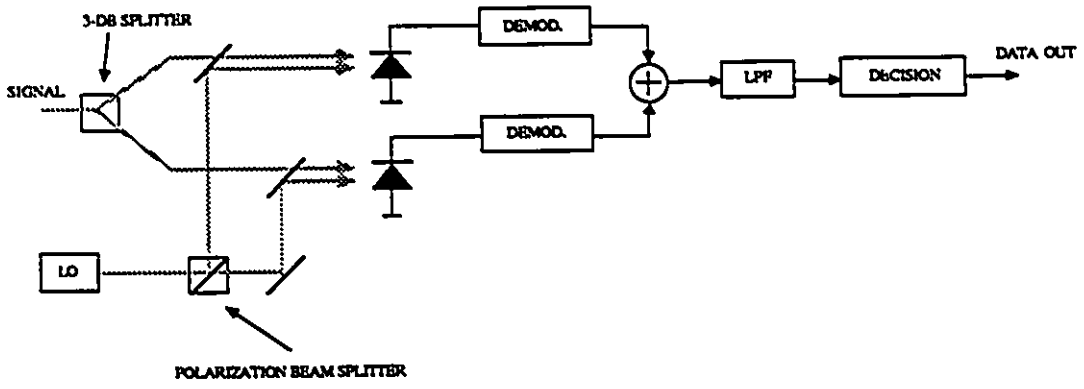

Figure 3.4: Polarization-diversity receiver.

3.4.3 Intensity Noise

Intensity fluctuations are present both in the transmitted signal and at the LO. The so-called *balanced receiver* can help in reducing the adverse effect of the LO fluctuations [54,59,69,70,71]. Fig. 3.5 shows the simplified receiver structure. The 180° optical hybrid is usually just a 3-dB coupler. The relative phase difference between the signal and LO is 0 and 180° respectively at the two output ports. In this way, the subtraction eliminates the large DC component due to the LO power (see eqn. 3.3). This technique proves to be very useful in multichannel optical networks [72].

3.4.4 Other Considerations

It should be pointed out that the techniques discussed so far are often combined within one receiver design. There are studies of balanced polarization-diversity receivers [65], polarization- and phase-diversity receivers [73,74], etc.. The analysis of such schemes is often quite complicated and not very well understood. A lot of research effort is needed in this direction.

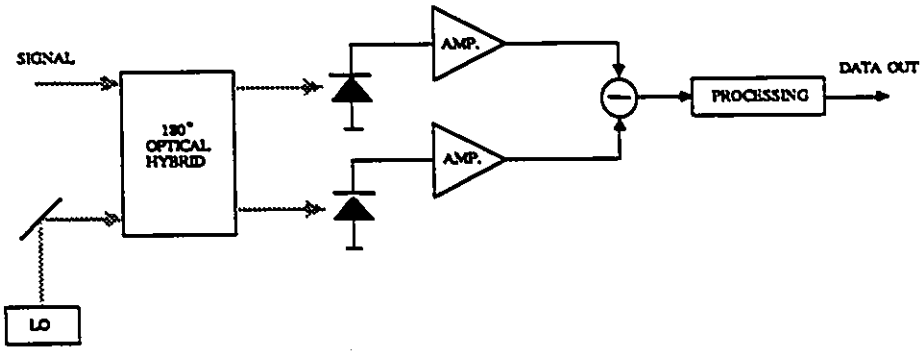

Figure 3.5: Balanced coherent optical receiver.

There are other problems that need further investigation. For example, the penalties in multi-channel networks [72,75,76] and the use of optical amplifiers in coherent optical systems [77,78,79,80]. However, we feel that the discussion presented was sufficient for our range of interest.

Chapter 4

Space Switching Using Spatial Light Modulators

4.1 Introduction

In this chapter, we present a feasibility study of SLMs as photonic switching elements for fibre-optic networks and systems. We address the problems of optical power division loss, crosstalk between the channels (Section 4.2) and implementation issues (Section 4.3).

Space switching is attractive, because once established the optical connection can carry a very high rate data stream. Simple transmission techniques can be used, like on-off keying (OOK) with direct detection, or fixed wavelength coherent transmission/detection. Most of the research lately has been concentrated on directional coupler switches built using Ti:$LiNbO_3$ technology [11,25]. Unfortunately, the size and the insertion losses of these devices make the implementation of large switching architectures impractical.

4.2 Limitations Due to Attenuation and Crosstalk

For the purpose of clarity, in this section we consider only the attenuation due to power division in the optical switch and the crosstalk produced by the finite contrast ratio of the SLM. Other detrimental factors will be addressed in the next section. The contrast ratio is defined as the ratio between the intensities of the light passing through a cell of the SLM in ON and OFF states.

The principle of operation of the SLM-based switch was illustrated in 2.1. The attenuation arising from power division is quite obvious to analyze from Fig. 2.1. It is equal to $10 \log M$ dB, where M is the number of *output* channels.

The effect of the crosstalk is more difficult to analyze, especially in digital systems, because it depends on the signal statistics of all interfering channels. However, when the number of interfering channels $(N-1)$ is relatively large, and the contribution of each interferer is small and independent from the others then, according to [S1], we can interpret the interference as additive white Gaussian noise as a direct result from the Central Limit Theorem. Thus, the power of the Gaussian noise is equal to the sum of the average powers of the individual interferers. For simplicity, we assume that all users transmit with the same average power. Then the interference is given by:

$$I = \frac{N-1}{C} P_0 \quad \text{[power units]} \tag{4.1}$$

where C is the contrast ratio of the SLM and P_0 is the average optical power of each channel (ignoring absorption in the material, since it is the same for all the channels). Consequently, the signal-to-interference ratio (SIR) is:

$$SIR = \frac{P_0}{I} = \frac{C}{N-1} \tag{4.2}$$

In order to obtain binary transmission error probability of 10^{-9}, it is necessary that $SIR \geq 16$ dB. A simple example using $C = 10^3$ (which is a rather good contrast ratio

for present devices [82]) shows that N should be less than 25 in order to meet the error rate requirements. This is a relatively small number of channels. The attenuation for 25 channels is only 14 dB, which is not a limiting factor in this case. This example suggests that some alternatives must be found to reduce the crosstalk. An obvious one is to increase the contrast ratio of the SLM. The other is to use multistage switching. Here we present the analysis for a three-stage non-blocking $N \times N$ Clos switch [83,84] shown in Fig. 4.1. For non-blocking operation, it is necessary that $k = 2n - 1$.

With careful inspection of Fig. 4.1, it can be seen that the attenuation of the signal is:

$$A = k \times \frac{N}{n} \times n = (2n-1)N \tag{4.3}$$

It increases linearly with n or N. The case $n = 1$ is equivalent to a single-stage switch.

Since the attenuation from power division is the same for the signal and the interferers, then the interference at the output of the switch is given by:

$$I = \frac{P_0}{C}[(n-1) + (N/n - 1) + (k-1)] \tag{4.4}$$

Consequently:

$$SIR = \frac{C}{(n-1) + (N/n - 1) + (k-1)} \tag{4.5}$$

If N is kept fixed, then the optimum value of n which minimizes the interference is $n = \sqrt{N/3}$.

Very useful expressions for the relationship between N and n can be obtained if fixed values for A and SIR are used. From (4.3), for the attenuation we obtain:

$$N = \frac{A}{2n-1} \tag{4.6}$$

From (4.5), for the interference we have:

$$N = n(4 + C/SIR) - 3n^2 \tag{4.7}$$

As mentioned before, SIR must be greater than 16 dB (i.e. 40). Equations (4.6) and (4.7) form a system with two unknowns. Solving the system would give the optimum

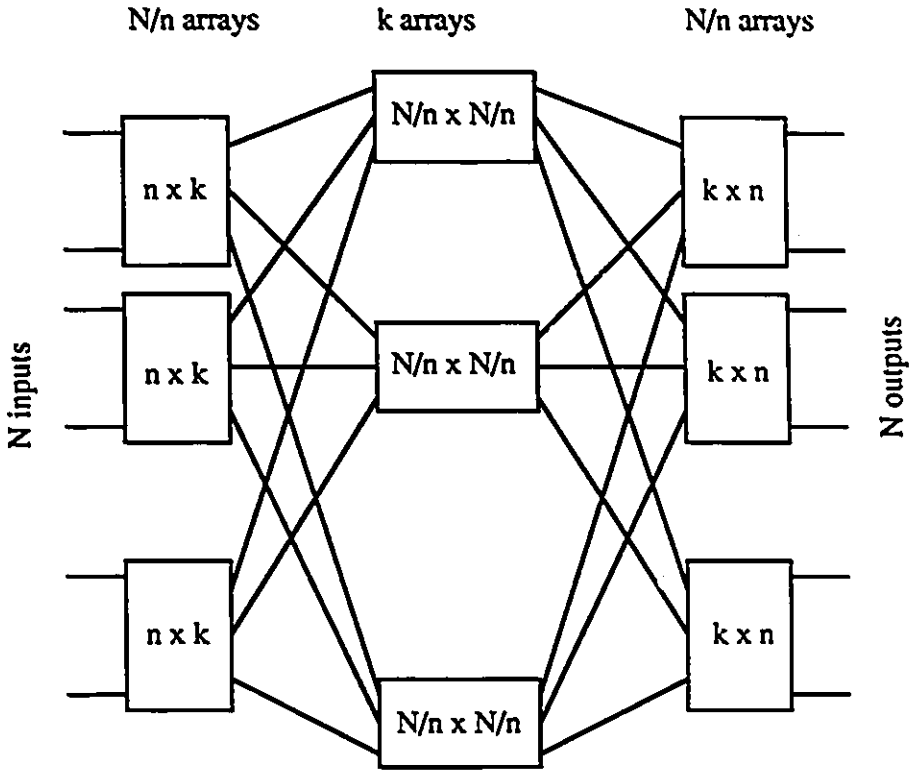

Figure 4.1: A three-stage Clos switching matrix.

value of n and the maximum number of channels N for specified attenuation A and contrast ratio C. A graphical representation is much more comprehensive. Fig. 4.2 shows plots of (4.6) and (4.7) for two different values of A and C, respectively. The points corresponding to a realizable system must be located below *both* of the pair of curves that are determined by the chosen values of A and C. It can be seen that for $C = 10^3$ and $A = 30$ dB the maximum number of channels is determined solely by the interference curve, and is approximately 70 for $n = 5$. The attenuation in that case is:

$$A = (2n - 1)N = 630 = 28\text{dB}$$

For the combination of $A = 30$ dB and $C = 10^4$, we see that $N_{max} \cong 400$ for $n = 2$. If an attenuation of 40 dB is tolerable, then the total number of channels could be as high as 1000 for $n = 5$.

Note: In interpreting the graphs, it should be clear that n and N can assume only integer values. Moreover, it is desirable that N is an integer multiple of n and also $n \leq N/2$.

4.3 Implementation Issues

4.3.1 Attenuation

Attenuation of 30 or 40 dB may seem too large at first, but such high losses are quite common in passive lightwave systems (e.g., passive star or bus topologies). Optical amplifiers (OAs) could be used to solve the attenuation problem [85]. An optical amplifier can boost the signal power by 20 dB. For example, if OAs were used after each stage of the switch in Fig. 4.1 the signal would be amplified by 60 dB. On the other hand, the number of amplifiers needed to do this would be:

$$N_{OA} = \frac{N}{n} \times k + k \times \frac{N}{n} + \frac{N}{n} \times n = \frac{N}{n}(5n - 2) \tag{4.8}$$

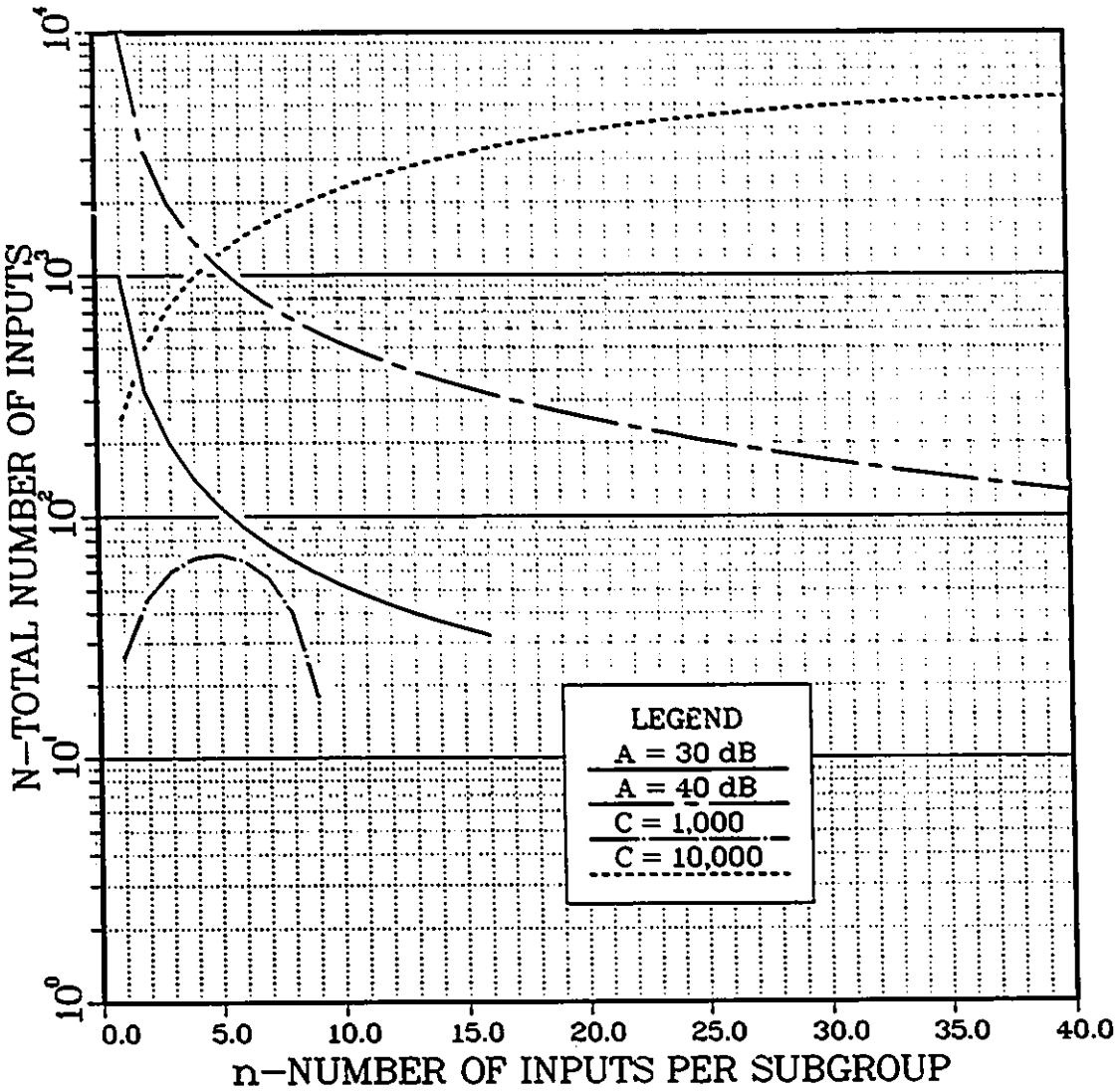

Figure 4.3: Total number of inputs N versus the number of inputs per subgroup n for different values of A and C.

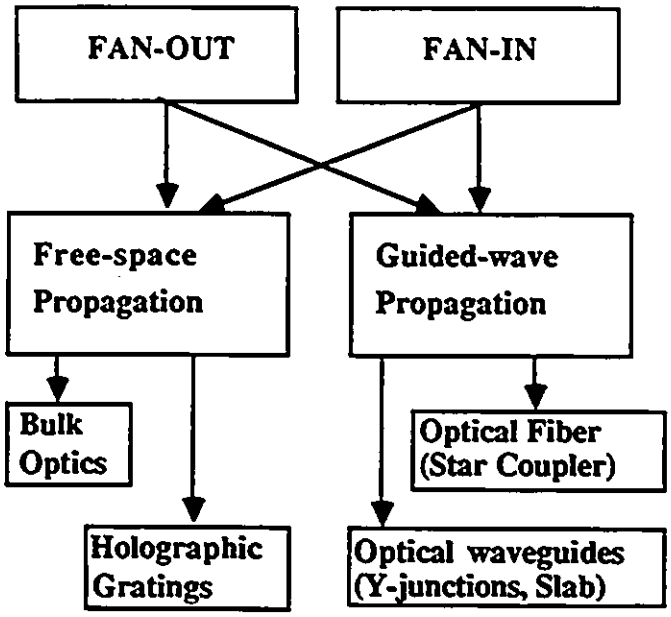

Figure 4.3: Alternatives for fan-out and fan-in.

Depending on n, we have:

$$3N \leq N_{OA} \leq 5N.$$

Thus, the number of OAs can become very large. Therefore, it would be very useful to have a method of amplifying several channels using a common pump laser, or being able to use large arrays of semiconductor OAs. Caution must be taken also to consider the noise contribution of the optical amplifiers.

4.3.2 Fan-in and Fan-out

A great challenge for the implementation of the proposed switch are the fan-out and fan-in problems. Fig. 4.3 summarizes the approaches that can be used. The optical interconnections have been studied for a variety of applications: inter-chip and inter-processor connections [86,87], optical computing and neural networks [88,

89,90], optical memory [91]. Holographic techniques seem to be suitable for fan-out applications, as demonstrated in [91,92,93]. Optical fan-out has also recently been demonstrated using a slab waveguide [94]. We feel that stacked slab waveguide tapers can be used for both the fan-out and the fan-in. The idea is illustrated in Fig. 4.4. The refractive indices of the guiding layers and of the reflecting layers are denoted by n_1 and n_2, respectively. It is necessary to provide for a low crosstalk between the adjacent layers. A promising approach for this application is the ARROW (Antiresonant Reflecting Optical Waveguide) [95,96].

There is another limitation on the maximum size of the single-stage switch — the length of the optical taper. Since the taper must be very gradual, in order to avoid losses, its length can become prohibitive. The length of the optical taper can be expressed as:

$$L = \frac{H}{2}\cot(\theta/2) \tag{4.9}$$

where H is the width of the SLM, and θ is the taper angle. For example, if $\theta = 2°$ and $H = 1$ cm, then $L = 57$ cm. It is clear that d should be small, so that the overall size of the switch remains practical for relatively large N. This condition is better satisfied by using single-mode fibres.

There is a possibility to provide an elegant solution to the attenuation problem. This can be done by adding rare-earth dopants to the output tapered waveguides, and pumping the entire medium with a powerful laser, thus achieving optical amplification of all output channels at the same time. This approach requires that all channels operate within a narrow optical spectral region.

4.3.3 Other Problems

The analysis of the three-stage switch can be extended to switch architectures using a larger number of stages. However, our opinion is that such architectures would not be advantageous, because the interconnection problem would become very complicated.

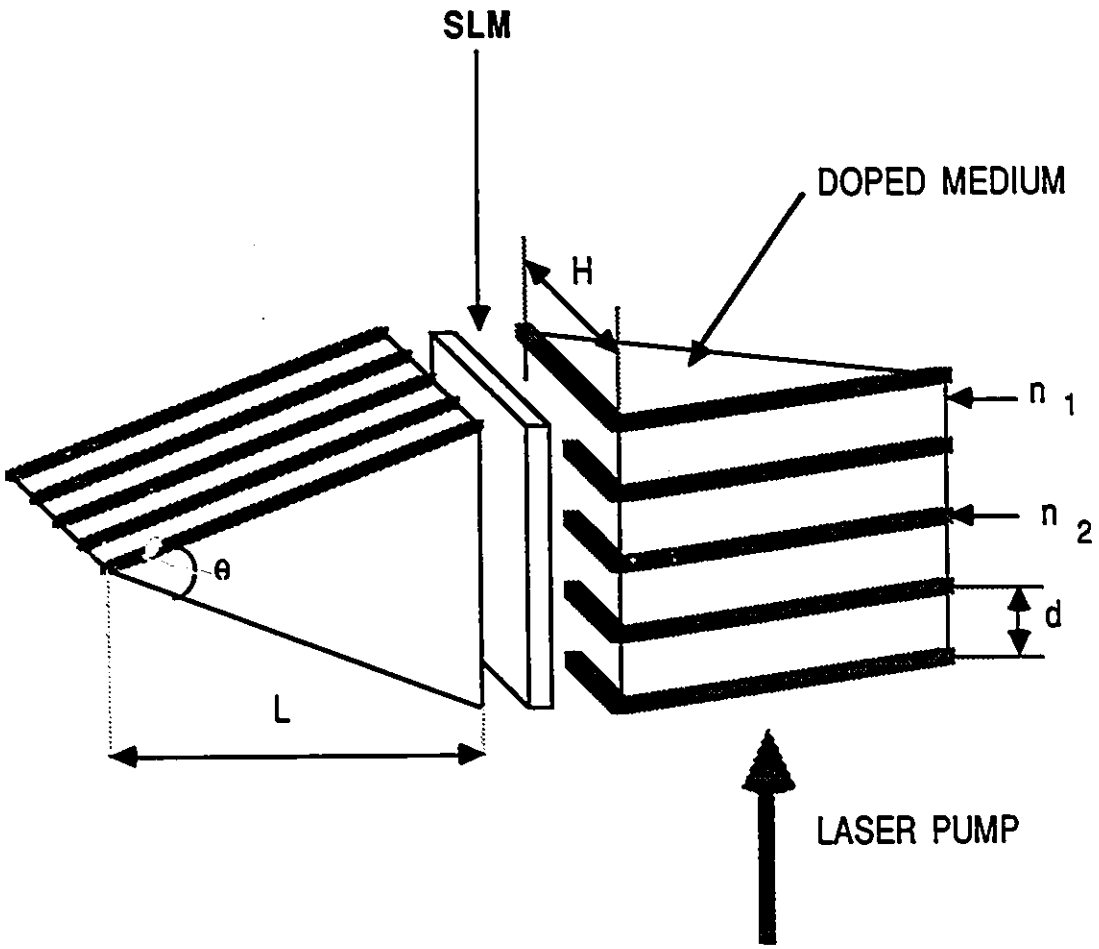

Figure 4.5: Optical crossbar switch using an SLM and stacked slab waveguide tapers for fan-out and fan-in.

The losses from splicing, insertion, fan-out and fan-in will increase dramatically. Compactness and reliability will suffer too. As a matter of fact, it is desirable to have as few stages as possible, preferably just one. By using a multistage switch, we trade attenuation for immunity to interference. For the above reasons, it is necessary to fabricate an SLM with the highest possible contrast ratio.

In [82] a comparison between different types of SLMs is presented. It is shown that the most promising devices are based on the magneto-optic effect. Currently available commercial devices from Semetex Corp. [97] exhibit a 10^3 contrast ratio with the potential to increase this value to 10^5. The size of the array could be made as large as 2048 $\times$ 2048 cells [98], the cell size varying largely between several μm and several hundred μm. The switching time for an individual cell is 100 ns which is adequate for interconnection purposes. All cells can be accessed individually and in parallel.

Presently available SLMs are mainly used for two-dimensional signal processing. They are optimized to work with light in the visible spectrum. For use in the optical communications field new devices are necessary which will operate with light in the spectral region around 1.3 – 1.55 μm wavelength.

Polarization could also be a problem. The magneto-optic SLM, for instance, uses two crossed polarizers to operate. Thus, the polarization of the input light is crucial for the operation of the device. One way to deal with this problem is to use polarization scrambling and accept the 3 dB power penalty that will result from the rejection of half of the incident optical energy. Other techniques for polarization control could also be used.

A hybrid approach of implementing the switch is also possible. By hybrid we mean a system which uses different types of switching elements. From Fig. 4.2 it can be seen that the optimum value of n (the number of channels in a subgroup) is relatively small. Thus, it may not be practical to use SLM in the first and the third stages. On the other hand, directional coupler switches fabricated by Ti:$LiNbO_3$

technology can be used to implement these stages quite easily. A decision must be made whether to preserve the broadcast capability of the switch in this case or not. The crosstalk analysis must be modified, because the directional couplers may have different crosstalk characteristics than the SLM.

A potential bottleneck for the operation of the switch could be the control mechanism, i.e., call setup, arbitration, etc., especially if fast circuit or packet switching is required. We are not going to elaborate on this issue. Some architectural and control considerations can be found in [99,100,101].

4.4 Summary

In this chapter, we have demonstrated that it is possible to anticipate the feasibility of a photonic crossbar switch using spatial light modulators. The number of channels could reach 1000×1000. Advances are needed in the fabrication of SLM, particularly in increasing the contrast ratio. Optical amplifiers are also needed. Fan-out, fan-in and polarization problems must be solved. Whenever possible, the use of a single-stage switch is preferable. We were unable to pursue experimental research due to lack of facilities.

Chapter 5

Fiber-Optic Transmission of Microwave 64-QAM Signals

5.1 Introduction

Lately, fibre-optic analog transmission of microwave signals has received considerable attention from researchers. This is due to several reasons, among them the high capacity of the fibre as a transmission medium, the availability of relatively low-cost microwave components, the ease of the subcarrier multiplexing (SCM) approach, compared to time-division multiplexing (TDM), etc.. Technological progress, mainly in the production of high-speed lasers [41], has also contributed to increased interest in SCM systems.

The optical analog microwave transmission is intended to be a near-term, low-cost implementation of wideband networks. The possible applications are numerous: analog video distribution [102]-[103], transmission of digitally-modulated RF (radio frequency) carriers [6,35,104], transmission of a mixture of digital and analog channels [34], multiple-access networks [39], etc.. There is little doubt that video distribution is the main motivation for the anticipated wide-spread penetration of the optical fibre in the local loop. Moreover, the fibre-optic transmission is probably the only alternative

in sight for the distribution of digital HDTV (high-definition TV). A recent paper by Kanno and Ito [105] describes a subcarrier-multiplexing approach for the distribution of digital HDTV. The advantage of the digital TV transmission is that the quality of the transmission is much better than in analog systems.

The purpose of our work in this chapter is two-fold. First, we want to demonstrate, in general, the practicality of fibre-optic transmission of a microwave signal digitally modulated using a 64-level quadrature-amplitude modulation (64-QAM) format. Second, we like to assess the usefulness of the multi-level QAM (M-QAM) format for digital HDTV distribution. M-QAM has been widely accepted for terrestrial microwave communications, hence simple interfacing between radio and fibre systems is possible. Another advantage of the M-QAM format is its spectral efficiency. Although the total bandwidth of the optical fibre is very large, in the SCM systems the available bandwidth is limited by the electronic components, and it should be used efficiently. Of course, wavelength-division multiplexing (WDM) can be used together with SCM [106], but this is a separate issue.

We conducted an experiment at 90 Mb/s transmission rate. This transmission rate was chosen not because it was particularly tailored to digital HDTV distribution (to the best of our knowledge, there is no universal standard for digital HDTV formats yet.), but because of the availability of radio equipment, namely 90 Mb/s C-band microwave digital radios.

The chapter is organized as follows. In Section 5.2 the experimental setup is described. In Section 5.3, the theoretical SNR and bit-error rate (BER) analysis is presented. The effects of thermal noise, intrinsic laser intensity noise, and reflection-induced laser noise on the system performance are discussed, together with methods for improving the performance: minimization of reflections and the use of error-correction coding techniques. Measurement results are presented and interpreted in Section 5.4. Section 5.5 deals with the possible applications of the transmission technique under investigation. In Section 5.6, the problem of laser nonlinearity is

addressed and some theoretical results are presented.

5.2 Experimental Setup

A block diagram of the experimental test set is shown in Fig. 5.1. The RF signals from two 90 Mb/s 64-QAM radio transmitter units, after being attenuated, are combined and used to intensity modulate a laser diode. A polarization controller (or optical isolator) is used to reduce the reflection-induced laser intensity noise. An optical attenuator is used to simulate the optical path loss. At the receiver end, the optical signal is detected and down-converted to an intermediate frequency (IF), where white Gaussian noise is added from a noise generator. By adding a controlled amount of Gaussian noise, it is possible to obtain experimental data about the BER as a function of bit energy per noise spectral density. After the IF stage, a 90 Mb/s 64-QAM receiver recovers the digital information and sends it to a BER test set (which also generates the pseudo-random bit sequence provided to the transmitter).

The radio system is equipped with an error-correcting codec using a shortened rate 18/19 self-orthogonal convolutional code similar to the one described in [107]. The effective coding rate is $R_c = 12/13$. As will be demonstrated in subsequent sections, the error correction capability greatly enhances the system performance. The experimental setup permits the measurement of the error probability before error correction decoding (using a cyclic redundancy check error-detecting code embedded in the transmitted bit-stream for frame synchronization), as well as after decoding, using the BER test set.

The parameters of the 90 Mb/s 64-QAM digital radio system are as follows:

carrier frequency $\cong$ 4 GHz;

overall bit rate = 95.96 Mb/s;

RF bandwidth = 20 MHz;

IF frequency = 70 MHz;

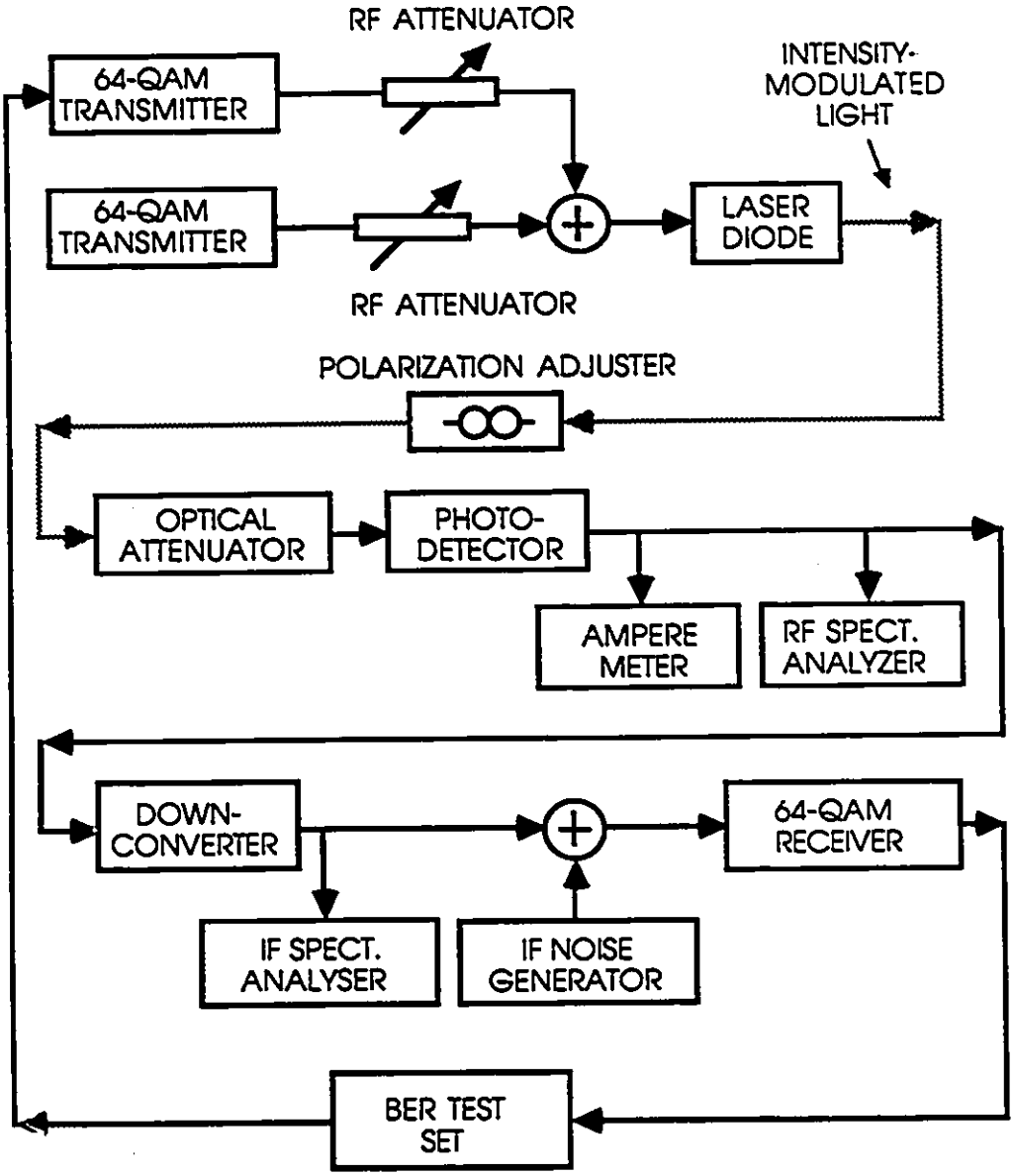

Figure 5.1: Experimental system setup in laboratory.

symbol rate = 15.99 Mbaud;

spectral efficiency = 4.8 b/s/Hz;

receiver noise figure = 4.5 dB.

The laser diode has a central wavelength of about 1.3 μm and a full-width-half-maximum (FWHM) linewidth of about 2 nm. Its 3-dB bandwidth is at 6 GHz, and the relaxation oscillation frequency is near this point. The photo-detector used in the experiment has a responsivity of 0.6 A/W.

The polarization controller reduces the effect of the reflected light in the following way. The polarization of the light in the direct path is rotated by 45°. On the reflected path, it is rotated by another 45° in the same direction (the material used is not isomorphic). Therefore, the polarization of the reflected beam becomes practically orthogonal to that of the light beam on the direct path. Hence, the intensity noise effect is reduced. Even better results can be obtained by using an optical isolator.

5.3 SNR and BER Analysis

There are several sources of noise in this system: receiver thermal noise, Gaussian noise added at the receiver IF stage, laser intensity noise (intrinsic and reflection-induced), dark-current noise, and shot noise. The dark-current noise is negligible, compared to the others, therefore it may be neglected. For the moment, we concentrate on the case of a single subcarrier, so that the effects of harmonic distortion, intermodulation and cross-modulation distortion can be set aside.

Laser intensity noise has long been recognized as a major detrimental factor in analog fibre-optic transmission. A very comprehensive analysis of the effects of the laser-diode intensity noise on system performance is presented in [108]. A detailed theoretical and experimental study of the characteristics of the intensity noise itself can be found in [109,110]. The intrinsic intensity noise is determined by the laser design and cannot be improved subsequently. However, measures can be taken to

minimize the reflection-induced intensity noise. In our subsequent discussions, we use the notion of laser intensity noise minimization as applied to the reflection-induced noise.

A quantitative measure of the laser intensity noise is the RIN (relative intensity noise), defined as [6,108]:

$$\text{RIN} = \frac{\Delta\overline{P}^2}{\overline{P}_0^2} \qquad \text{dB/Hz} \tag{5.1}$$

where $\overline{P}_0$ is the time-averaged laser light intensity and $\Delta\overline{P}^2$ is the mean-square intensity fluctuation spectral density of the light output. The RIN spectrum exhibits a maximum at the laser relaxation oscillation frequency, but within a relatively narrow frequency band (such as a modulated subcarrier), it can be assumed to be flat. For a laser diode biased well above threshold, the intensity noise can be assumed to have Gaussian distribution [109,110].

The optical modulation index is defined as:

$$m_o = \frac{P_{max} - P_0}{P_0} \tag{5.2}$$

where P_{max} is the peak transmitted light power and P_0 is the average transmitted light power.

The symbol error rate on one rail (in-phase or quadrature-phase) of an M-QAM signal is given by [111]:

$$P_s(e) = \left(1 - \frac{1}{\sqrt{M}}\right) \text{erfc}\left(\sqrt{\frac{3}{2(M-1)}\gamma_s}\right) \tag{5.3}$$

where γ_s is the average signal-to-noise ratio defined for QAM symbols, and:

$$\text{erfc}(x) = \frac{2}{\sqrt{\pi}} \int_x^\infty e^{-t^2} dt \tag{5.4}$$

Considering the peak power of the corner points in a 64-QAM signal constellation, it is important to define an effective value for the optical modulation index (m_e). For now, the SNR at the output of the photo-diode, conditioned on a given 64-QAM level r_i, is:

$$\text{SNR}|_{r_i} = \text{SNR}_0 r_i^2 \tag{5.5}$$

where

$$\mathrm{SNR}_0 = \frac{\frac{1}{2}m_o^2 I_D^2}{4kTBF/R_L + 2eI_DB + \mathrm{RIN}I_D^2B + N_0B} \tag{5.6}$$

where:

I_D — average detected photocurrent,

B — receiver IF bandwidth (double-sided),

k — Boltzmann's constant (1.38×10^{-23} J/° K),

T — absolute temperature (290 ° K),

e — electron charge (1.602×10^{-19} C),

F — electronic receiver amplifier noise figure,

R_L — photo-diode load resistor with a 50 Ω nominal value.

The effect of the Gaussian noise added at IF is shown in (5.6) by the term N_0B in the denominator, where N_0 is the equivalent spectral density height.

In a symmetrical 64-QAM signal space, the maximum amplitude belongs to the corner signal points. For an adjacent-point signal spacing d, it is:

$$\max r_i = \frac{7}{\sqrt{2}}d \tag{5.7}$$

For proper optical intensity modulation, it is necessary that:

$$0 < m_o r_i \leq 1 \tag{5.8}$$

for all i. To assure this, we assume a normalized peak value 1 for r_i, that is:

$$d = \frac{\sqrt{2}}{7} \tag{5.9}$$

Now, the average SNR for the 64-QAM signal is:

$$\gamma_s = \mathrm{SNR}_0 \left(\frac{1}{64} \sum_{i=1}^{64} r_i^2 \right) = \frac{21}{2} d^2 \mathrm{SNR}_0 = \frac{3}{7}\mathrm{SNR}_0 \tag{5.10}$$

Therefore:

$$\gamma_s = \frac{\frac{1}{2} \times \frac{3}{7} m_o^2 \times I_D^2}{4kTBF/R_L + 2eI_DB + \mathrm{RIN}I_D^2B + N_0B} \tag{5.11}$$

In (5.11), m_o is the optical modulation index whose value can be between zero and one. The effective modulation index is $m_e = \sqrt{3/7}m_o$. For example, for $m_o = 0.3$, the effective modulation index $m_e = 0.196$. Therefore, the effective index is less than $\sqrt{3/7} \cong 0.65$ for a distortion-free signal constellation.

Equations (5.1) to (5.11) can be used to find the BER analytically as a function of SNR, or the received optical power, knowing that:

$$I_D = R_0 P_0 \tag{5.12}$$

where R_0 is the responsivity of the photo-diode in Ampere/Watt.

We present part of our results in terms of bit energy-to-noise density E_b/N_0 in the forthcoming sections. E_b/N_0 can be related to the SNR Γ_s by:

$$\Gamma_s = \frac{E_b}{N_0} \times \frac{R_b}{B} \tag{5.13}$$

where R_b is the bit rate.

The usefulness of error-correction techniques in fibre-optic systems has been recognized and exploited [112,113]. Forward error-correction coding (FEC) is a particularly valuable approach to compensate for power-dependent BER impairments [114]. It can also be used to reduce error-rate floors and/or relax the stringent technological requirements otherwise present for various optical and electronic components.

The performance of the type of error-correction code used in this experiment is described in detail in [107]. Self-orthogonal codes are a class of convolutional codes that are rather simple to implement, and they can be decoded with majority-logic decoding. The particular code used in this experiment can correct up to 2 bit errors within a constraint length $N_c = 949$ bits. The parameter that is most needed for the present analysis is the relationship between the input and the output BER of the decoder, and it can be found in [107,115] as:

$$P_b \leq \frac{12}{18} \times \frac{1}{N_c R_c} \sum_{i=3}^{N_c} \binom{N_c}{i} p^i (1-p)^{N_c - i} \tag{5.14}$$

where P_b is the bit error probability after decoding, and p is the BER at the decoder input. Expression (5.14) is a reasonable approximation for values of p less that 10^{-4}.

5.4 Measurement Results

The optical modulation index m_o is 0.3 throughout all experiments. The first measurement is the average BER on one rail of the QAM signal versus the E_b/N_0, without intensity noise minimization. The received average photocurrent is kept constant at 0.6 mA. The value of E_b/N_0 is controlled by inserting the appropriate amount of white Gaussian noise at the IF of the receiver. The results obtained are shown in Fig. 5.2. The ideal performance of the 64-QAM signaling (i.e., with only the Gaussian noise source) is plotted as a reference. The large penalty due to intensity noise is clearly seen from the error rate curve at the decoder input. This is measured by a cyclic redundancy check code that performs error detection for frame synchronization. The error-correction decoding improves the performance of the system dramatically, bringing it very close to the ideal one down to an error probability equal to 10^{-6}.

Fig. 5.3 shows the results of a test, where the Gaussian noise source is removed, and the optical signal is gradually attenuated. No intensity noise minimization took place. In this case, the RIN is worse than in the previous measurement. This is due to the presence of the optical attenuator which introduces more connectors and, consequently, more reflections. One can clearly see the occurrence of an error floor for large values of received optical power. Again, the performance at the decoder output is substantially better.

In the next experiment, intensity noise is minimized using a polarization controller. The same measurements of BER versus E_b/N_0 are taken, both before and after error-correction decoding. The results are shown in Fig. 5.4. Clearly, the situation is much better than in the previous two experiments. The curve, which is closest to the reference one, represents the case of the measured back-to-back performance of the

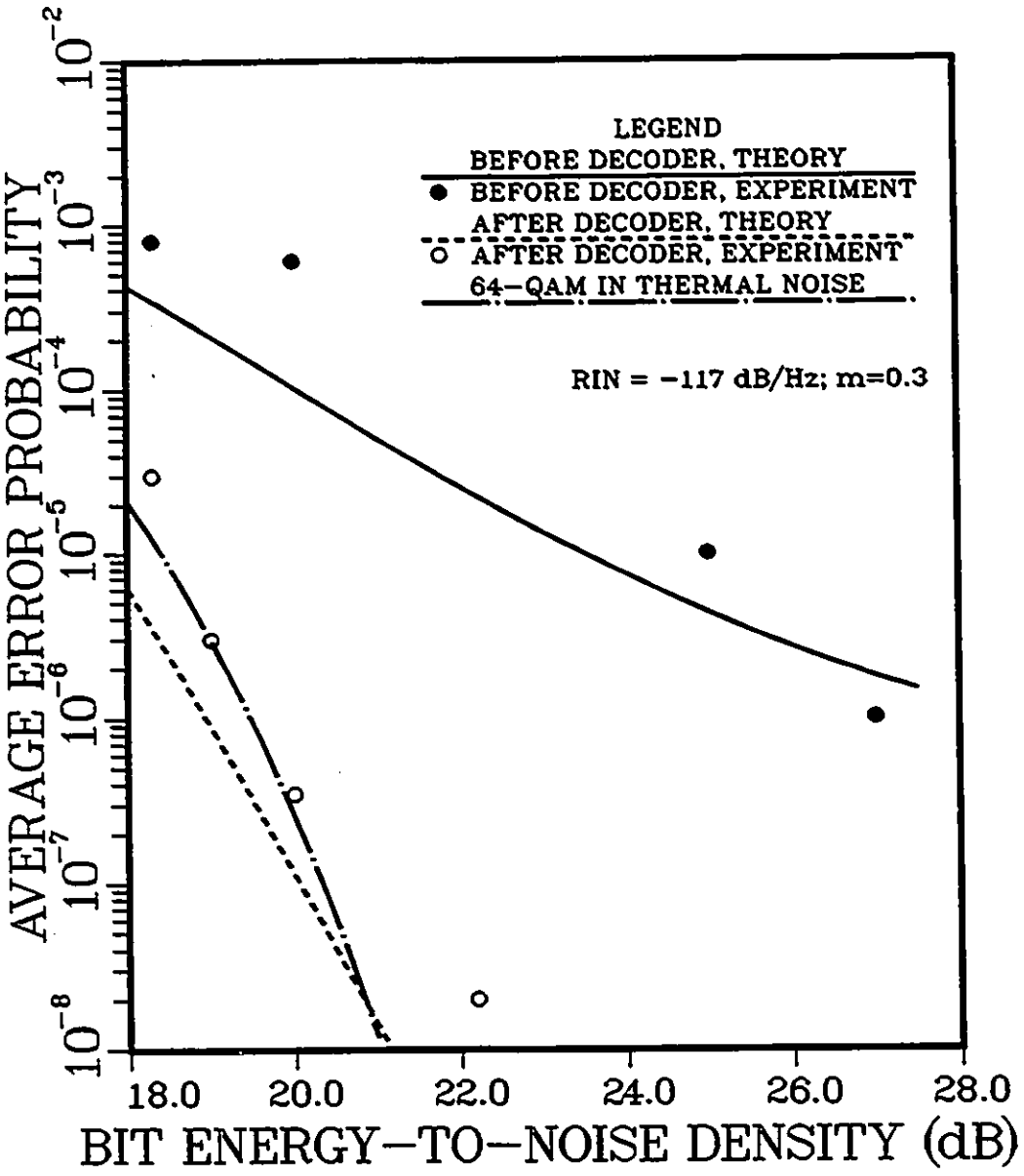

Figure 5.2: Error probability performance versus required E_b/N_0 in the presence of intensity noise, before and after error correction decoding of the 64-QAM signal.

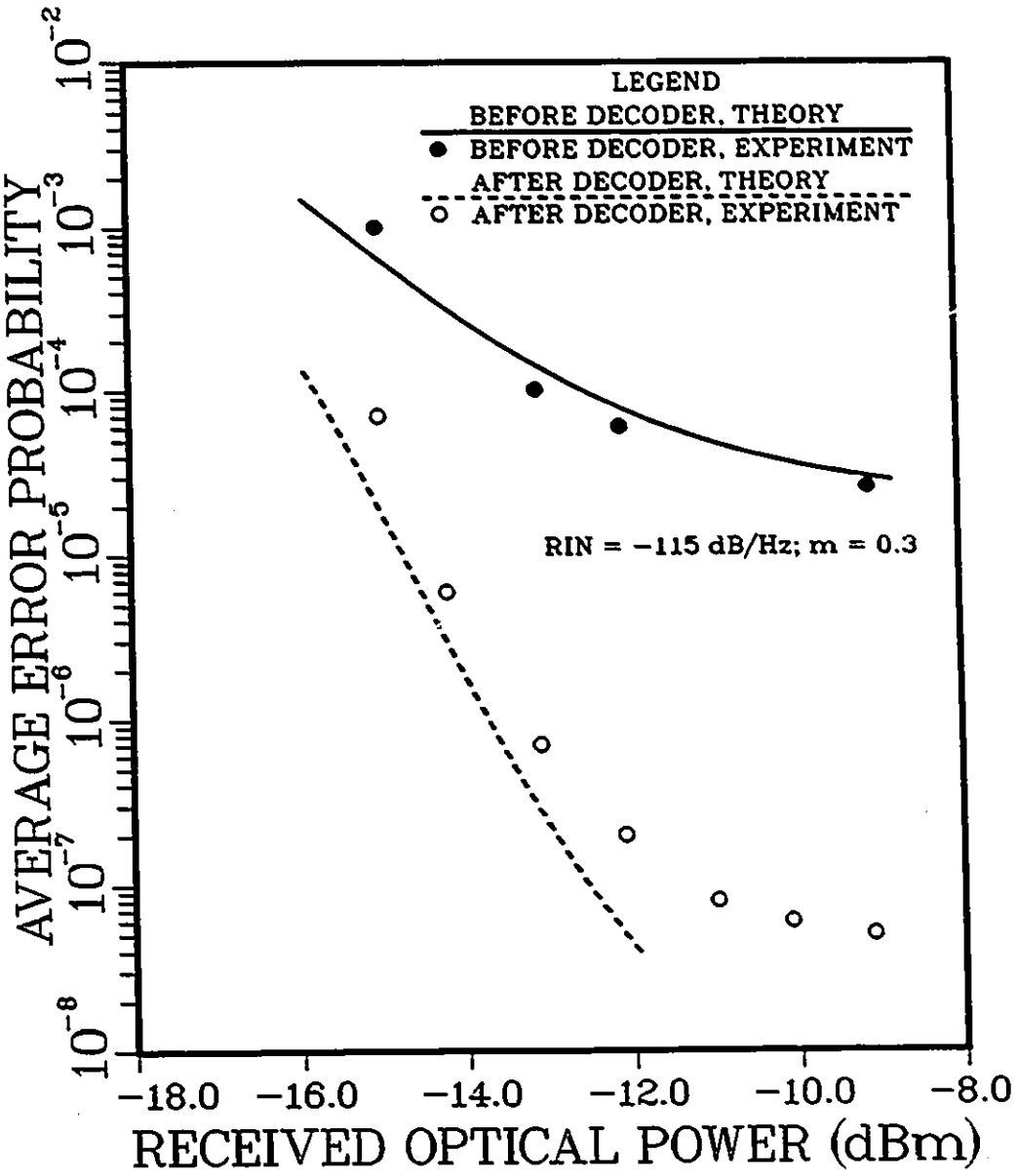

Figure 5.3: Average error probability versus received optical power in the presence of intensity noise.

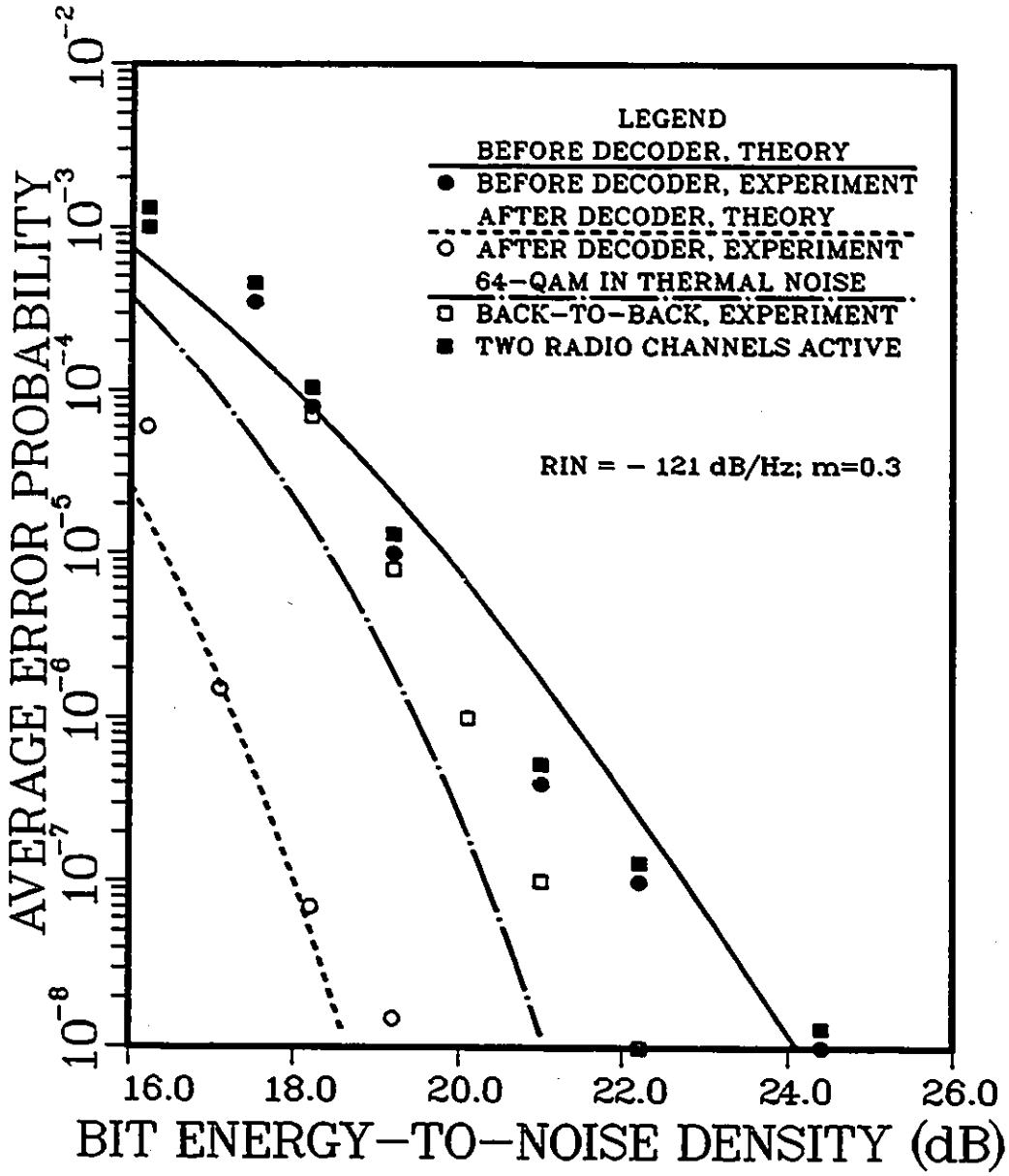

Figure 5.4: Error probability performance versus required E_b/N_0 with minimized intensity noise, before and after error correction decoding of the 64-QAM signal, for one and two active modulated carriers.

radio, i.e., when the optical parts are replaced by an RF attenuator such that the same nominal power is received by the radio receiver. There is about 1 dB implementation degradation at an error probability of 10^{-8}. In the same experiment, another radio is added for simultaneous transmission. The power budget of the system will change, of course, but the important fact is that there is no sign of BER degradation from interference, or nonlinear distortion, at least for two 64-QAM signals. The guard band between the two signals is equal to the receiver bandwidth, i.e., 20 MHz, and appears to be adequate.

The results of the fourth experiment are shown in Fig. 5.5. The BER versus received average optical power is measured in the case of minimized intensity noise. Down to a BER=10^{-8}, there is no error floor, even on the error rate curve measured at the decoder input. However, this floor will still occur at higher optical power levels, since the intrinsic intensity noise of the laser is still present.

We note that the values for the RIN are quite high, even when the reflections are minimized. The reason for this is the relatively high microwave input power transferring low-frequency noise into the transmission band (e.g., see [108]). The intrinsic RIN of the free-running unmodulated laser, as specified by the manufacturer, is typically about -129 dB/Hz. This figure can get larger by up to 10 dB, in the case of a high RF power at the laser input. In our case, 8 dBm of RF power was needed to achieve $m_0 = 0.3$. To avoid the above-mentioned effect, the RF power must be reduced to below 3 dBm, and then $m_0 \leq 0.17$.

The experimental results are generally in good agreement with the theoretical predictions. The occasional larger differences are due to system imperfections not accounted for. One should also keep in mind that the decoder input error rate is not measured by the BER test set, and therefore, cannot be very accurate. Also, (5.14) is an approximate expression that gives accurate results only under conditions specified in the previous section.

Fig. 5.6a shows the received RF spectrum and signal constellation when two signals

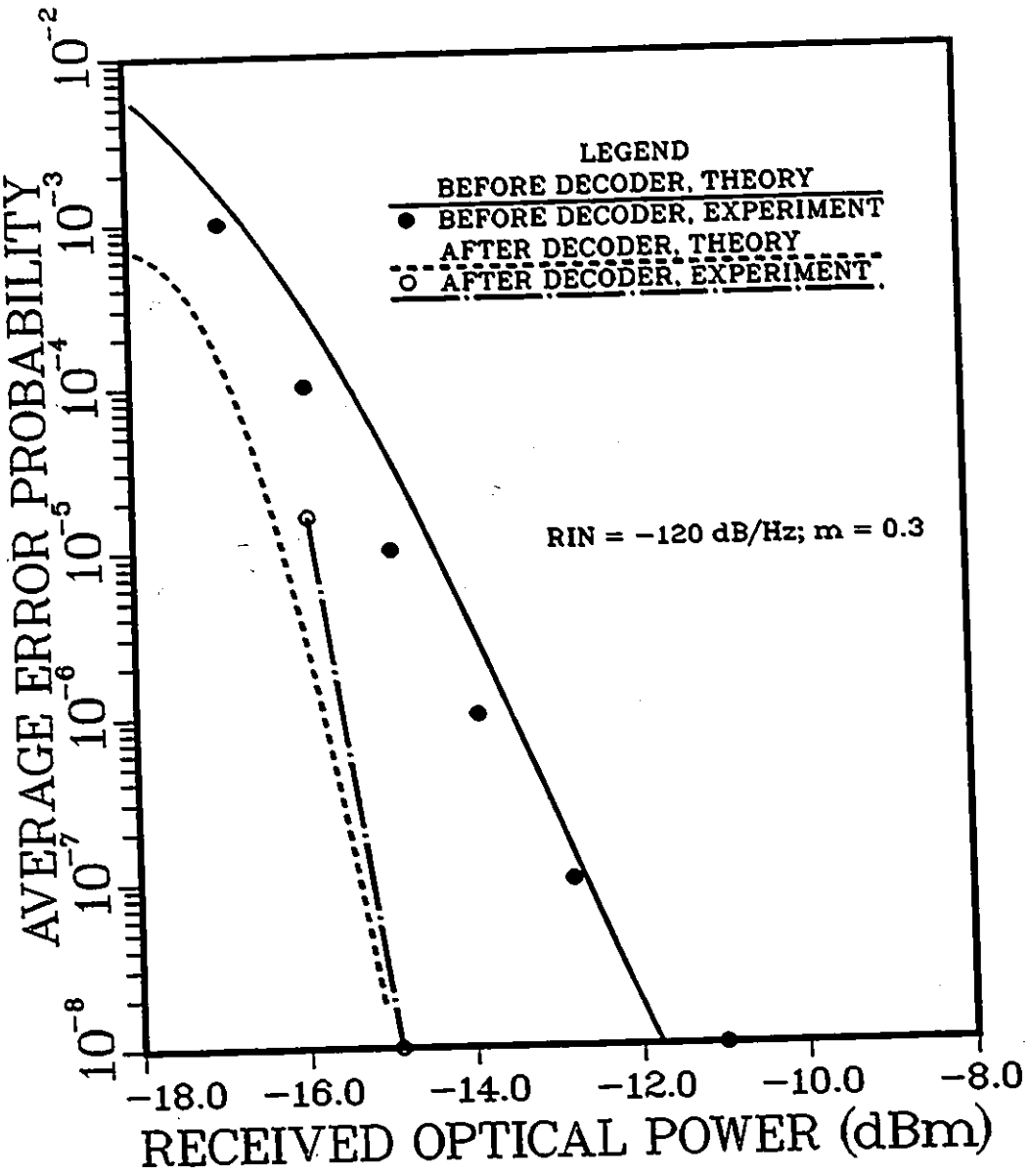

Figure 5.5: Average error probability versus received optical power with minimized intensity noise.

are transmitted simultaneously. The RIN was minimized. The optical power was kept constant at 0 dBm. Fig. 5.6b, c, and d correspond to different levels of added Gaussian noise. Fig. 5.6d corresponds to a BER = 4×10^{-4}.

Next, we want to assess the performance of the system when a laser with a lower RIN is used. Fig. 5.7 shows a comparison for two values of the RIN: −120 dB/Hz and −155 dB/Hz. The second value has been achieved with good semiconductor lasers. It can be seen from Fig. 5.7 that the error floor does not appear, even at BER = 10^{-10} for the −155 dB/Hz case. It can also be observed that the RIN affects the performance of the system after the decoder to a much lesser degree than before the decoder. This demonstrates the robustness of the error-correction scheme. We can be fairly confident in our theoretical projections for the BER at −155 dB/Hz RIN, because the theoretical model was proven to achieve results in good agreement with the experimental data.

5.5 Potential Applications

As mentioned in the introduction, the optical transmission technique under investigation is suitable for various kinds of digital information. Our intention though, is to assess the applicability of the findings to digital HDTV distribution networks. The transmission capacity required for an uncompressed digital HDTV signal is about 1 Gb/s. With sophisticated image coding techniques, a transmission rate of about 150 Mb/s is possible, without significant picture-quality degradation. Work is under way on 45 Mb/s transmission of digital HDTV using inter-frame coding. Therefore, each of our carriers can transmit two digital HDTV channels. A tentative power budget can be found using Fig. 5.5 and the following assumptions: launched optical power by the transmitter = 0 dBm; fibre loss including splicing and connectors = 0.6 dB/km. This results in a repeaterless transmission distance of 25 km. Moreover, the optical modulation index can be increased from 0.3 to 0.6, provided that

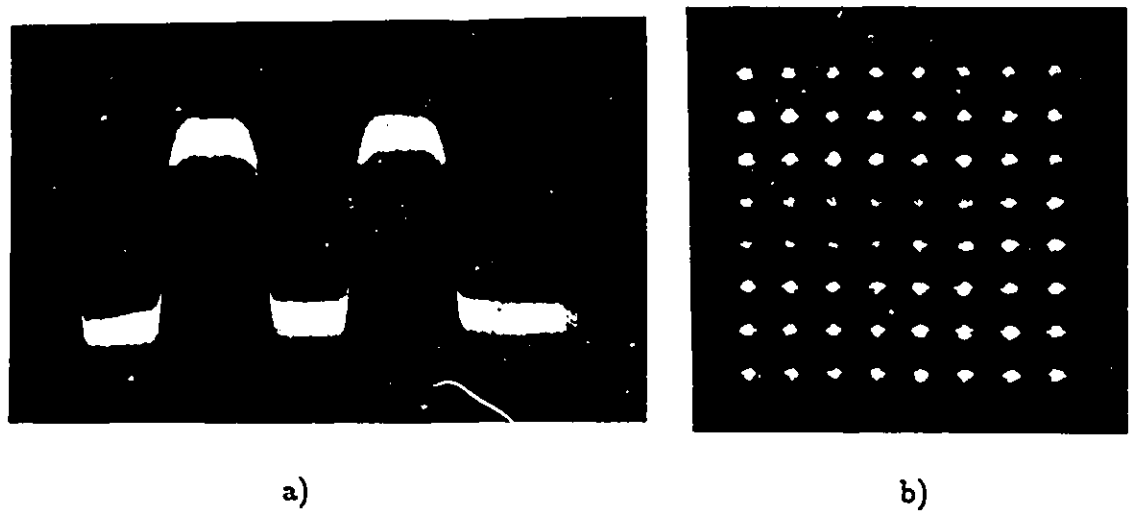

a) b)

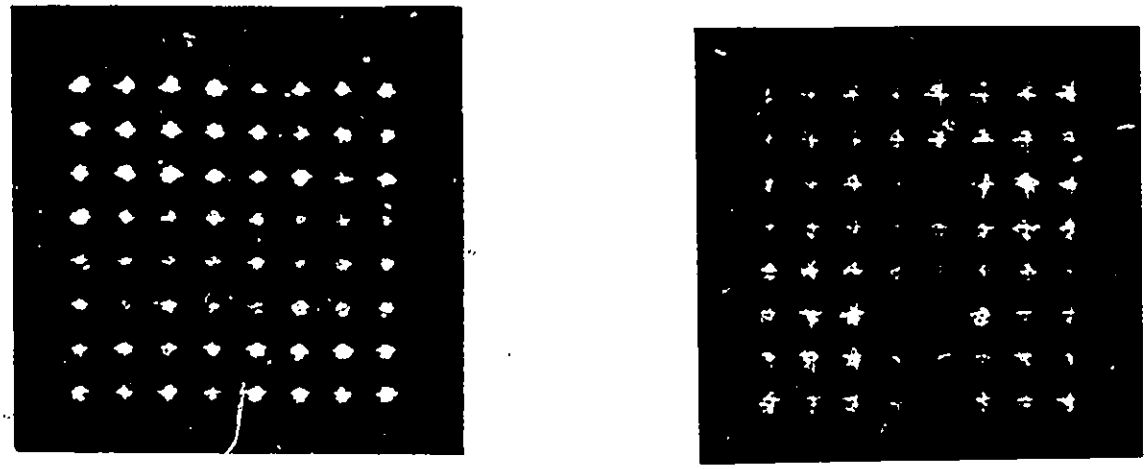

c) d)

Figure 5.6: Received two-channel signal with minimized intensity noise, $P_0 = 0$ dBm: a) RF spectrum with two radio signals received; b) Reference received signal constellation for error-free (BER $\leq 10^{-8}$) received bitstreams; c) Received signal constellation with increased eye-closure compared to case-b; d) Received signal constellation for BER $= 4 \times 10^{-4}$.

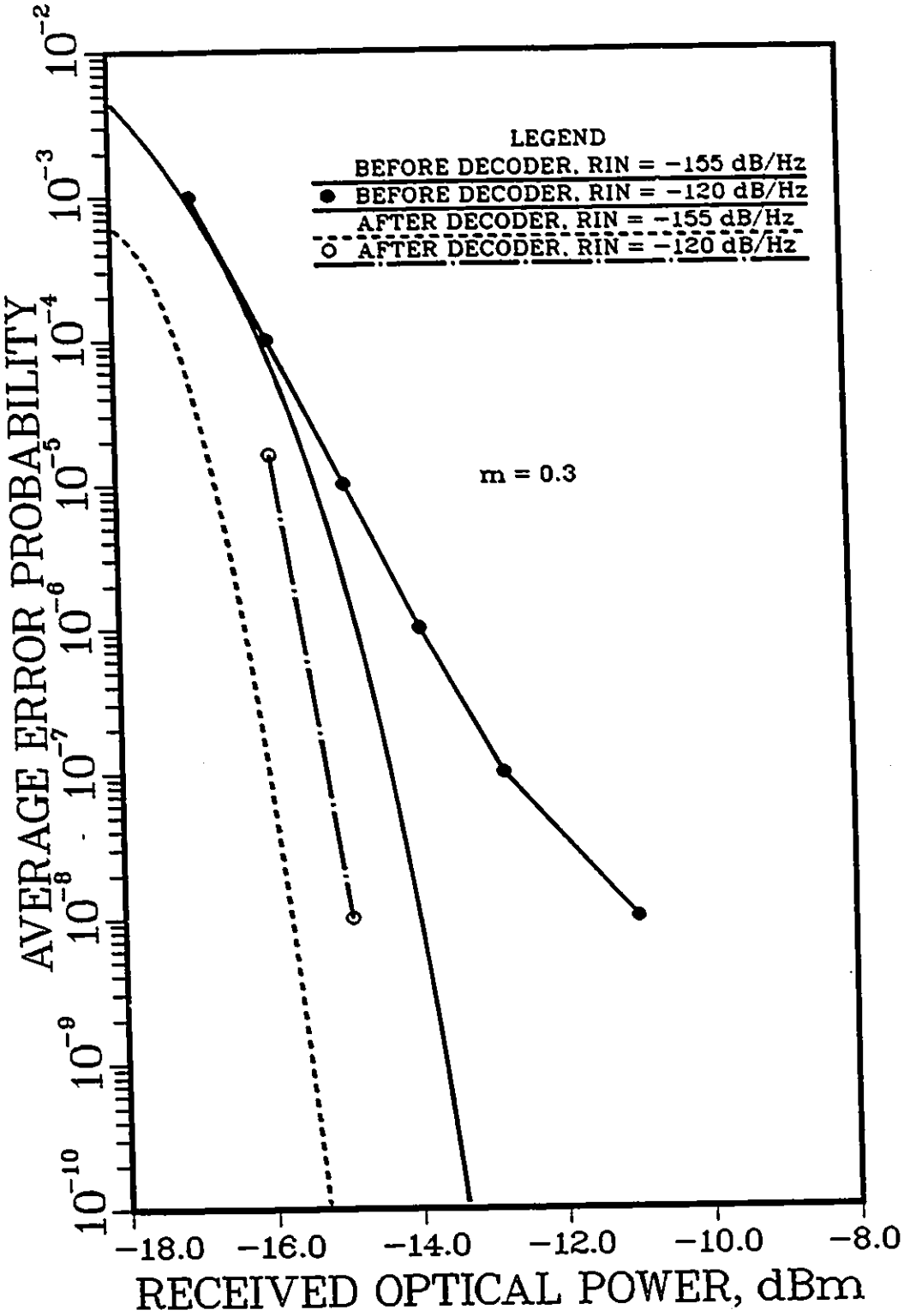

Figure 5.7: Comparison of BER performance for two values of the RIN.

	Transmission distance (km)						
No. of channels	2	4	8	16	32	64	128
$m_t = 0.3$	25	20	15	10	5	–	–
$m_t = 0.6$	35	30	25	20	15	10	5
	Total bandwidth (MHz)						
	20	60	140	300	620	1260	2540

Table 5.1: Transmission distance and total required bandwidth as a function of the number of HDTV channels. There are two TDM-multiplexed TV channels per subcarrier.

nonlinearities cause no problem. This will increase the power budget by 6 dB.

If transmission of many (e.g., more than 5) TV channels is required, then the individual subcarrier modulation indices can be selected so that their values satisfy the relationship [34]:

$$m_t = \sqrt{\sum_{i=1}^{N} m_i^2} \tag{5.15}$$

where N is the number of subcarriers, m_i's are the individual modulation indices, and m_t is the total modulation index. Assuming all m_i's are equal:

$$m_t = m_i\sqrt{N} \tag{5.16}$$

This means that the power budget for an N-carrier transmission is decreased by $10\log_{10} N$ dB, compared to a single-carrier transmission. Table 5.1 gives the point-to-point transmission distance as a function of the number of channels for two values of m_t, under the previous assumptions. In the same table is also given the required bandwidth for transmission, assuming guard bands between the carriers equal to the receiver bandwidth. The spectral efficiency of the scheme is evident. It should be mentioned here, that the FEC increases the required bandwidth slightly, whereas the BER improvement is significant. The codec can be built using standard TTL integrated circuits [107], or advanced CMOS chips.

The use of optical amplifiers [32,103] can substantially increase the system power budget, resulting in longer transmission distances and/or larger number of users.

If higher than 90 Mb/s bit-rates are required, then two alternatives are possible: a) increase the transmission rate of the individual subcarriers, or b) use several subcarriers per channel, as in [108]. Since m_t and m_i are related as in (5.16), the two approaches are equivalent in terms of power budget. The first approach will need less receiver bandwidth, since fewer guard bands will be necessary, but the logic must work at a higher speed. Approach b) is less bandwidth-efficient, but in return can use lower-speed digital electronic circuits. The optimum trade-off is a task for the system designer.

5.6 Nonlinearity Considerations

Laser nonlinearity has been a major source of concern in subcarrier multiplexed photonic systems [36,37,116,117]. Appendix A of this thesis provides a brief background on nonlinearities in communication systems.

Because of the spectral efficiency of the 64-QAM transmission format, single-octave (SO) mode of operation is most likely to be used in the system under consideration. The definition of single-octave and multi-octave mode of operation is given in Appendix A. In SO mode of operation, the dominant source of distortion are third-order intermodulation products (IMPs), and the channel worst affected is the middle one. For a reasonably large number of channels (e.g., 10 or more), the number of IMPs is quite large, therefore the interference can be treated as additive Gaussian noise. The noise contribution of the third-order IMPs can be expressed as:

$$\sigma_{3d}^2 = I_D^2 m_j^6 A_3^2 h_3 K_3 \tag{5.17}$$

where:

A_3 is a nonlinearity coefficient,

K_3 is the number of IMPs falling within the passband of the middle channel,

h_3 is a coefficient that determines how much of the IMPs power falls within the passband of the channel (see Appendix A).

Therefore, for the j-th channel we have:

$$\gamma_{sj} = \frac{\frac{1}{2} \times \frac{3}{7} m_j^2 \times I_D^2}{4kTBF/R_L + 2eI_D B + \mathrm{RIN} I_D^2 B + I_D^2 m_j^6 A_3^2 h_3 K_3} \tag{5.18}$$

Consider $N = 40$ subcarriers (corresponding to 80 TV channels in the previous example). Using information from Appendix A, we can determine that $K_3 = 551$, and $h_3 \approx 1/\sqrt{3} = 0.577$. The data sheet of the laser diode that we used in our experiment provides information about the linearity of the device. In a three-tone test, at $P_{in} = 0$ dBm RF power, the third-order IMP is 50 dB below the carrier. From this value, we can determine $A_3 = 5.8 \times 10^{-3}$. The j-th modulation index is determined as:

$$m_j = \frac{m_0}{\sqrt{N}} = \frac{0.6}{\sqrt{40}} = 0.095 \tag{5.19}$$

Now we can determine the BER for the worst channel as a function of the received optical power. The results are shown in Fig. 5.8, where for comparison are also shown BER curves of a distortionless system. The distortion penalty is clearly present, but it is not an overwhelming problem. When error-correction coding is applied, the penalty is less than 0.5 dB at a BER = 10^{-9}.

5.7 Summary

From the results presented in this chapter, it is evident that the fibre-optic transmission of a 64-QAM microwave signal is feasible and practical. Two important ways of improving the system performance were discussed and demonstrated — laser intensity noise minimization, and the use of error-correction coding. The transmission technique investigated is suitable for many different types of digital information. It could be particularly attractive as a cost-effective approach to the distribution of digital video services.

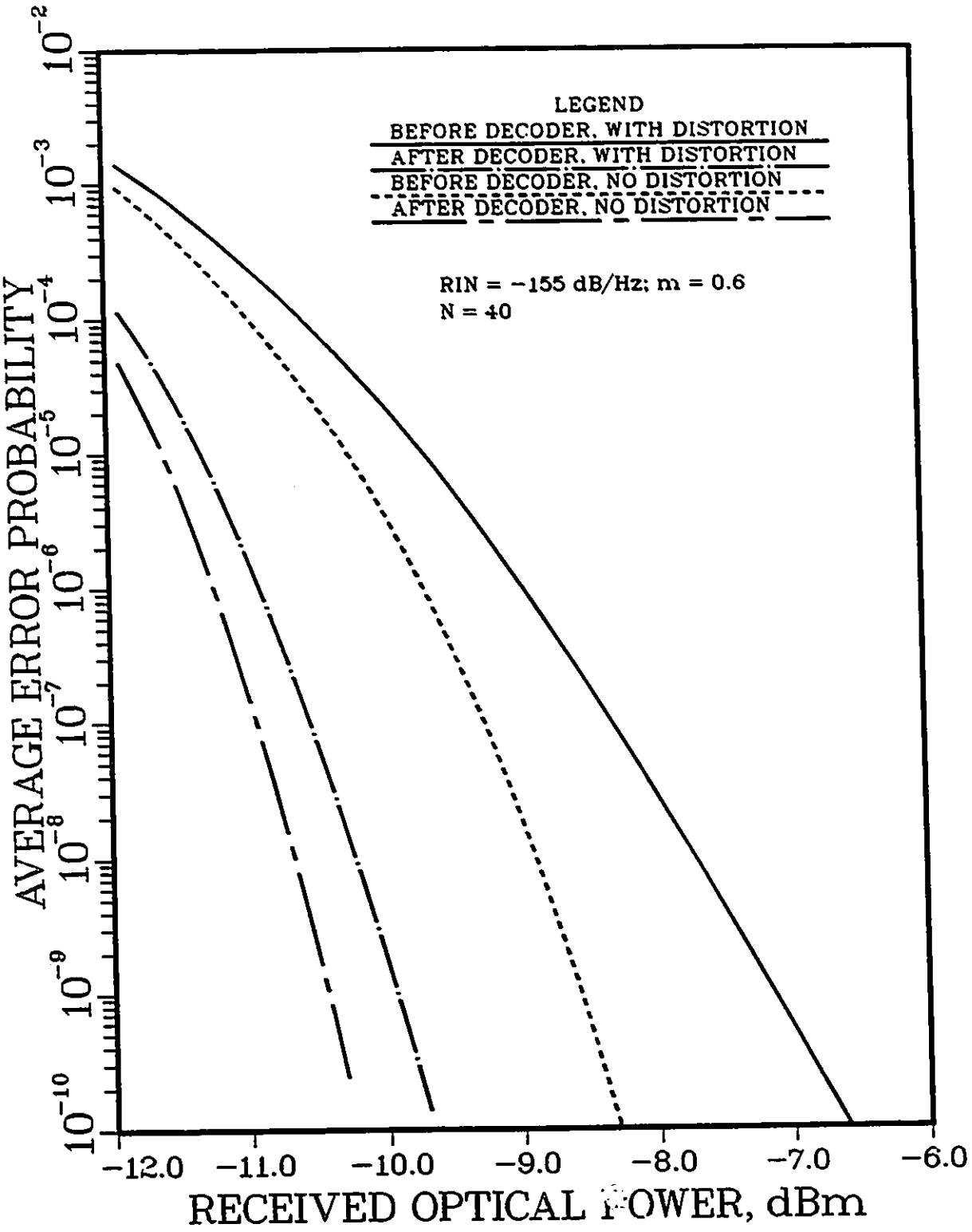

Figure 5.8: Error probability performance versus received optical power for a 40-channel transmission, with or without nonlinearity. RIN = −155 dB/Hz.

Chapter 6

SCM/CD Networks

6.1 Introduction

In this chapter of the thesis, we address SCM/CD systems. We discuss the system topology, the optical and RF modulation methods that can be used, the possible number of users, and several implementation issues.

There has been a limited number of reports on SCM/CD systems in the literature. The topics investigated include completely analog systems [45,46], as well as systems with digitally modulated subcarriers [48]–[50].

In a conventional SCM/DD system, optical intensity modulation (IM) is used. In SCM/CD systems there are some unique problems. Because of the spectral selectivity property in coherent optical detection, the individual channels (subcarriers) must be separated in the optical, as well as in the RF (radio frequency) domains. This can be achieved by appropriate optical modulation, which will create optical sidebands carrying the information. Fig. 6.1 helps to illustrate the principle of creating optical channels by using the sidebands that result from optical modulation. Another way of looking at this process is as a frequency shifting of the optical signal. From communication theory, we know that amplitude modulation (AM) preserves the spectrum of the baseband (modulating) signal. Hence, it would be most suitable to use AM

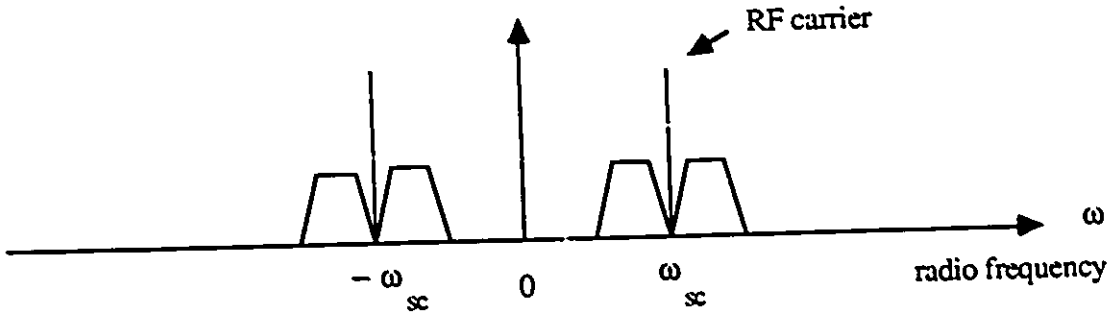

a) Baseband signal spectrum (modulated subcarrier)

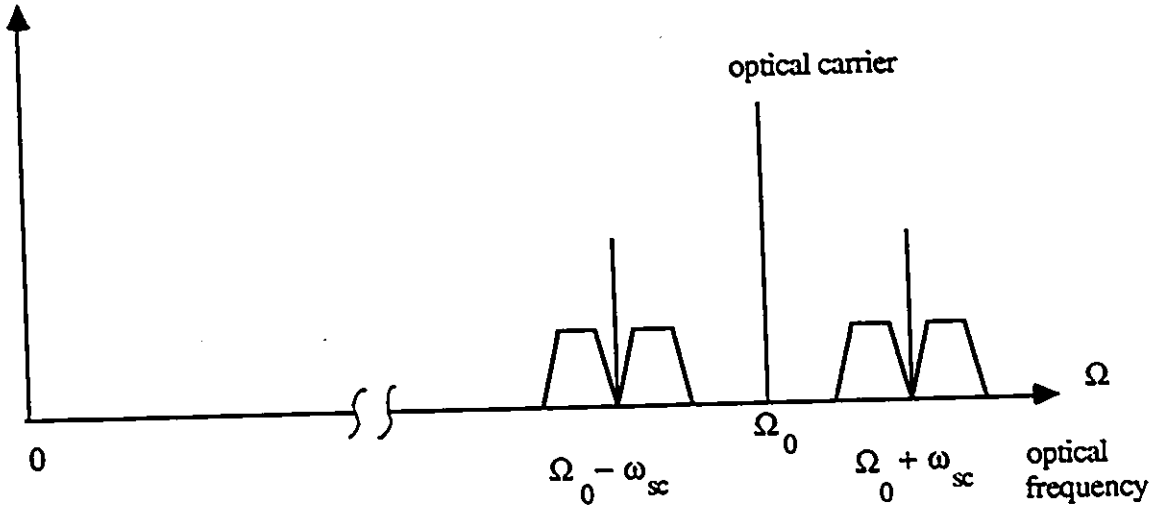

b) Optical spectrum after optical modulation

Figure 6.1: Optical spectrum after modulation with an RF signal (shown above). Nonlinear effects are not considered.

for optical modulation. Unfortunately, to the best of our knowledge, true optical AM has not been demonstrated yet. Therefore, optical IM or angle modulation must be used, in order to achieve "quasi-AM" performance. This is the approach in [48]-[50], where optical PM (phase modulation) is used.

The problem with using the IM or PM is that they are inherently nonlinear, and the associated distortions degrade the system performance. The penalties occurring when using PM are discussed in [48]-[50]. Our intention in this paper is to extend the analysis found in these papers to include the case of optical IM. Distortion penalties due to nonlinearities in the case of DD have been investigated by a number of researchers [34,36,37,77,78],[116], including the use of external modulators [117,118]. In the case of coherent detection, the analysis is quite different, as it will be seen later in this chapter.

Our research has shown that direct IM offers no advantage in terms of linearity, compared to PM. Moreover, modulating the laser injection current causes optical frequency modulation which is unwanted and difficult to suppress. Because of the cited reasons, we are going to discuss only external IM using electro-optic modulators.

There are several possibilities to be considered: multiple subcarriers per laser, or a single subcarrier per laser (for multiple-access networks); single-octave versus multi-octave operation; optical intensity modulation (OIM) versus optical phase modulation (OPM), etc.. For the purpose of clarity, other system degradation factors, such as laser phase and intensity noise, polarization fluctuations, etc., are not considered for the moment.

This chapter is organized as follows. In Section 6.2, the general concepts of multi-carrier (distribution) and multiple-access SCM/CD networks are presented. Section 6.3 addresses the details of the system performance for multi-carrier networks. Section 6.4 deals with multiple-access networks. Section 6.5 gives an estimate of the number of users for each system configuration. The problems of polarization control are discussed in Section 6.6. In Section 6.7, some other general considerations are

presented. Finally, our findings and conclusions are summarized in Section 6.8.

6.2 General System Concepts

Fig. 6.2 illustrates schematically the multi-carrier SCM/CD transmission. In this architecture, N RF subcarriers modulated by analog and/or digital signals, are combined together and used to modulate an optical carrier by means of an external electro-optic modulator. Note that the optical modulation is always analog in this case (because the modulating signal is an RF waveform), whereas this is not necessarily so for the RF one. At the receiver end, the incoming optical signal and the light from a local laser oscillator are mixed on the surface of a photodiode. Hence, the optical signal is down converted to the RF/microwave domain, where the individual subcarriers can be selected using conventional radio techniques. Such a system uses only one laser to transmit many channels, and it can offer significant savings when compared to the systems that use a separate laser for each channel. Such a system will typically be used for distribution of services.

Next, we present a multiple-access photonic network that combines both subcarrier multiplexing and coherent optical detection. Fig. 6.3 illustrates the idea. M network users are connected by a passive $M \times M$ star coupler. All users transmit at the same single optical wavelength. There is only one tunable RF subcarrier per user. At the receiver, a subcarrier can be selected by tuning either the local laser, or by tuning an RF oscillator. This way, a communication channel can be established between any two users in the network. A similar concept was proposed by Darcie in [39], the difference being that in [39] direct detection was assumed. A major limitation on the number of users in [39] is the excess shot noise produced by the optical power coming from all users, including unwanted ones. In our SCM/CD system, this limitation is overcome, since in coherent systems the major source of shot noise is the local laser. The effect of the excess shot noise is quite small [75].

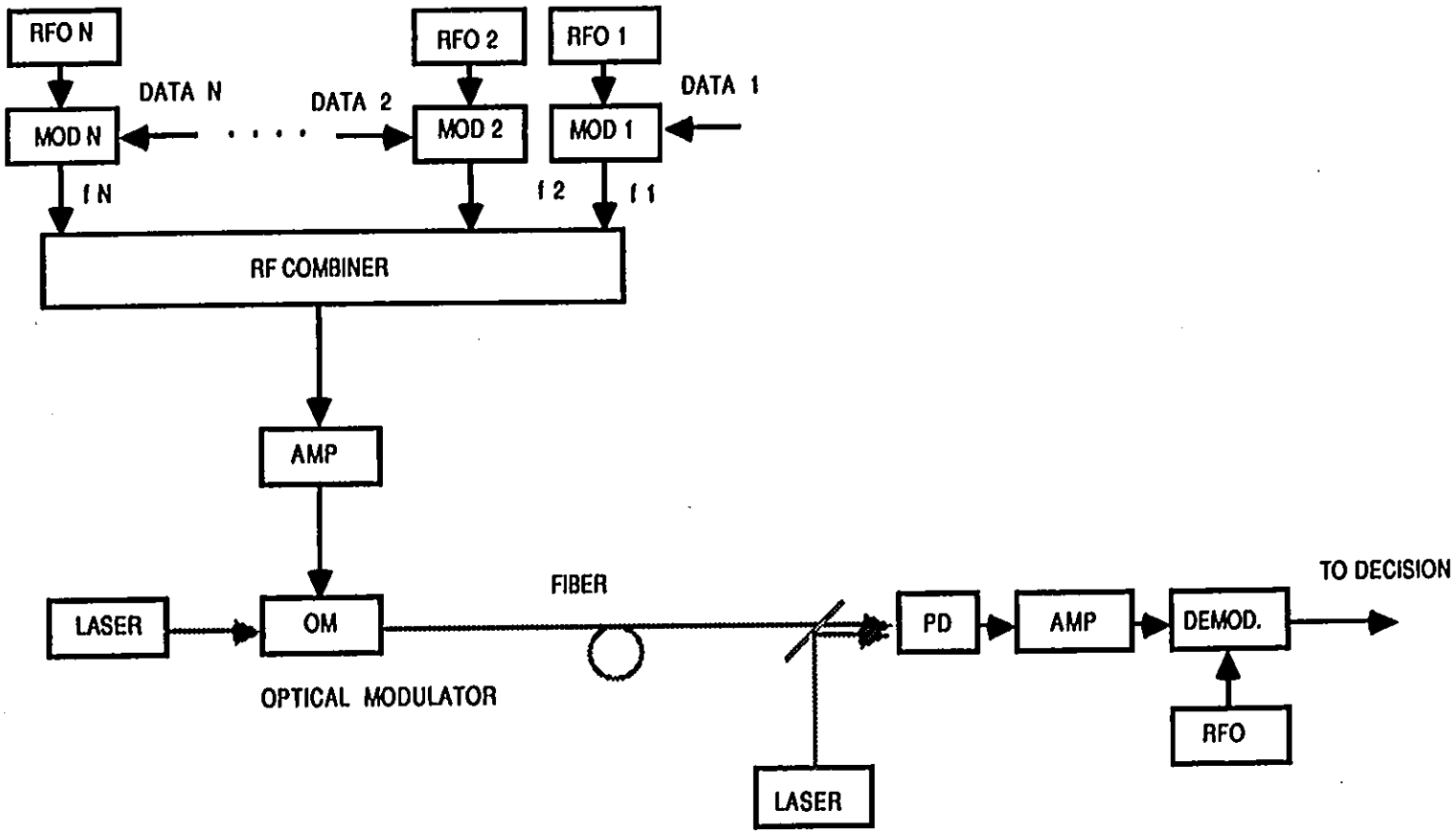

Figure 6.2: Schematic diagram of an SCM/CD system.

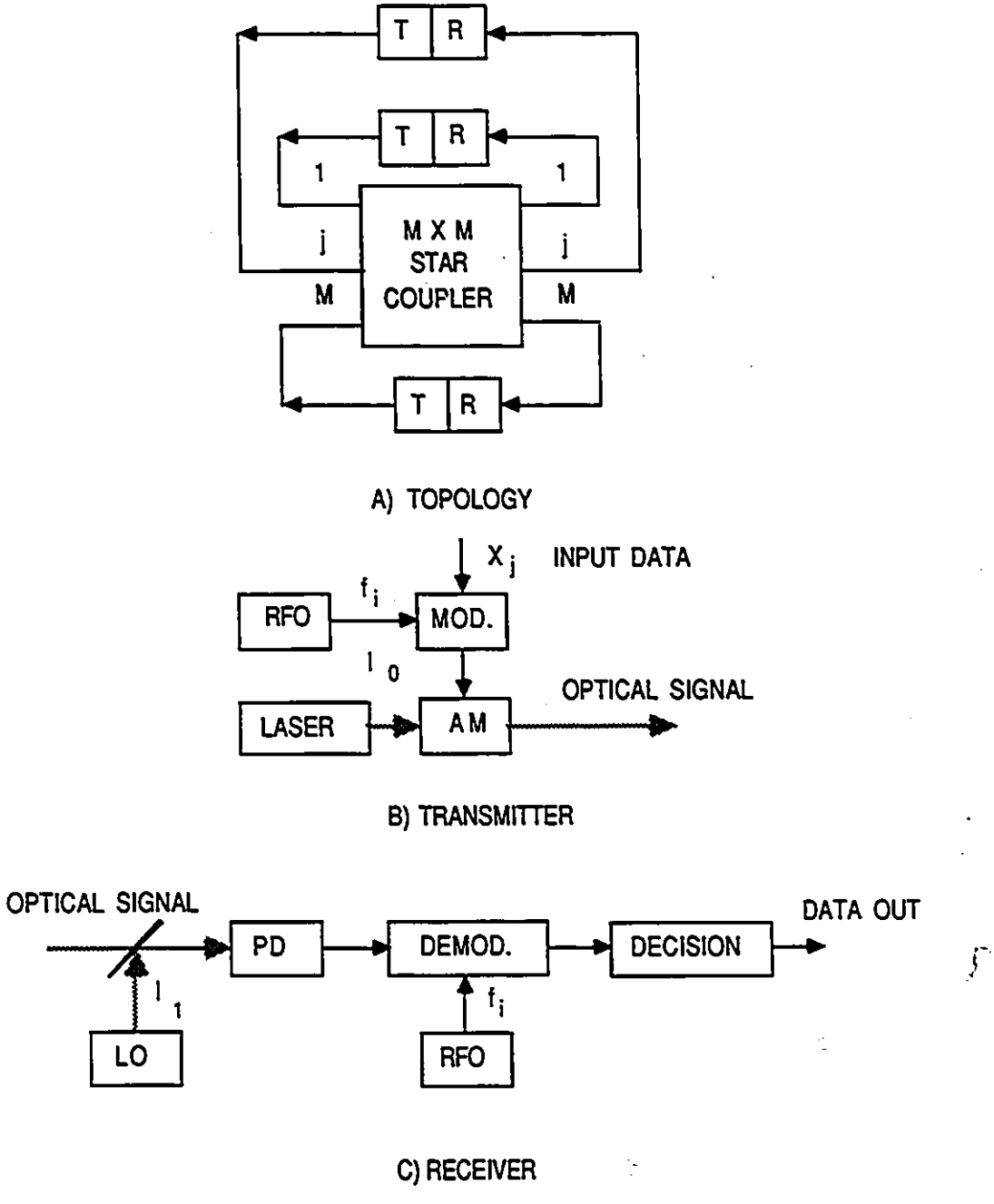

Figure 6.3: Diagram of an SCM/CD multiple-access network.

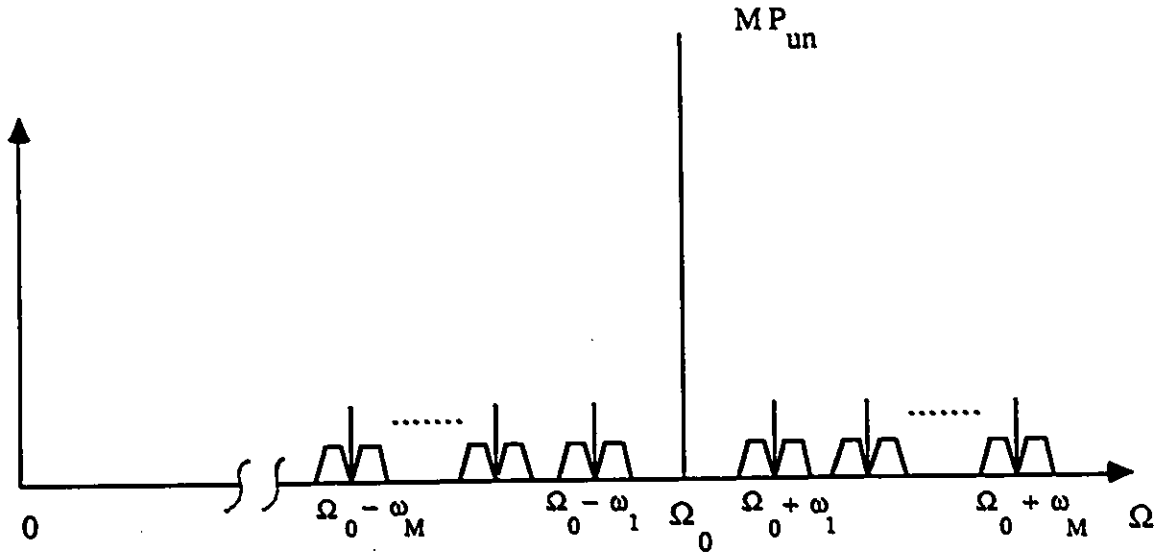

Figure 6.4: Single-sided spectrum of the combined optical signals from all users.

The spectrum of the combined optical signals from all users looks like Fig. 6.4. There is a strong component at Ω_0 (the lasing frequency in CW mode) due to the sum of all unmodulated optical carriers. The power left in the unmodulated carriers depends on the type of modulation and the optical modulation index. One can see that the individual channels remain spectrally separated in the optical domain. After the mixing with the LO light, the spectrum will be shifted down again to the RF domain, where the desired channel can be selected using RF techniques.

In the case of SCM/DD networks, the wavelength of operation of the individual transmitting lasers is relatively unimportant within a broad range of optical frequencies. In the proposed SCM/CD network this is a crucial issue. As mentioned in Chapter 3, absolute laser frequency stabilization has always been a difficult problem. Fortunately, several solutions are available that are suitable for our particular case.

The first possible alternative is to distribute to all users a stable optical reference coming from a centrally-located, powerful, narrow-linewidth laser source. The local lasers can be locked to this reference. Even if the reference optical frequency drifts, all

local lasers will drift accordingly, thus preserving the spacing between the channels. In the case of two different wavelengths λ_0 and λ_1, for the transmitting laser and for the LO respectively, there are techniques [22,23] to tune and lock another laser to a wavelength that is at a specified spectral distance from the reference one.

Another possible approach does not use a distribution of an optical reference. Instead, atomic or molecular absorption spectra are used as an absolute reference at each user location. There have been reports of a successful implementation of this technique [119].

Yet another possibility is to use Zeeman lasers which can be tuned to a desired wavelength without an external reference [120].

In all three cases the implementation is greatly facilitated by the fact that wide-range high-speed tunability is not required from the lasers when the network is operated as a stand-alone, i.e., not a part of an optical FDM system.

The performance of the proposed system is inferior to that of coherent FDM systems with tunable lasers, because a significant part of the optical power is "lost" in the unmodulated carrier which does not carry information (as mentioned before, the information resides in the sidebands). The number of channels will also be smaller. However, it can offer an intermediate step between operation on a single wavelength and a full FDM system. The frequency registration problem in coherent FDM systems has not been completely solved yet. The proposed SCM/CD system can provide many independent channels on a single wavelength. The concept can be extended to users transmitting on several wavelengths in a WDM (wavelength-division multiplexing) system, however, more sophisticated interconnect protocols are needed. As mentioned before, the SCM/CD system outperforms the SCM/DD significantly, as will be shown later in this chapter.

6.3 Multi-carrier Networks

In a way similar to [50], the carrier-to-noise ratio (CNR) for one modulated subcarrier filtered out at the receiver can be expressed in terms of the mean square (MS) value of the current components at the output of the photodiode:

$$\text{CNR} = \frac{AR^2 P_{LO} P_s m_e^2}{\sigma_{sh}^2 + \sigma_{th}^2 + \sigma_{2d}^2 + \sigma_{3d}^2} \tag{6.1}$$

where:

R — photodiode responsivity,

P_{LO} — local laser oscillator power,

P_s — average received signal power,

m_e — effective optical AM index,

σ_{sh}^2 — shot noise power,

σ_{th}^2 — thermal noise power,

σ_{2d}^2 — second-order distortion power,

σ_{3d}^2 — third-order distortion power,

A — constant.

Also,

$$\sigma_{th}^2 = \frac{4kT^\circ FB}{R_L} \tag{6.2}$$

where:

k — Boltzmann's constant,

T° — absolute temperature (290 °K),

B — receiver noise bandwidth,

F — amplifier noise figure,

R_L — photodiode load resistance (50 Ω),

and:

$$\sigma_{sh}^2 = 2eRP_{LO}B \tag{6.3}$$

where:

e — electron charge,

P_{LO} — local laser power.

The values of m_e, σ_{2d}^2, and σ_{3d}^2 remain to be determined for each particular case. All noise sources, including the distortion terms, are assumed to be Gaussian. This assumption is reasonable, except for a few cases that will be specified subsequently. We assume that the adjacent-channel crosstalk is negligible.

The receiver photo-current can be expressed as:

$$i(t) = R\left\{P_{LO} + P_s(t) + 2\sqrt{P_{LO}P_s(t)}\cos[(\Omega_c - \Omega_{LO})t + \phi(t)]\right\} + \eta(t) \qquad (6.4)$$

where:

Ω_c — optical carrier angular frequency,

Ω_{LO} — local laser oscillator angular frequency,

$\phi(t)$ — optical angle modulation,

$\eta(t)$ — additive noise.

In the OPM case, P_s is not a function of time, whereas with OIM $\phi(t)$ does not carry any information, i.e., it represents phase noise which can be neglected under the assumptions in the introduction.

For the optical PM we have:

$$\phi(t) = \sum_{j=1}^{N} \beta_j \cos[\omega_j t + x_j(t)] \qquad (6.5)$$

where β_j is the individual phase modulation index of the j-th subcarrier. Throughout the paper, we assume that the individual subcarriers use narrow-band FSK (frequency shift keying) modulation format, as in [50]. Therefore, for the j-th subcarrier:

$$x_j(t) = 2\pi f_d \int_{-\infty}^{t} \sum_i a_i g(\tau - jT)d\tau \qquad (6.6)$$

where:

f_d — peak frequency deviation,

a_i — binary information,

$g(t)$ — rectangular pulse, and

T — bit period.

We assume that all subcarriers have the same β_j and f_d. Ignoring the DC terms in (6.4), which do not carry useful information, we can write [50,121]:

$$i_{PM}(t) = 2R\sqrt{P_{LO}P_s}\sum_{n_1=-\infty}^{+\infty}\cdots\sum_{n_N=-\infty}^{+\infty}J_{n_1}(\beta)\cdots J_{n_N}(\beta)\cos\{(\Omega_c-\Omega_{LO})t+ n_1[\omega_1 t+x_1(t)]+\cdots+n_N[\omega_N t+x_N(t)]\}+\eta(t) \quad (6.7)$$

where J_n denotes a Bessel function of the first kind of order n. Another assumption to be made is that the optical detection is heterodyne, i.e., only one of the optical sidebands is used. From (6.7), we can express:

$$m_{cPM} = J_1(\beta)[J_0(\beta)]^{N-1} \quad (6.8)$$

For β small, $m_c \approx \beta/2$. For σ_{2d}^2 and σ_{3d}^2 we have:

$$\sigma_{2d}^2 = 2h_2K_2R^2P_sP_{LO}J_1^4(\beta)[J_0(\beta)]^{2N-4} \quad (6.9)$$

$$\sigma_{3d}^2 = 2h_3K_3R^2P_sP_{LO}J_1^6(\beta)[J_0(\beta)]^{2N-6} \quad (6.10)$$

where:

K_2 — number of second-order intermodulation products (IMPs),

K_3 — number of third-order IMPs,

h_2 and h_3 — coefficients that take into account the spectral form of the IMPs and the receiver filtering [50], i.e., the spectral overlap between the useful channels and the interference.

For more details see Appendix A. The procedure for calculating K_2 and K_3 is given in [116,122], and in Appendix A. Finally, $A_{PM} = 2.0$.

The second modulation method to be considered is external electro-optic IM. The driving-voltage-to-light intensity relationship is given (e.g., see [43,123]) by:

$$P_o = P_i\sin^2\left(\frac{\pi}{2}\times\frac{V}{V_\pi}\right) \quad (6.11)$$

where:

P_o — output light intensity,

P_i — input intensity,

V — driving voltage, and

V_π — voltage that causes a phase shift of π of the light passing through the material.

This equation applies to intensity modulators that use a phase modulator and a polarizer/analyzer pair. For the Mach-Zehnder interferometric modulators, the relationship (6.11) is given by "$\cos^2$" which is essentially the same nonlinearity and the treatment for it is similar. The received optical power can be expressed as:

$$P_s(t) = P_m \sin^2 \left[\frac{\alpha\pi}{4} + \frac{\pi}{2} \times \frac{V_m}{V_\pi} y(t)\right] \tag{6.12}$$

where:

P_m — hypothetical maximum received optical power (i.e., the power that would be received if the modulator output were set to a maximum),

α — coefficient which determines the bias of the modulator,

V_m — voltage amplitude of each subcarrier (all assumed to have equal V_m values), and

$y(t)$ — sum of N modulated subcarriers with unit amplitude:

$$y(t) = \sum_{j=1}^{N} \cos[\omega_j t + x_j(t)] \tag{6.13}$$

The RMS (root-mean-square) amplitude of the optical field is:

$$\sqrt{P_s(t)} = A(t) = \sqrt{P_m} \sin \left[\frac{\alpha\pi}{4} + \frac{\pi}{2} \times \frac{V_m}{V_\pi} y(t)\right] \tag{6.14}$$

The voltage-intensity curve is shown in Fig. 6.5a, and the voltage-amplitude curve is shown in Fig. 6.5b. In SCM/DD systems, the modulator is usually biased at the inflection point of the voltage-intensity curve, which eliminates the second-order distortions. The voltage-amplitude curve, however, does not have an inflection point.

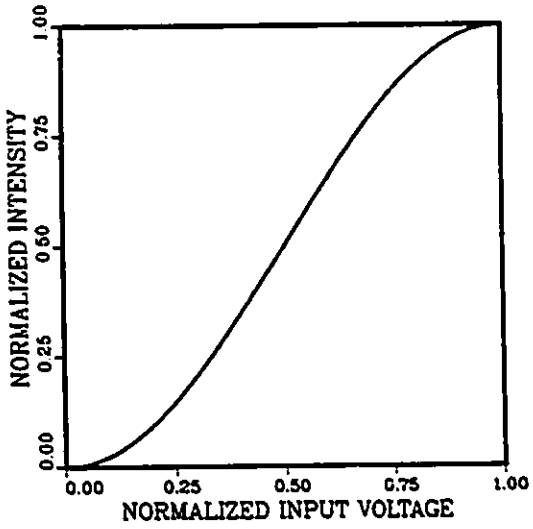

a)

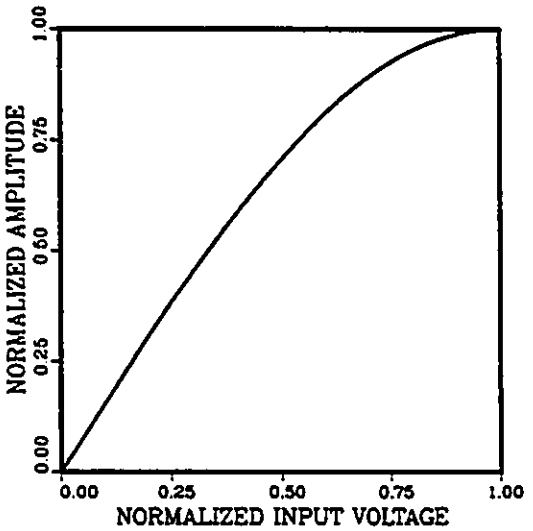

b)

Figure 6.5: a) Light intensity, and b) Light field amplitude versus applied voltage for an electro-optic intensity modulator.

As seen from Fig. 6.5b, the linear zone is at lower bias voltages. But reducing the bias voltage restricts the dynamic range (or the total modulation depth) of the system. Therefore, the modulator bias is a crucial parameter in SCM/CD systems using intensity modulation, and needs optimization.

After power series expansion, (6.14) becomes:

$$A(t) = \sqrt{P_m}\left\{\sin\left(\frac{\alpha\pi}{4}\right) + m_{eI}y(t)\cos\left(\frac{\alpha\pi}{4}\right) - \frac{1}{2!}[m_{eI}y(t)]^2\sin\left(\frac{\alpha\pi}{4}\right) + \frac{1}{3!}[m_{eI}x(t)]^3\cos\left(\frac{\alpha\pi}{4}\right) + \cdots\right\} \tag{6.15}$$

where:

$$m_{eI} = \frac{\pi}{2} \times \frac{V_m}{V_\pi} \tag{6.16}$$

The terms in (6.15) of order higher than 3 are ignored, as insignificant. From (6.4) and (6.15), the receiver photocurrent becomes:

$$i_{IM}(t) = RP_s(t) + \sqrt{P_{LO}P_m}\left\{\sin\left(\frac{\alpha\pi}{4}\right) + m_{eI}y(t)\cos\left(\frac{\alpha\pi}{4}\right) - \frac{1}{2!}[m_{eI}y(t)]^2\sin\left(\frac{\alpha\pi}{4}\right) + \frac{1}{3!}[m_{eI}x(t)]^3\cos\left(\frac{\alpha\pi}{4}\right) + \cdots\right\} \times \cos[(\Omega_c - \Omega_{LO})t] + \eta(t) \tag{6.17}$$

Nonlinearity of the polynomial type as in (6.15) has been analyzed in [116,122,124] and is discussed in Appendix A. As shown in Appendix B, the second-order IMPs power is determined as:

$$\sigma_{I2d}^2 = \frac{1}{8}h_2K_2R^2P_mP_{LO}\sin^2\left(\frac{\alpha\pi}{4}\right)m_{eI}^4 \tag{6.18}$$

Similarly, for the third order IMPs, the power is expressed as:

$$\sigma_{I3d}^2 = \frac{1}{32}h_3K_3R^2P_mP_{LO}\cos^2\left(\frac{\alpha\pi}{4}\right)m_{eI}^6 \tag{6.19}$$

The average received optical power is:

$$P_{sIM} = P_m\sin^2\left(\frac{\alpha\pi}{4}\right) \tag{6.20}$$

Finally, also from Appendix B:

$$A_{IM} = \frac{1}{2}\cos^2\left(\frac{\alpha\pi}{4}\right). \tag{6.21}$$

Two additional problems exist when using intensity modulation. First, there is the direct detection term $RP_s(t)$ (e.g., see (6.17)) which can fall within the passband of certain channels. In most practical cases, however, it will be 20 to 30 dB below the coherent detection term. Moreover, with careful intermediate frequency selection, one can adjust this interference to fall within the guardband between subcarriers. The second problem is the fact that m_{cI} is restricted not only by distortion considerations, but should not exceed the limits for proper IM. The condition is:

$$V_m < \frac{\alpha V_\pi}{2\sqrt{N}} \qquad \text{or} \qquad m_{cI} < \frac{\alpha\pi}{4\sqrt{N}} \tag{6.22}$$

In order to be specific, in our analysis we assume certain system parameters. The IMPs power depends on the frequency allocation plan for the subcarriers, the optical and the RF modulation formats, and the number of channels. The main system parameters used in all subsequent calculations are: FSK index $D = 2f_dT = 0.75$, bit rate per channel = 100 Mb/s, channel spacing = 200 MHz, receiver bandwidth = 120 MHz, receiver noise figure = 3.8 dB, local laser oscillator power P_{LO} = 0 dBm, wavelength of operation = 1.3 μm. The subcarriers are situated at odd multiples of 100 MHz (e.g., 2.1, 2.3, 2.5, ... etc. GHz). The reason for this is to minimize the effect of the second-order IMPs [50].

6.3.1 Multi-Octave Operation

In the case of multi-octave (MO) operation (i.e., when the bandwidth allocated to the subcarriers starts from frequency f_1 and extend beyond frequency $2f_1$; for more information see Appendix A), the worst channel is the first one, where second-order IMPs dominate the distortion penalty. The best channel is the middle one, with only third-order IMPs. When using PM, the difference in CNR (or receiver sensitivity)

N	20	40
K_2, ch. 1 (worst)	19	39
K_3, middle ch.	126	551
K_3, ch. 1	81	361

Table 6.1: Number of intermodulation products.

between the best and the worst channel can be several dBs [50]. Here, we show that by using the option of variable bias, we can make the IM-based system more linear and thus improve the system performance.

We find that the receiver sensitivity is a more useful measure of performance than the CNR, because it provides a better way to optimize the system performance when maximum transmission distance is required. If the CNR is kept constant, (6.1) can be solved for P_s (or P_m). For the OPM case, we have:

$$P_s = \frac{\sigma_t^2 + \sigma_{sh}^2}{2R^2 P_{LO}\{(m_{cPM}^2/CNR) - K_2 h_2 m_{cPM}^4 - K_3 h_3 m_{cPM}^6\}} \tag{6.23}$$

Similarly, for the OIM case we obtain:

$$P_m = \frac{\sigma_t^2 + \sigma_{sh}^2}{R^2 P_{LO}\left[\frac{m_{cI}^2 \cos^2\left(\frac{\alpha\pi}{4}\right)}{CNR} - \frac{K_2 h_2 \sin^2\left(\frac{\alpha\pi}{4}\right) m_{cI}^4}{8} - \frac{K_3 h_3 \cos^2\left(\frac{\alpha\pi}{4}\right) m_{cI}^6}{32}\right]} \tag{6.24}$$

Fig. 6.6 shows the receiver sensitivity in the case of optical IM as a function of m_{cI} for the first (worst) and the middle (best) channels, for different values of α. The CNR is assumed fixed at 18 dB (which is enough to achieve 10^{-9} bit-error rate, given the Gaussian nature of all the sources of disturbance in this work), $N = 20$, $h_2 = 0.24$, and the values for K_2 and K_3 can be found in Table 6.1.

Reducing α improves the performance of both channels considerably, particularly channel No. 1. For $\alpha = 0.6$, both channels have the same sensitivity within 1 dB difference. One can show that $\alpha = 0.6$ is optimum for this particular system. Further reduction of α will be counterproductive, because m_{cI} will also decrease, and the thermal noise will dominate.

Fig. 6.7 shows a direct comparison between PM and external IM. For fair com-

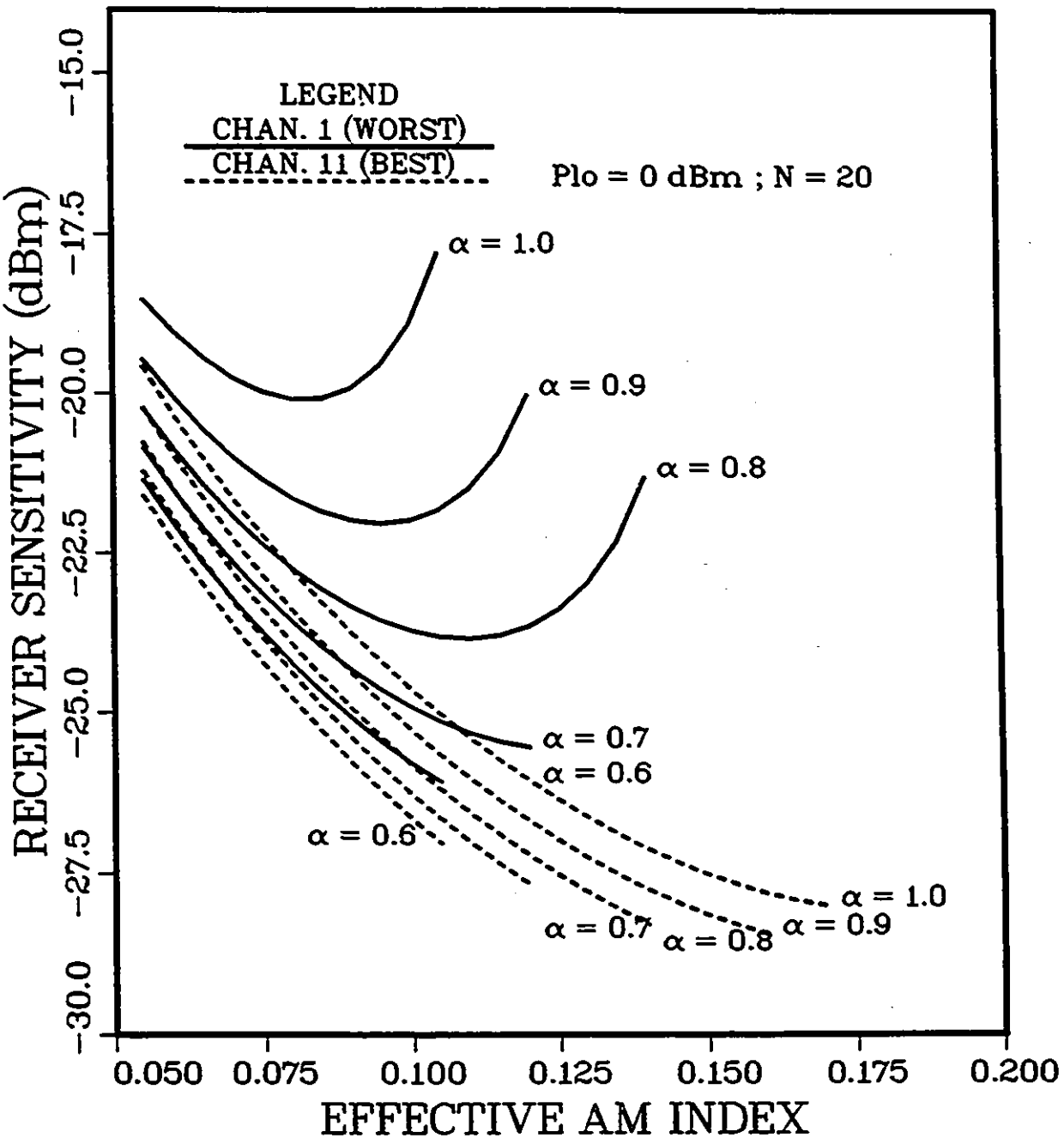

Figure 6.6: Best and worst channel sensitivity as a function of m_{eI} for the OIM format and several values of α. Multi-octave operation, $N = 20$.

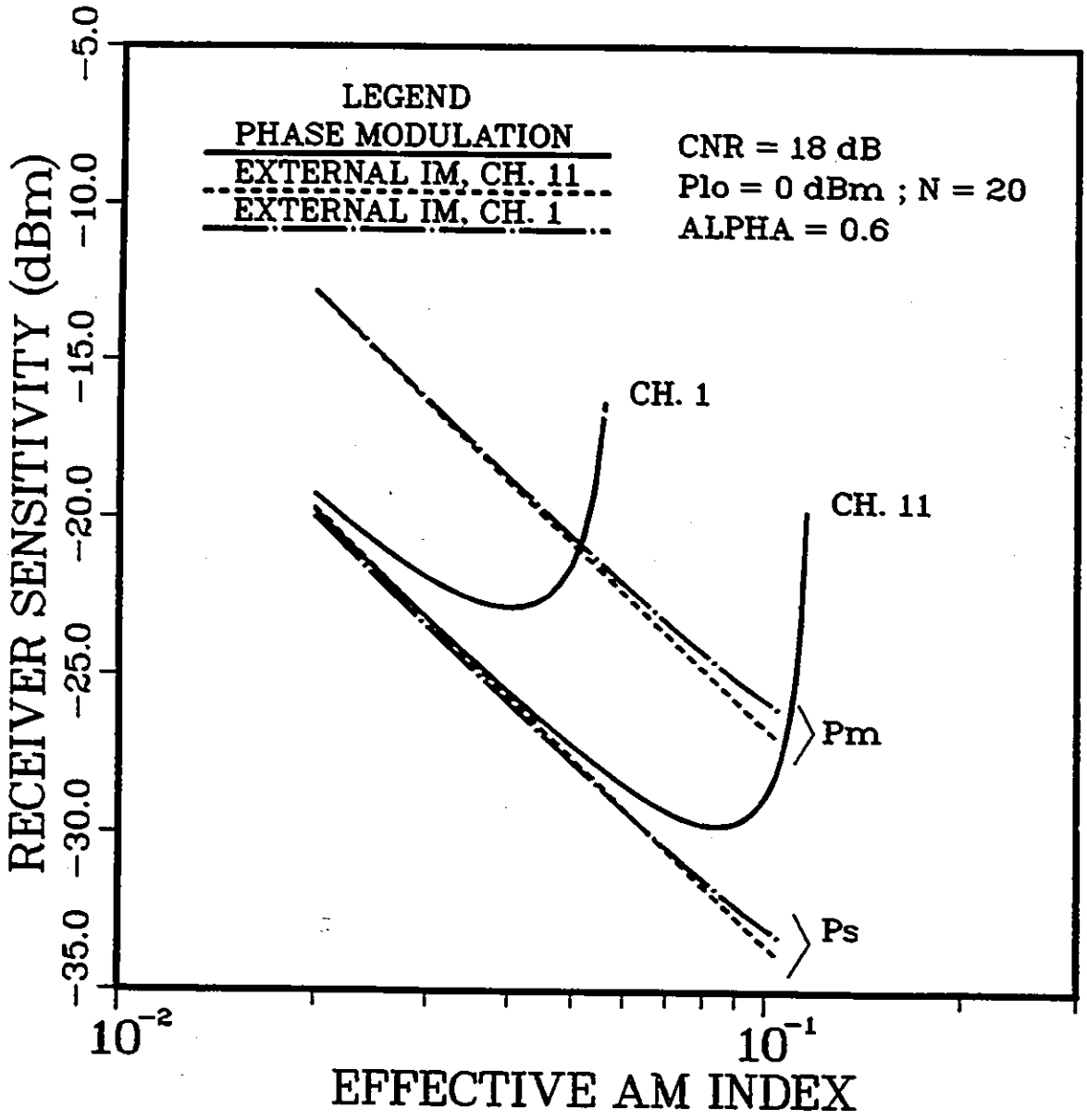

Figure 6.7: Comparison between OIM and OPM receiver sensitivity in multi-octave operation for $N = 20$.

parison, P_m should be used as received optical power when calculating the receiver sensitivity in the IM case. Both P_{sIM} and P_m are shown. The sensitivity when using IM falls in between the best and the worst channel for PM. The overall performance of the IM system, determined by the worst channel, will be better.

As the number of channels increases, the performance of both modulation schemes will remain generally the same, relative to each other. We have verified this numerically for $N = 40$. The results are shown in Fig. 6.8.

6.3.2 Single-Octave Operation

In single-octave (SO) mode of operation, second-order IMPs are not present. The CNR degradation is due to third-order IMPs. The worst channel in this case is the middle one. The results for SO operation can be seen from Fig. 6.6, Fig. 6.7, and Fig. 6.8 by considering the middle channel. The number of third-order IMPs is the same for SO or MO mode of operation. One can see that the PM offers better performance than IM in SO mode of operation.

6.3.3 BER Performance

In order to evaluate the BER performance, we need to assume a specific receiver structure. Due to the simplicity of its implementation, and good performance, FSK delay-line demodulator receivers, shown schematically in Fig. 6.9, have gained increasing popularity [39,50,125]. We also chose this receiver model for our analysis. When ignoring the laser phase noise, the expression for the BER is given by [125]:

$$P_b \cong \sqrt{\frac{1+\sin\psi}{(1-\sin\psi)(8\pi\sin\psi)}}\exp[-\rho(1-\sin\psi)] \tag{6.25}$$

where ρ is the signal-to-noise ratio, and:

$$\psi = \frac{\pi(1-D)}{2} \tag{6.26}$$

for $0 < D < 1$. Using (6.25) and the formulas for the CNR, the BER can be calculated. Fig. 6.10 shows plots of P_b as a function of the received optical power for the OIM

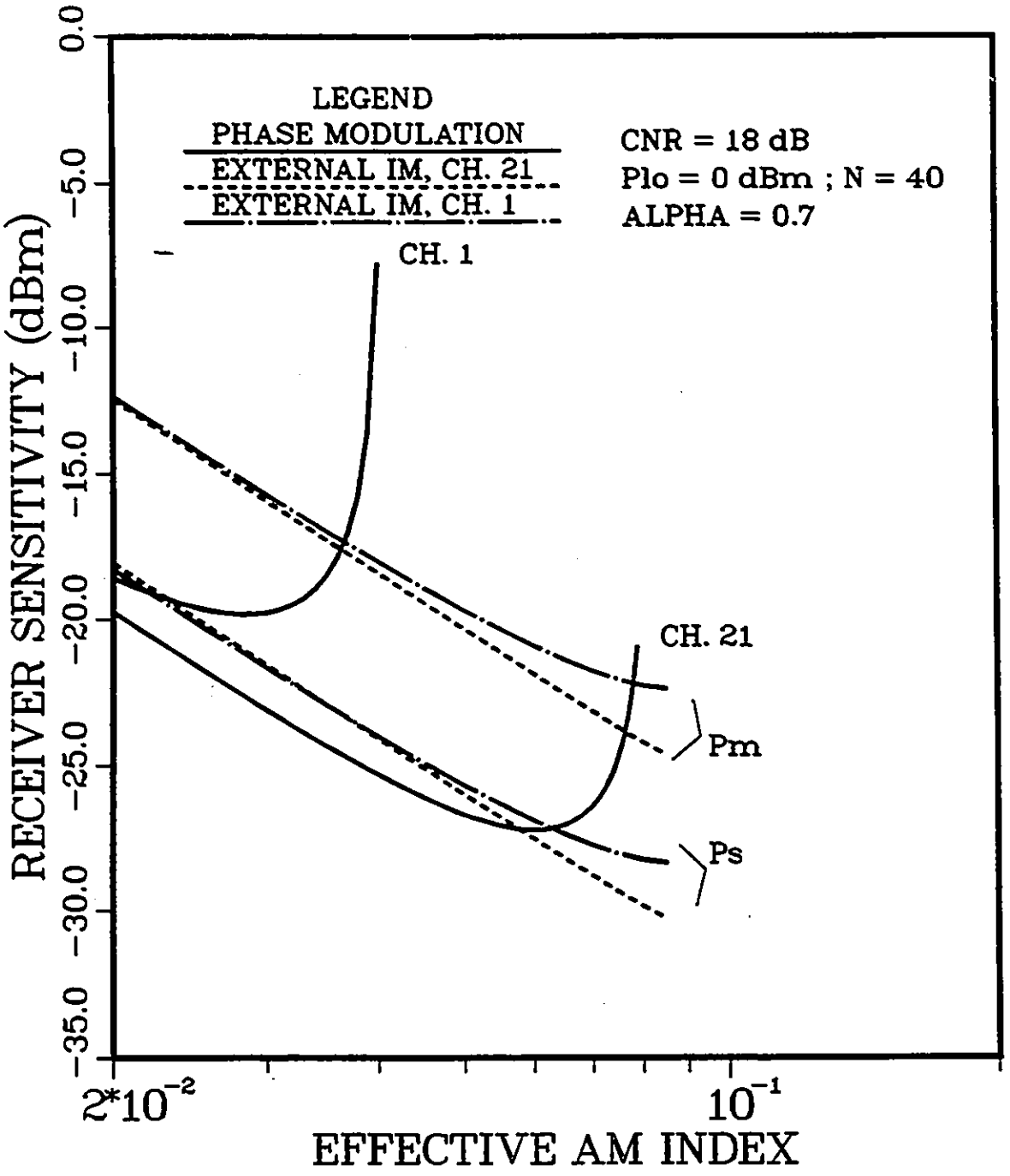

Figure 6.8: Comparison between OIM and OPM receiver sensitivity in multi-octave operation for $N = 40$.

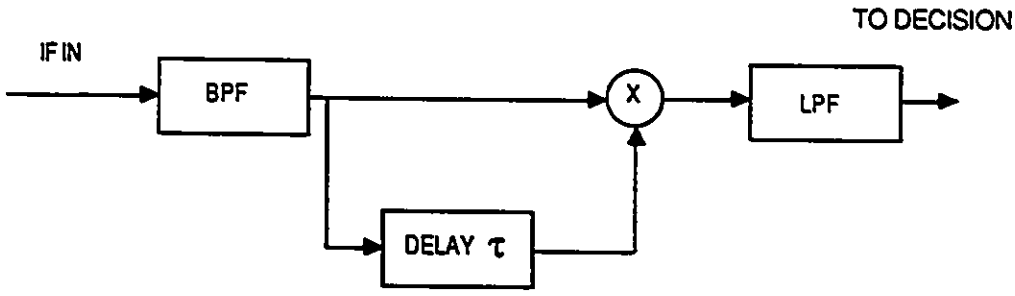

Figure 6.9: Schematic diagram of an FSK receiver with delay demodulation.

and OPM for $N = 20$ in multi-octave operation mode. The points are experimental data from [50]. The parameters used for the theoretical calculations for PM are the same as in [50]. The theoretical and experimental results for OPM are in a very good agreement.

The effective AM index and the bias α for the OIM case are selected to be the optimum ones, as indicated by Fig. 6.6 ($m_{eI} = 0.1, \alpha = 0.6$). The overall performance (i.e., the worst channel case) of IM is superior to PM. Here we can show a possibility to improve somewhat on the performance of the PM case. In [50], the optimum OPM index β is selected under the assumption of -30 dBm received optical power and a maximized CNR. It is found that β should be 0.13. This approach does not give the maximum achievable receiver sensitivity. When using the plots of receiver sensitivity versus m_e (Fig. 6.7), we find that $\beta_{opt} = 0.05$. Fig. 6.11 shows plots of BER for this value of β. The performance of channel one (worst) of the OPM case is slightly better, but the OIM still retains its superiority.

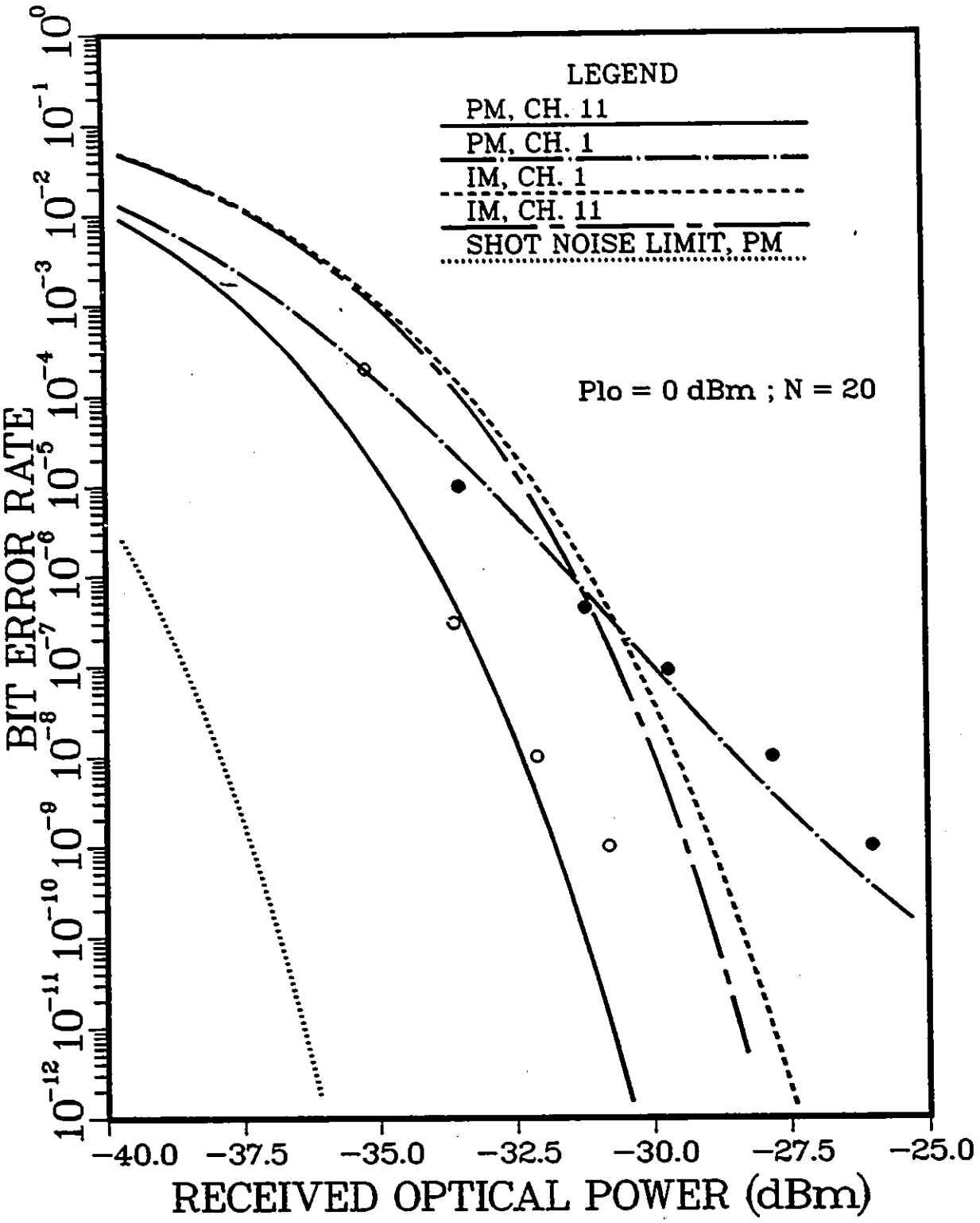

Figure 6.10: Bit error rate curves as a function of received optical power for OIM and OPM cases, multi-octave operation, $N = 20$, $\alpha = 0.6$, $m_{eI} = 0.1$, $m_{ePM} = 0.13$. The data points are experimental results from [50]:• — OPM, channel 1 (worst); ∘ — OPM, channel 11 (best).

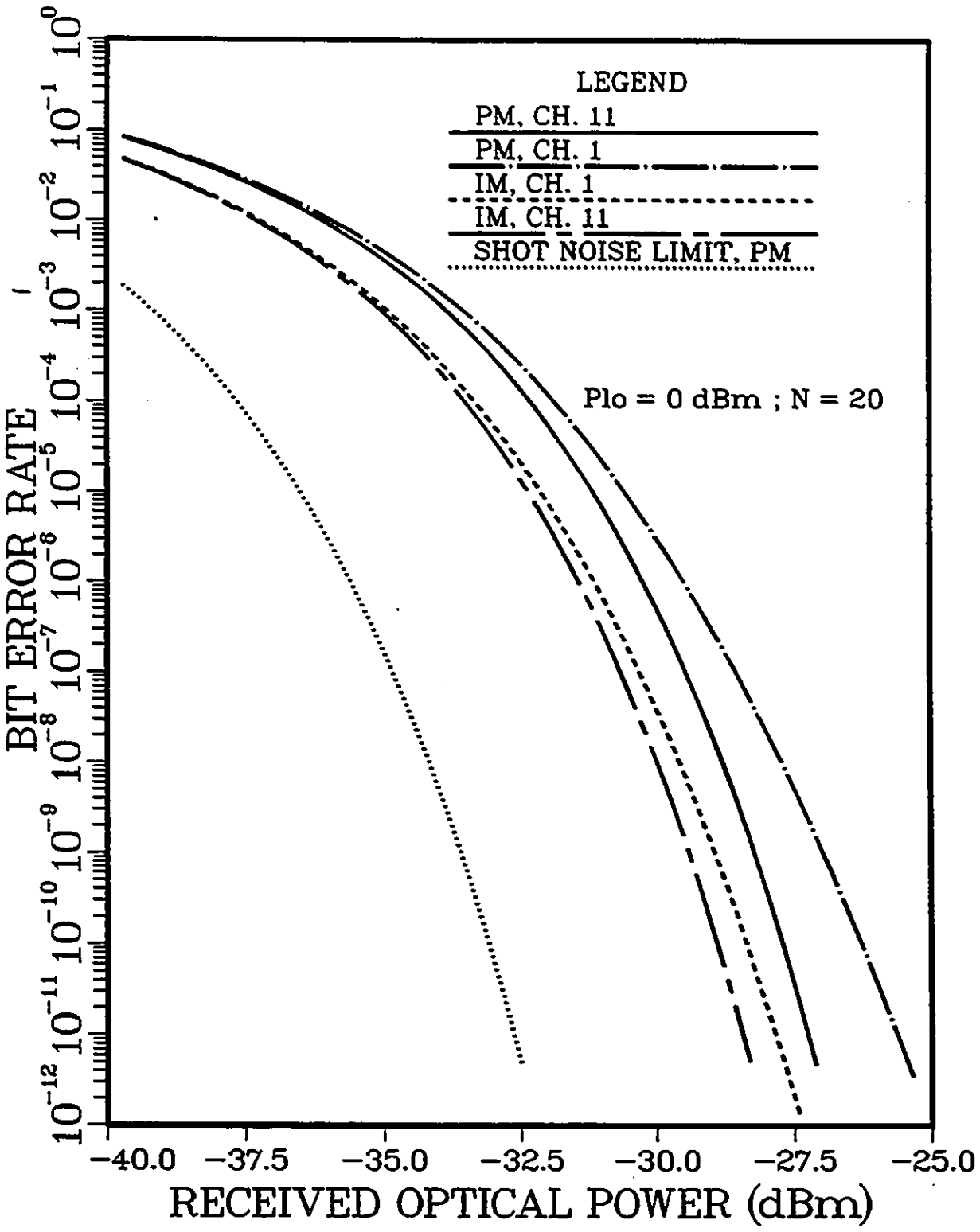

Figure 6.11: Bit error rate curves as a function of received optical power for OIM and OPM cases, multi-octave operation, $N = 20$, $\alpha = 0.6$, $m_{cI} = 0.1$, $m_{cPM} = 0.05$.

6.4 Multiple-Access Systems

Since in this scheme there is a pair of sidebands created by one subcarrier per transmitter, the nonlinearity problem is considerably less severe. There are no interfering intermodulation products, only harmonics. The amplitude of the harmonics is less than the amplitude of the IMPs, and their number is also much smaller. The receiver sensitivity for any particular channel depends in general on the transmitted power from each user and on the optical power loss between each transmitter and the receiver under consideration. In order to make the problem tractable, we assume that all users transmit with the same average optical power, and that the optical path loss is the same between any two users.

6.4.1 Single-Octave Operation

In single-octave operation, the modulation index is not restricted by any nonlinearity considerations. Hence, in order to maximize the power budget, the maximum achievable effective AM index should be chosen. For the OPM case, as seen from (6.8), the effective AM index is simply $J_1(\beta)$, and its maximum value is ≈ 0.58 for $\beta \approx 1.8$. For the OIM case, the maximum m_c, and the optimum value of α are determined from Fig. 6.12. Note that in Fig. 6.12 the received optical power considered is P_{sIM}. As mentioned before, the total shot noise at the receiver is due to the local laser oscillator and to the optical power received from all network users. The additional shot noise power is dependent on the number of transmitting users at any particular time, and the contribution of each of them. For simplicity, we assume that the excess shot noise power is half of that due to the LO. This is a rather conservative estimate.

Using the parameters assumed above, and the ones assumed in the previous sections, we can determine the receiver sensitivity. For the OIM case, the best sensitivity $P_{sIM} = -46.3$ dBm is obtained for $\alpha = 0.6$ and $m_{cI} = 0.46$. From this and (6.20), we obtain $P_{m|min} = -39$ dBm for the OIM case. Also, $P_{s|min} = -49$ dBm for the OPM

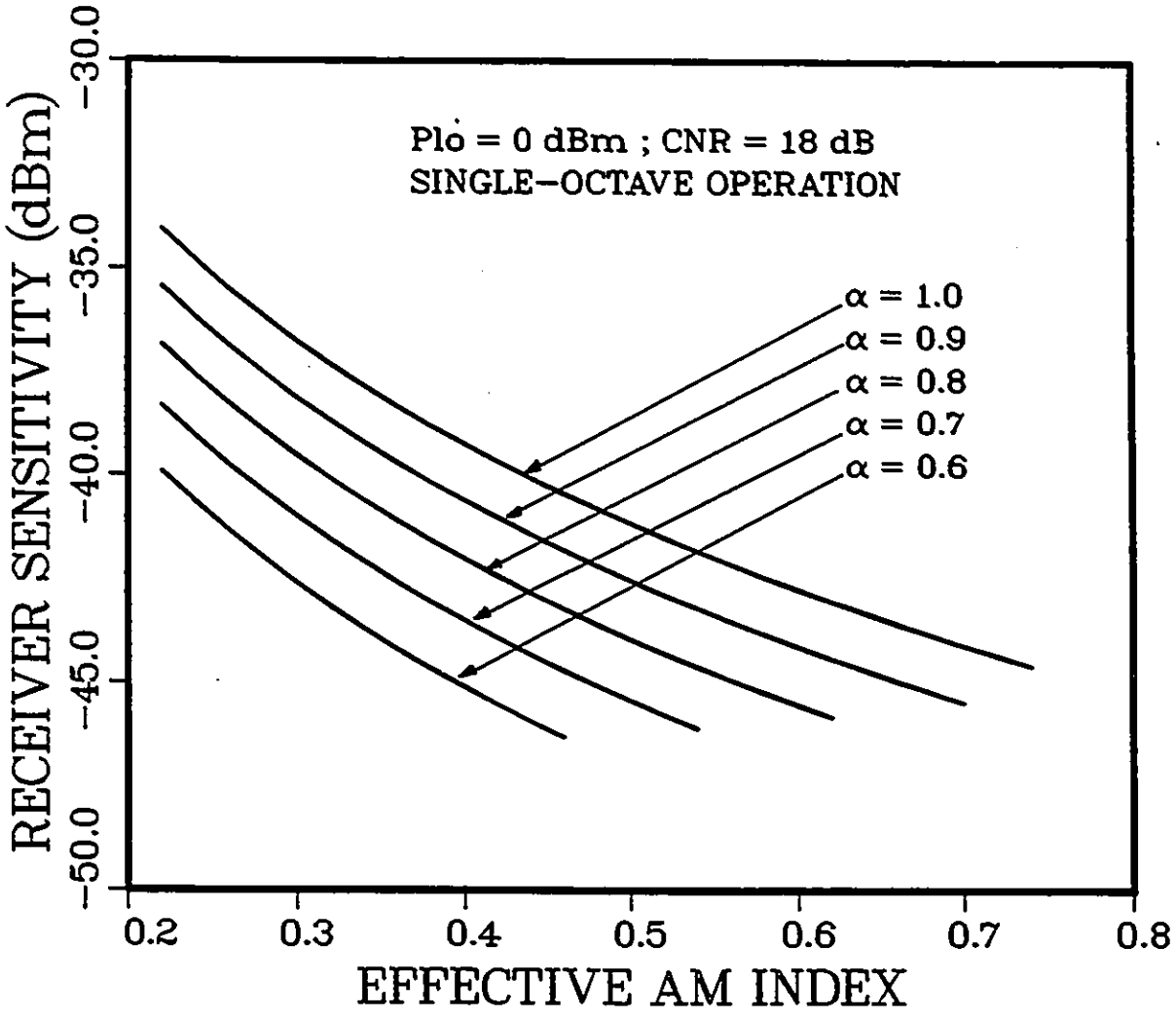

Figure 6.12: Receiver sensitivity versus effective AM modulation index for several values of α. Multiple-access case, single-octave operation.

case. We can see the advantage of PM for multiple-access networks.

6.4.2 Multi-Octave Operation

In multi-octave operation, the channels with the worst CNR are the ones affected by second harmonic interference. The frequency allocation plan assumed previously will ensure that the second-order harmonics (SOH) will fall in the guardband between the channels. The maximum number of SOH is two. For such a small number of interferers, the assumption of Gaussian statistics for the interference power is not accurate. Nevertheless, the Gaussian approximation can still be used, because it gives reasonably good estimates [72], and simplifies the analysis considerably.

By inspection of (6.7), we determine the second-harmonic interference for the PM case:

$$\sigma^2_{2hPM} = 2R^2 P_{LO} P_s K_2 h_2 [J_2(\beta)]^4 \tag{6.27}$$

Using information from Appendix B, for the IM case we have:

$$\sigma^2_{2hIM} = \frac{1}{8} R^2 P_{LO} P_s K_2 h_2 m^4_{cIM} \sin^2\left(\frac{\alpha\pi}{4}\right) \tag{6.28}$$

These values of σ^2_{2h} can be used in the formulas for calculating the CNR and the receiver sensitivity. Note that $K_2 = 2$ and $h_2 = 0.24$.

The same method for finding the optimum bias of the intensity modulator is used once again. All relevant system parameters are the same as before. Fig. 6.13 shows the result: $\alpha_{opt} \cong 0.6$. This value is used for direct comparison with the OPM. Fig. 6.14 shows the receiver sensitivity for the OIM and OPM cases as a function of m_c. The sensitivity for single-octave operation is also shown in the figure for comparison. The results of the comparison are clearly in favor of the OPM. Moreover, the difference in both cases between SO and MO mode of operation is not very pronounced. This is because the nonlinearity is a lesser problem in the case of a single subcarrier per laser.

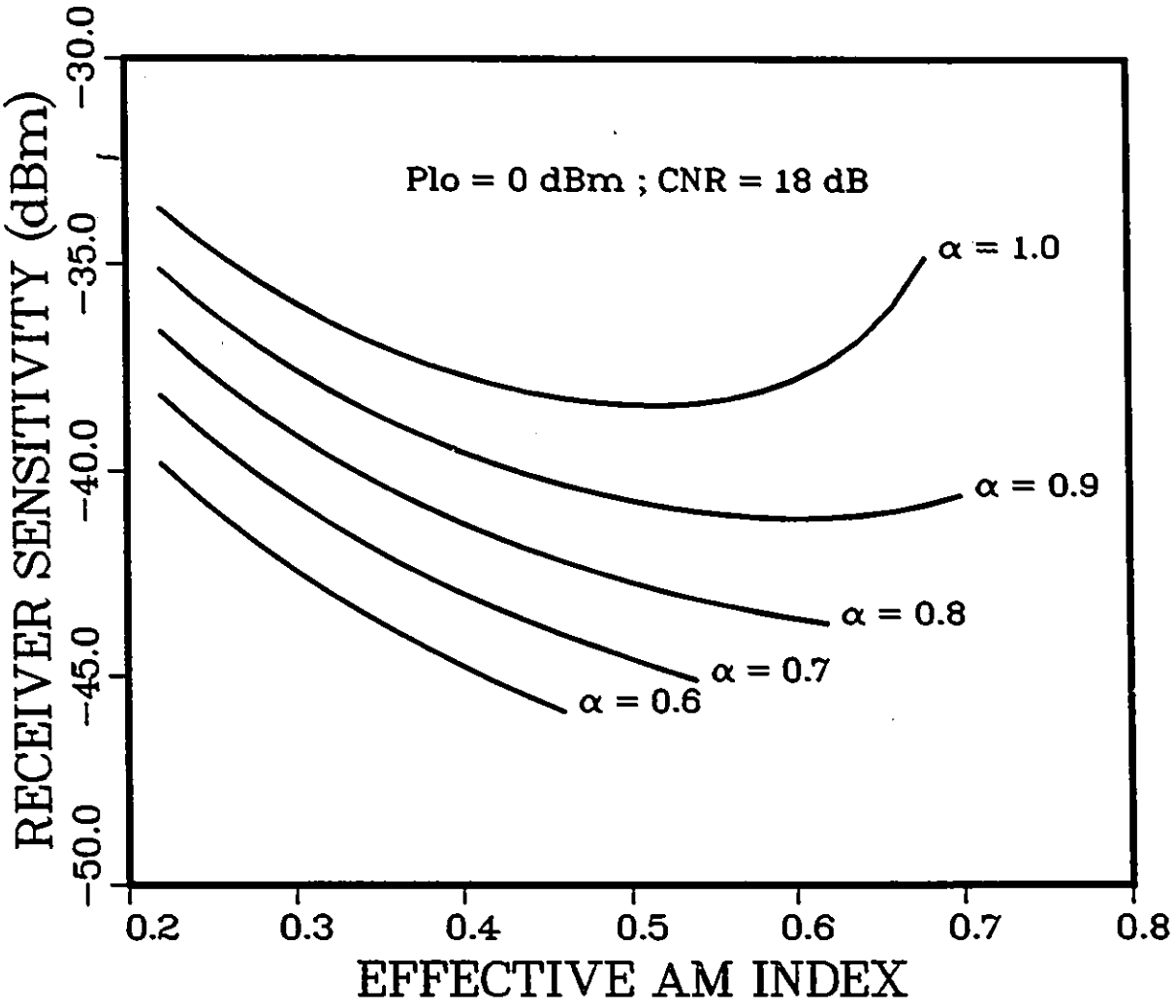

Figure 6.13: Receiver sensitivity versus effective AM modulation index for several values of α. Multiple-access case, multi-octave operation, worst channel (No. 1).

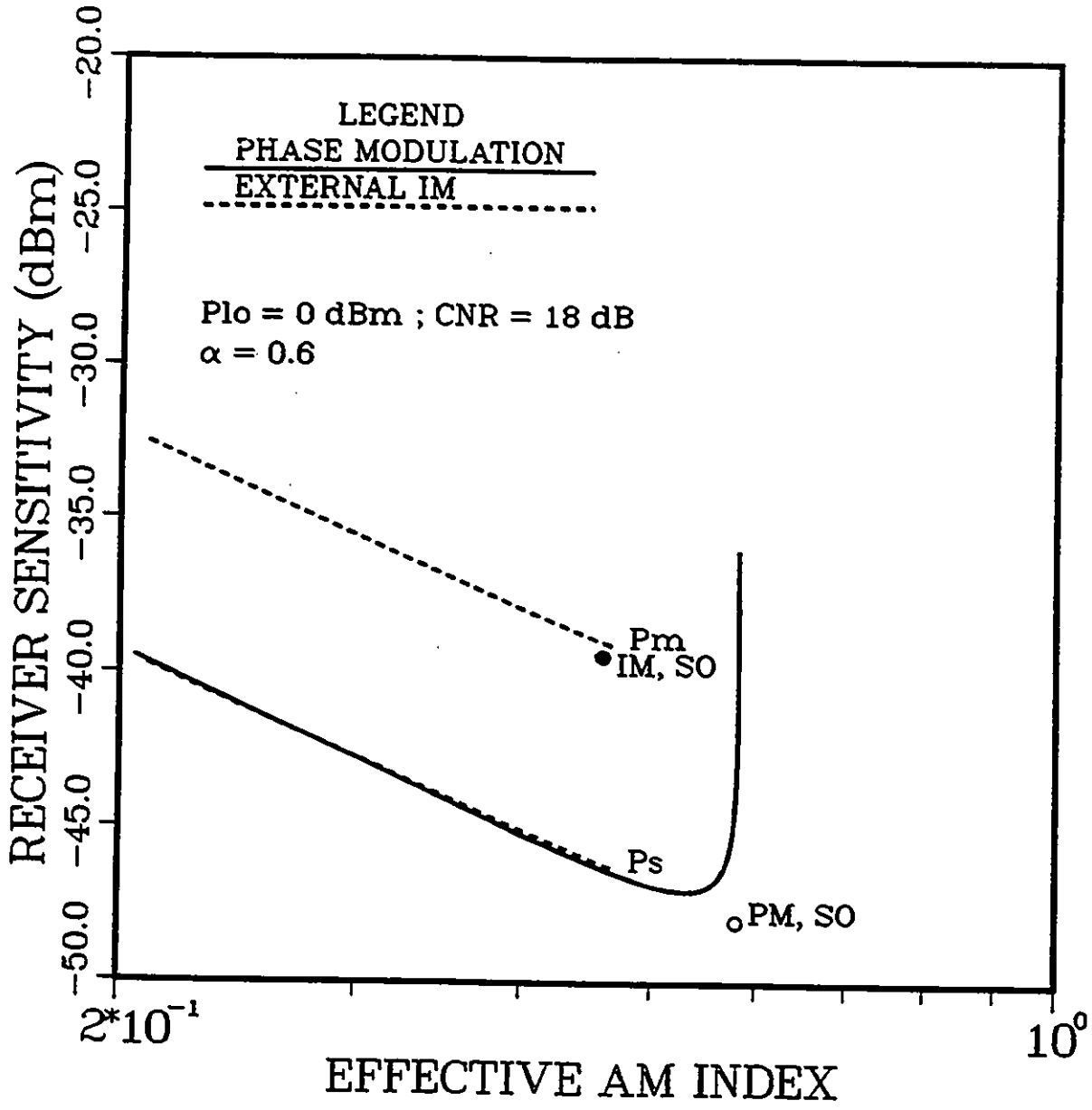

Figure 6.14: Comparison between OIM and OPM receiver sensitivity in a multiple-access system for both single- and multi-octave operation.

CASE	OPM	OIM
Multi-channel, single-octave N = 20	$P_s = -30.5$ dBm $256 < M < 512$	$P_s = -28$ dBm M = 256
Multi-channel, multi-octave N = 20	$P_s = -23.5$ dBm $64 < M < 128$	$P_s = -27$ dBm $128 < M < 256$
Single-channel, single-octave	$P_s = -49$ dBm $16,384 < M < 32,768$	$P_s = -39.5$ dBm $2,048 < M < 4,096$
Single-channel, multi-octave	$P_s = -47$ dBm M=16,384	$P_s = -38$ dBm $M \leq 2,048$

Table 6.2: Projected number of users of SCM/CD systems of different types.

Fig. 6.15 shows plots of BER versus received optical power when all system parameters are optimized for each case. The same receiver model, as before, is used.

6.5 Number of Users

In this section, we present an estimate of the potential number of users for each of the cases discussed so far. We introduce some assumptions about the power loss in the network. First, we assume that the star coupler of size M×M is built by using n stages of 2×2 couplers ($M = 2^n$). The maximum number of stages is given by:

$$n_{max} = \frac{P_t(\text{dBm}) - P_{s|min}(\text{dBm}) - l_f(\text{dB})}{3 + l_c(\text{dB})} \tag{6.29}$$

where P_t is the transmitted power from each user, $P_{s|min}$ is the receiver sensitivity, l_f is the fibre loss, and l_c is the coupler excess loss. Then:

$$M_{max} = 2^{\text{int}[n_{max}]} \tag{6.30}$$

where int[$*$] denotes the integer part. We assume $P_t = 0$ dBm, $l_f = 3$ dB (i.e., ≈ 6 km), $l_c = 0.1$ dB. Table 6.2 shows the summarized results.

A comparison of the results for the multiple-access networks with the direct-detection ones in [39] shows that the SCM/CD networks allow for a significantly larger number of users. The use of optical amplifiers in the DD networks is going to

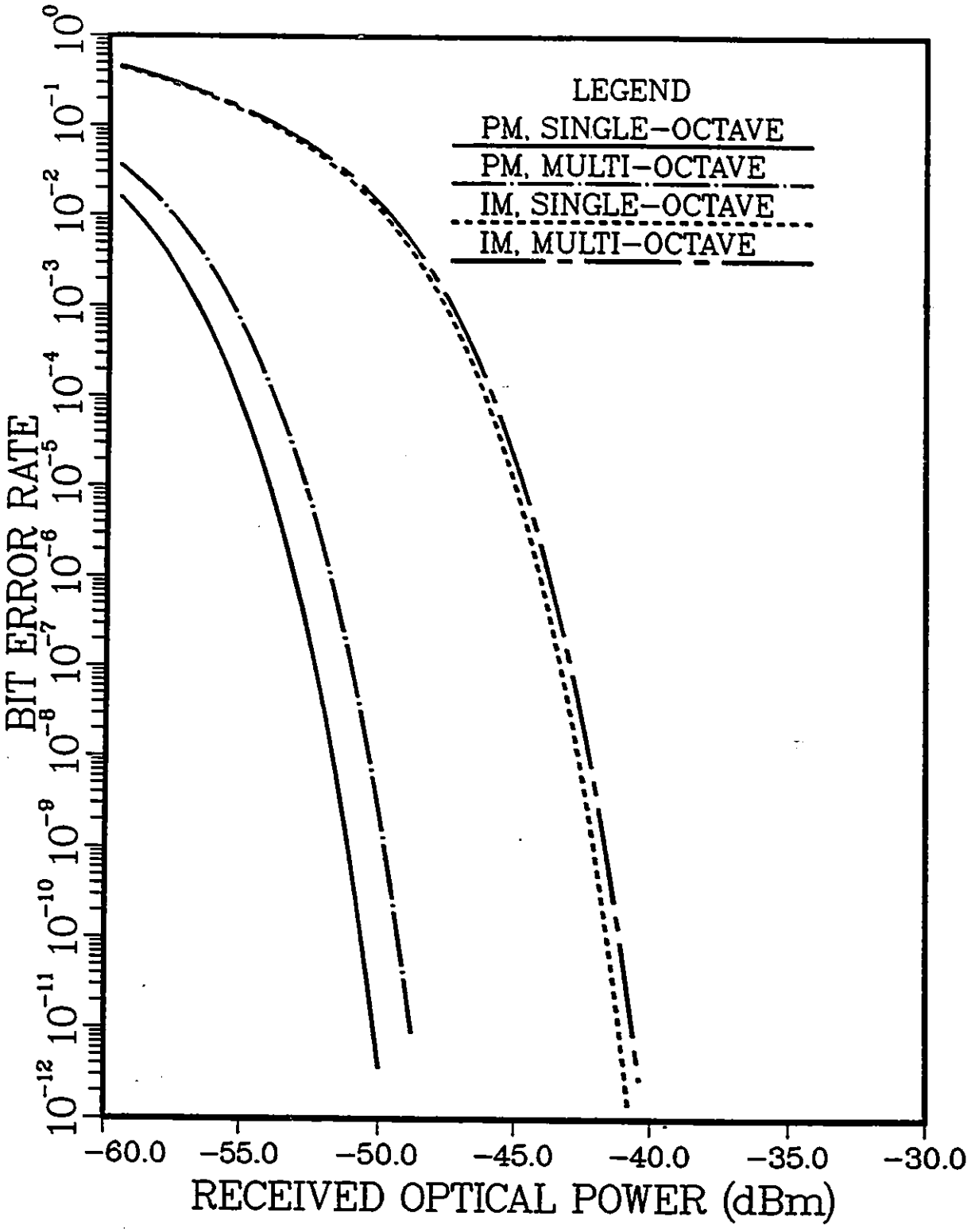

Figure 6.15: Bit error rate curves as a function of received optical power from one user in multiple-access SCM/CD systems. All parameters are optimized for maximum performance.

help only partially, because the excess shot noise is going to increase as a result of the amplification.

6.6 Polarization Control

The need for good polarization matching between the optical signal and the LO was discussed in Chapter 3. All polarization control techniques can in principle be used for the SCM/CD network. However, some of them are more suitable for our purposes than others.

For instance, one can use polarization-maintaining fibres (PMF). In a LAN environment the higher losses of the PMF, compared to a regular fibre, may not be a significant disadvantage. For this approach to work, the star coupler and the other optical components must also preserve the polarization of all the optical signals. This could be a very difficult requirement to satisfy.

Polarization-tracking techniques are often rather complicated and in most cases do not provide endless polarization control, i.e., more than 360°. For this reason, we favor polarization-diversity techniques. Since we are inclined to use phase-diversity techniques, in order to avoid excessive complexity and too many processing branches, it is attractive to use polarization switching [68] (discussed in Section 3.4.2). The transmission rate in the individual channels is not very high, so it is not a problem to switch the polarization of the LO laser a few times during each bit interval.

6.7 Other Considerations

So far, we did not address the possibility to balance the performance of all channels in the OPM multi-carrier SCM/CD system by using different optical modulation indices β_i for different channels. Such a technique would make the theoretical analysis of the system performance more difficult. The tuning and operation of such a system will also be difficult in practice. We feel that the use of optical IM can considerably

simplify both. Moreover, the response of the intensity modulator could be further linearized by electronic means, alleviating the need for reducing the bias. This could lead to an even better power budget for the case of OIM.

It is possible to use optical frequency modulation (OFM) to create the sidebands. The theoretical analysis will be very similar to that for the OPM. The attractiveness of using FM is that it can be achieved by direct modulation of the laser. However, several problems exist. First, the optical FM index of every channel depends on the frequency of the respective subcarrier, thus requiring individual tuning of each channel. Second, the nonuniform FM response of semiconductor lasers can present significant difficulties. The maximum achievable FM modulation speed may not be enough for many SCM applications. In view of the above difficulties, we think that FM is not a suitable optical modulation method for SCM/CD systems.

The effect of the laser phase noise will be addressed in the next chapter.

One should note that the number of users of the multiple-access networks is not necessarily the same as the number of channels. The former is determined by the available power budget (i.e., the power losses and the receiver sensitivity) and networking limits, whereas the latter is restricted by the available system bandwidth and to some extent by the processing speed of the control electronics. It is likely that the number of users will exceed the number of channel pairs. Therefore, contention may be allowed in the network, which must be resolved by appropriate protocols.

6.8 Summary

In this chapter, we presented a theoretical analysis of two optical modulation methods that can be used for SCM/CD networks — OPM and external OIM. It was shown that OIM has the potential for improved performance, compared to the OPM, when used in multi-carrier (distribution) networks and multi-octave mode of operation. This is due to the possibility of improving the system linearity by properly adjusting

the modulator bias.

We also presented a multiple-access SCM/CD network conceptually. This type of network offers a larger number of users than a similar SCM/DD network. At the same time, the proposed concept can readily be extended to multiple optical wavelengths, which makes it compatible with the optical FDM networks. The proposed network can be implemented with presently available technology. In the case of multiple-access SCM/CD networks, the optical PM offers a better performance than the IM, as shown in our work.

Chapter 7

Laser Phase Noise in SCM/CD Systems

7.1 Introduction

While offering a superior performance compared to direct detection systems, coherent optical detection also introduces additional problems. One of the most severe problems is the laser phase noise [40,53]. Laser phase noise in coherent digital baseband systems has been studied extensively. However, few results have been published on the laser phase noise impact on analog coherent systems [45,46]. In this chapter, we address the problem of laser phase noise in SCM/CD systems from a different perspective than in [45] and [46].

Since there are two modulation stages — RF and optical — the system's immunity to phase noise depends on both of them. It is possible and convenient to consider the optical and the RF modulation separately.

Section 7.2 presents a discussion of several optical modulation formats in relationship with the laser phase noise. Section 7.3 addresses the effect of the RF modulation format on the system performance in the presence of laser phase noise.

7.2 Phase Noise and Optical Modulation

The optical modulation creates optical sidebands around the carrier that are subsequently used at the receiver. We can express the modulated optical signal as follows:

$$E(t) = A(t)\exp\{j[\Omega_0 t + \theta(t) + \phi_n(t)]\} \tag{7.1}$$

where $A(t)$ is the amplitude, Ω_0 is the optical angular frequency, $\phi_n(t)$ represents the phase noise, and:

$$\theta(t) = K_{PM}x(t) \qquad \text{for PM} \tag{7.2}$$

$$\theta(t) = K_{FM}\int_0^t x(\tau)d\tau \qquad \text{for FM} \tag{7.3}$$

where K_{PM} and K_{FM} represent optical modulation indices and $x(t)$ is the information signal (modulated subcarrier). We can also write:

$$\beta_{FM} = \frac{K_{FM}}{2\pi f_c} \tag{7.4}$$

where f_c is the subcarrier frequency, and

$$\beta_{PM} = K_{PM} \tag{7.5}$$

The laser phase noise affects the FM and PM systems in three ways: as additive noise during optical modulation, by creating a noisy phase reference for the subsequent RF demodulation, and by making the spectrum of the received signal wider, thus requiring larger passband and consequently allowing more noise into the system. In IM systems, phase noise is not a consideration during optical modulation, but has the same implications for the RF demodulation.

For simplicity, let us consider the case of a single subcarrier. The laser frequency noise consists of three components [40]: white Gaussian noise component, $1/f$ low-frequency noise, and noise due to the laser relaxation oscillations. The most significant component by far is the white noise one. The power spectral height of the white frequency noise is:

$$S_f(f) = \frac{\Delta\nu}{\pi} \tag{7.6}$$

where $\Delta\nu$ is the combined linewidth of the received light and the local laser light beams.

Let us derive expressions for the signal-to-noise ratio when the phase (frequency) noise is treated as an additive noise. For the case of FM, we have:

$$SNR_{FM} = \frac{K_{FM}^2}{2\sigma_f^2} \tag{7.7}$$

where σ_f^2 is the variance of the frequency noise, which can be expressed as:

$$\sigma_f^2 = \frac{\Delta\nu B}{\pi} \tag{7.8}$$

where B is the receiver bandwidth. From (7.4)–(7.8), we have:

$$SNR_{FM} = \frac{2\pi^3 \beta_{FM}^2 f_c^2}{\Delta\nu B} \tag{7.9}$$

For the PM case, we can write:

$$SNR_{PM} = \frac{\beta_{PM}^2}{2\sigma_\phi^2} \tag{7.10}$$

where σ_ϕ^2 is the variance of the phase noise. Within a narrow bandwidth B around a frequency f_c, σ_ϕ^2 can be expressed as:

$$\sigma_\phi^2 = S_\phi(f_c)B = \frac{\Delta\nu B}{4\pi^3 f_c^2} \tag{7.11}$$

where $S_\phi(f_c)$ is the phase noise power spectrum at frequency f_c.

Combining (7.10) and (7.11) gives:

$$SNR_{PM} = \frac{2\pi^3 \beta_{PM}^2 f_c^2}{\Delta\nu B} \tag{7.12}$$

which is essentially the same as the expression (7.9) for SNR_{FM}, which was to be expected, given the duality of the FM and PM modulation formats.

Plots of SNR as a function of $\Delta\nu$ are shown in Fig. 7.1 for different values of β. Other parameters assumed are: $f_c = 4$ GHz; $B = 100$ MHz. The first-order sidebands are the strongest for $\beta \approx 1.8$. Small values of β have to be used when transmitting several subcarriers simultaneously. Because of the high frequency of the RF subcarriers, the requirements for $\Delta\nu$ are not very restrictive, even for small values of β.

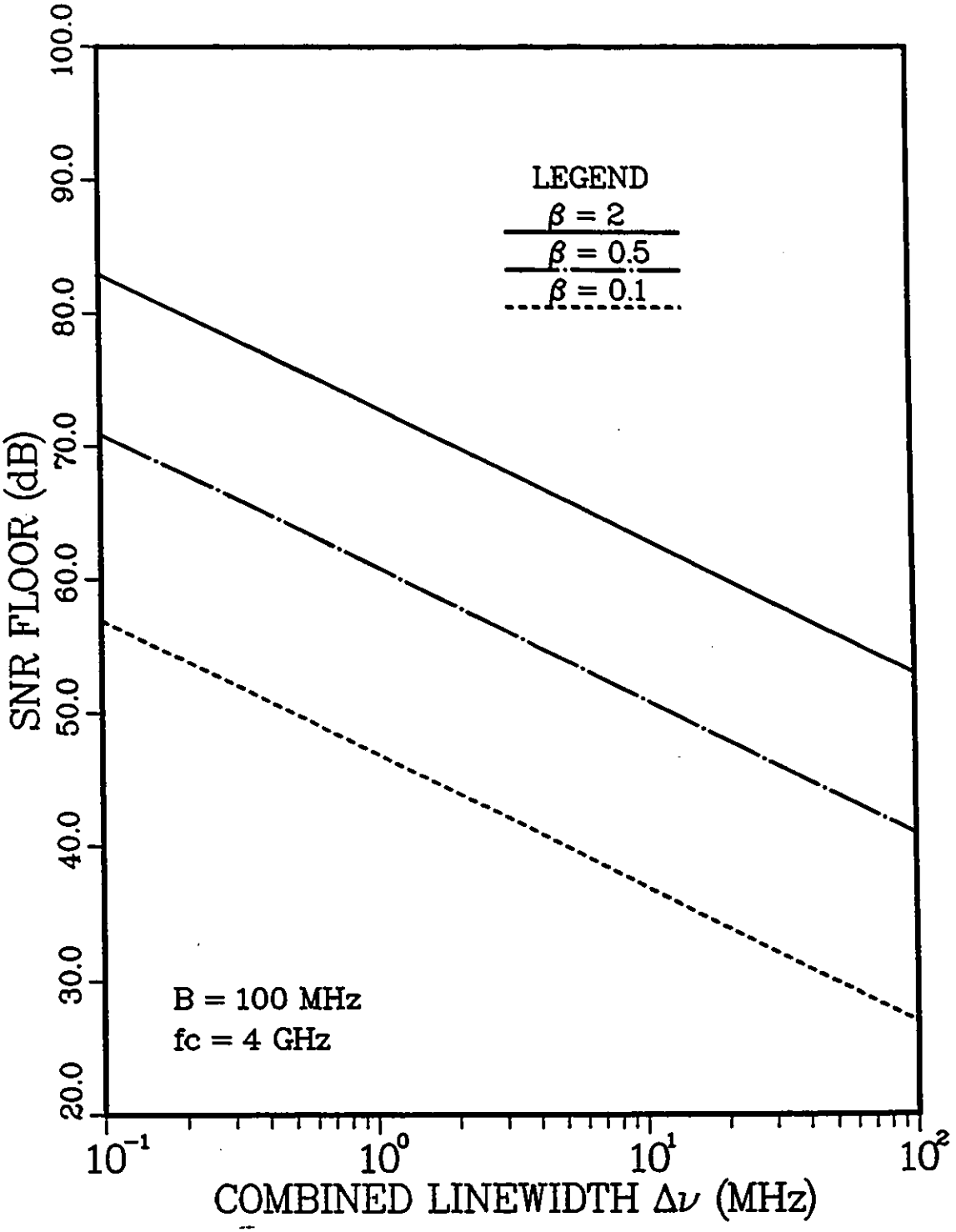

Figure 7.1: SNR floor in FM and PM systems resulting from additive phase noise.

7.3 Phase Noise and RF Modulation

We shall limit our discussion to systems that use digitally-modulated subcarriers. By realizing that the phase noise in the optical sidebands is the same as in the unmodulated carrier, we can use the results from previous studies of baseband coherent digital systems [40,53]. It is well known that the performance of systems employing synchronous demodulation is very sensitive to laser phase noise, as discussed in Chapter 3. On the other hand, systems using asynchronous FSK (Frequency Shift Keying) or ASK (Amplitude Shift Keying) can be very tolerant to phase noise. More details can be found in [52,62].

Our discussions so far have not considered the possibility for using phase noise cancellation techniques. SCM/CD systems offer this possibility naturally, since there is an unmodulated carrier present. This carrier contains the exact phase information and, unlike in baseband coherent systems, it is easy to separate from the information signal by filtering. Noise cancellation techniques of this type have been successfully demonstrated in [126].

7.4 Summary

The impact of laser phase noise in SCM/CD lightwave transmission systems has been analyzed. We found that the type of subcarrier modulation format is more important than the type of optical modulation with respect to phase noise immunity. As in baseband coherent systems, asynchronous modulation/demodulation formats should be used to overcome the phase noise restrictions. SCM/CD systems offer a simple way of implementing phase noise cancellation techniques. This will allow the transmission of relatively low bit-rate data using lasers with relaxed linewidth parameters.

Chapter 8

Phase-Diversity SCM/CD Receivers

8.1 Introduction

In this chapter we have two goals. First, we want to introduce the structure of a phase-diversity homodyne receiver for SCM/CD systems. In parallel with this, we give an example of the impact of the laser phase noise on the receiver performance.

Phase-diversity receivers were mentioned in Chapter 3. The phase-diversity scheme is a clever way to avoid the need for an optical PLL in homodyne optical detection. It has been analyzed theoretically and experimentally [52,64,65], [66,73,74] [127,128,129], for baseband coherent systems. It is straightforward to extend the analysis to SCM/CD systems.

Section 8.2 presents the receiver structure and the theoretical analysis of its performance. In Section 3, some numerical examples are given. First, we are going to demonstrate the need for some kind of phase control in SCM/CD homodyne systems. We can express the information part of the detected photo-current for the j-th channel, ignoring the additive noise, as:

$$i_j(t) = A_j \cos[(\omega_{IF} + \omega_j)t + \phi_j(t) + \Delta\phi(t)]$$

$$+ \quad A_j(t)\cos[(\omega_{IF} - \omega_j)t - \phi_j(t) + \Delta\phi(t)] \tag{8.1}$$

where:

$A_j(t)$ — amplitude,

ω_{IF} — intermediate frequency,

ω_j — subcarrier frequency,

$\phi_j(t)$ — possible angle modulation,

$\Delta\phi(t)$ — relative phase difference between the signal and the LO.

Suppose $\omega_{IF} = 0$. After simple trigonometry, we have:

$$i_j(t) = 2A_j(t)\cos[\omega_j t + \phi_j(t)]\cos[\Delta\phi(t)] \tag{8.2}$$

The $\cos[\Delta\phi(t)]$ term can cause a complete fading of the received signal, unless some preventive measures are undertaken. One measure is to lock the phase of the local laser to the phase of the incoming signal carrier. As is well-known, this is difficult to achieve, so phase-diversity techniques provide an attractive alternative.

8.2 Receiver Structure and Analysis

The receiver structure that we consider in this chapter is based on an 8-port 90° optical hybrid shown in Fig. 8.1 and described in [130,131]. At the outputs of the hybrid, the signal and the LO have different phase shifts relative to one another. Fig. 8.2 shows the schematic diagram of the whole receiver. The tunable RF oscillator (RFO) is used to select the desired channel and to convert it to the passband of the bandpass filter (BPF). For simplicity, no noise sources are shown in the figure. We assume, as in previous chapters, that the transmitted subcarriers are FSK modulated. The demodulation is implemented by delay-and-multiply type discriminators. The delay τ is much smaller than a bit period, therefore operating as a differentiator. The cross-multiplication of the in-phase and the quadrature channels is used to provide the immunity to phase variations and also has the added benefit of de-correlating the noise components in the noise×noise products.

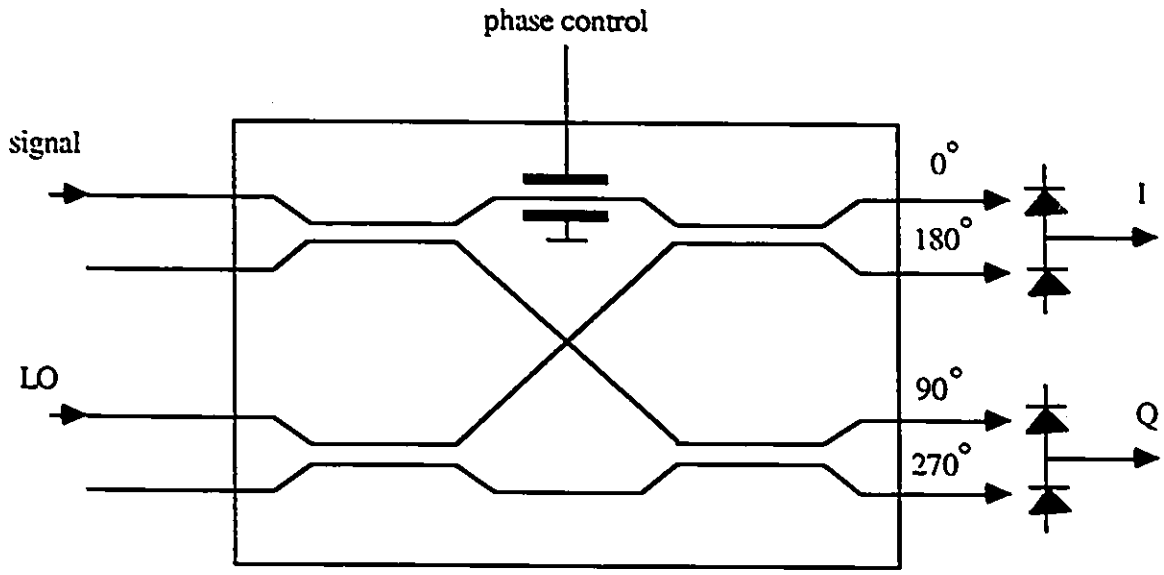

Figure 8.1: Schematic diagram of an 8-port 90° optical hybrid.

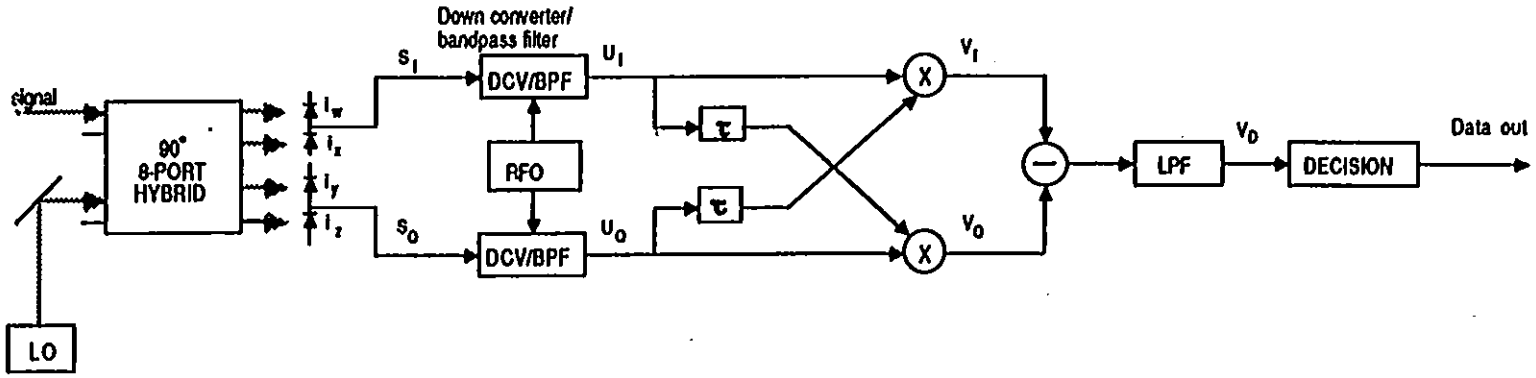

Figure 8.2: Schematic diagram of an SCM/CD phase-diversity homodyne receiver using an 8-port 90° optical hybrid.

We assume that the optical sidebands are created by phase modulation. For the current components of the j-th channel at the output of the photodiodes, we can write:

$$\begin{aligned} i_{jw}(t) &= \frac{1}{4}R\left\{P_s + P_{LO} - 2J_1(\beta)\sqrt{P_sP_{LO}}\sum_{l=-1,1}\cos[l(\omega_j t+\phi_j)+\Delta\phi]\right\} \\ &+ n_w(t) \end{aligned} \tag{8.3}$$

$$\begin{aligned} i_{jx}(t) &= \frac{1}{4}R\left\{P_s + P_{LO} + 2J_1(\beta)\sqrt{P_sP_{LO}}\sum_{l=-1,1}\cos[l(\omega_j t+\phi_j)+\Delta\phi]\right\} \\ &+ n_x(t) \end{aligned} \tag{8.4}$$

$$\begin{aligned} i_{jy}(t) &= \frac{1}{4}R\left\{P_s + P_{LO} + 2J_1(\beta)\sqrt{P_sP_{LO}}\sum_{l=-1,1}\sin[l(\omega_j t+\phi_j)+\Delta\phi]\right\} \\ &+ n_y(t) \end{aligned} \tag{8.5}$$

$$\begin{aligned} i_{jz}(t) &= \frac{1}{4}R\left\{P_s + P_{LO} - 2J_1(\beta)\sqrt{P_sP_{LO}}\sum_{l=-1,1}\sin[l(\omega_j t+\phi_j)+\Delta\phi]\right\} \\ &+ n_z(t) \end{aligned} \tag{8.6}$$

where $n_w(t)$, $n_x(t)$, $n_y(t)$, and $n_z(t)$ are shot noise components, which are independent from each other, Gaussian, and zero-mean. Furthermore:

$$\begin{aligned} S_I(t) = i_{jx}(t) - i_{jw}(t) &= RJ_1(\beta)\sqrt{P_sP_{LO}}\sum_{l=-1,1}\cos[l(\omega_j t+\phi_j)+\Delta\phi] \\ &+ n_x(t) - n_w(t) \end{aligned} \tag{8.7}$$

$$\begin{aligned} S_Q(t) = i_{jy}(t) - i_{jz}(t) &= RJ_1(\beta)\sqrt{P_sP_{LO}}\sum_{l=-1,1}\sin[l(\omega_j t+\phi_j)+\Delta\phi] \\ &+ n_y(t) - n_z(t) \end{aligned} \tag{8.8}$$

Note that the 8-port hybrid allows us to have a balanced receiver configuration, which helps in eliminating the noise due to the amplitude fluctuations (or RIN) of the LO laser [70].

Following the signal path further, we can write:

$$U_I(t) = \mathrm{BPF}\left\{C\sum_{l=-1,1}\cos[l(\omega_{IF}t+\phi_j)+\Delta\phi] + n_I(t)\right\} \tag{8.9}$$

$$U_Q(t) = \mathrm{BPF}\left\{C\sum_{l=-1,1}\sin[l(\omega_{IF}t+\phi_j)+\Delta\phi] + n_Q(t)\right\} \tag{8.10}$$

where BPF stands for bandpass-filtering operation, $C = RJ_1(\beta)\sqrt{P_s P_{LO}}$, and $n_I(t)$ and $n_Q(t)$ are sums of all the additive noise terms in the respective branches of the receiver, i.e., shot, thermal, intensity, etc. The decision variable V_D is obtained as:

$$V_D(t) = \text{LPF}\left\{U_I(t)U_Q(t-\tau) - U_Q(t)U_I(t-\tau)\right\} \tag{8.11}$$

where LPF stands for lowpass-filtering operation.

The derivation of the statistics for $V_D(t)$ is quite involved mathematically, because the signal×noise and noise×noise products. Tsao et al. [129] have performed the theoretical analysis of a baseband FSK phase-diversity receiver. In our case, the main difference is that not all the received optical power is used to calculate the signal-to-noise ratio, but only the power contained in the optical sidebands. We can modify their results for the case of the SCM/CD system, and using our notation for the probability of error, we have:

$$P_e = \frac{1}{2}\text{erfc}\left\{\frac{D}{\sqrt{2(W + 2XY + X^2Z/12)}}\right\} \tag{8.12}$$

where:

$$D \;-\; \text{normalized frequency deviation,} \tag{8.13}$$

$$W = \frac{\Delta\nu}{\pi R_b}, \tag{8.14}$$

$$X = \frac{qR_b}{RP_s[J_1(\beta)]^2}, \tag{8.15}$$

$$Y = D^2 + \frac{\Delta\nu}{\pi R_b} + \frac{1}{3}, \tag{8.16}$$

$$Z = 16D^3 + 36D^2 + 28D + \frac{15}{2} \tag{8.17}$$

and:

$\Delta\nu$ — combined laser linewidth,

R_b — bit rate,

q — electron charge.

Shot-noise limited detection was assumed for simplicity. As can be seen from (8.12) - (8.17), the BER depends on the received optical power, the laser phase noise, the bit rate, and the frequency deviation.

8.3 Numerical Results

For the purpose of a numerical example, we chose the following parameters: transmission bit rate $R_b = 150$ Mb/s, $\beta = 1.8$ (i.e., $J_1(\beta) \cong 0.58$). This value of β is applicable for a single subcarrier per laser. Figures 8.3, 8.4, and 8.5 show plots of the BER as a function of the received optical power for different laser linewidths and frequency deviations. As expected, the larger the frequency deviation, the less sensitive the system is to the laser phase noise.

8.4 Discussion

The phase-diversity receiver provides the same sensitivity as a heterodyne receiver. It has the advantage of requiring less bandwidth from the electronic components. Therefore, it is probably worth the extra complexity of implementation, because the receiver bandwidth is a limiting factor in SCM/CD systems. A homodyne receiver also has an advantage in optical FDM systems, because it allows for closer optical channel spacing.

The immunity to phase noise of heterodyne and phase-diversity receivers is about the same. As seen from Figures 8.3to 8.5, the receiver structure under investigation is reasonably tolerant to laser phase noise. There is a trade-off between frequency deviation (and therefore electronics bandwidth required) and tolerance to the phase noise. These parameters should be optimized for any particular system.

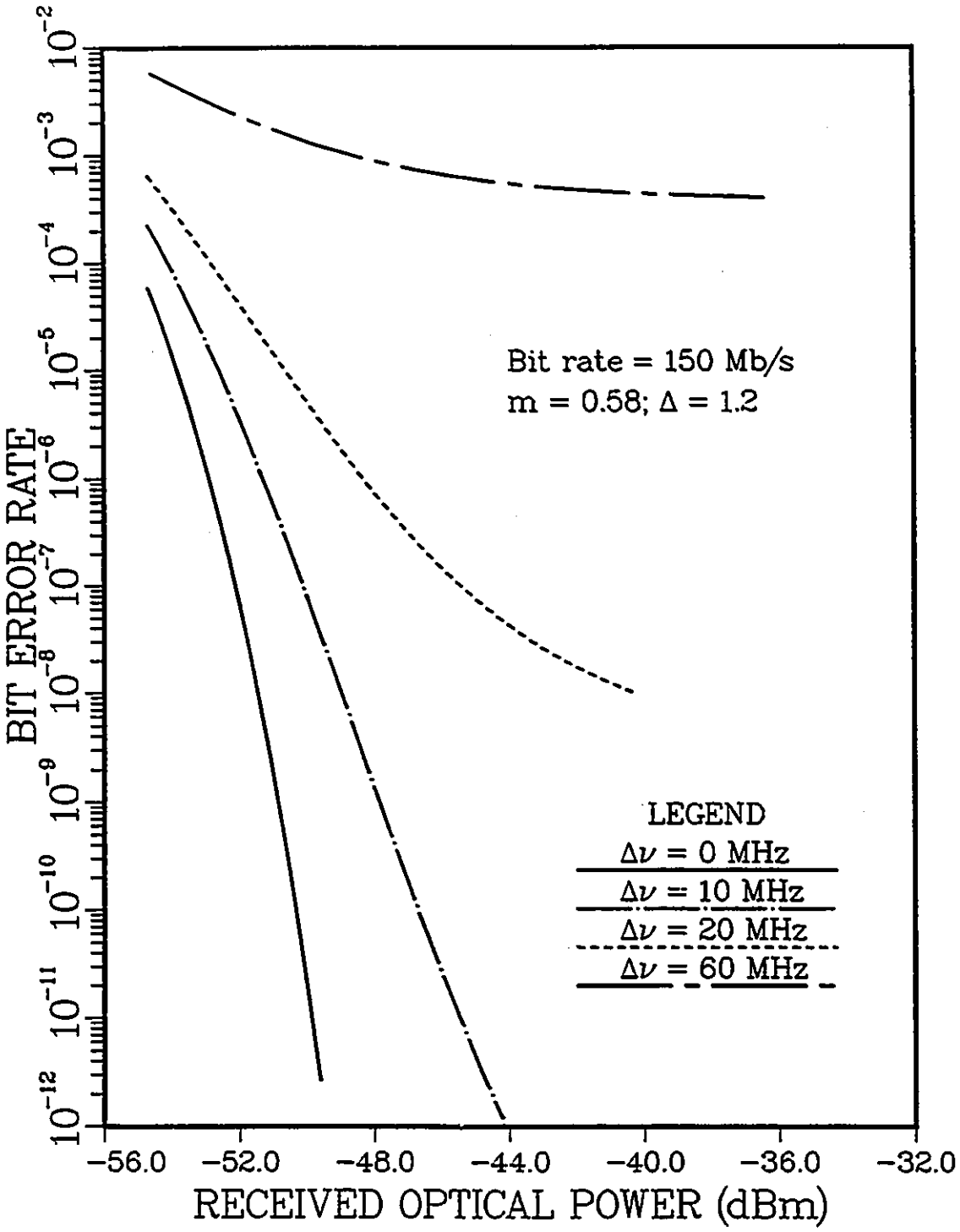

Figure 8.3: BER as a function of received optical power for a phase-diversity SCM/CD homodyne receiver. The normalized frequency deviation is $D = 1.2$.

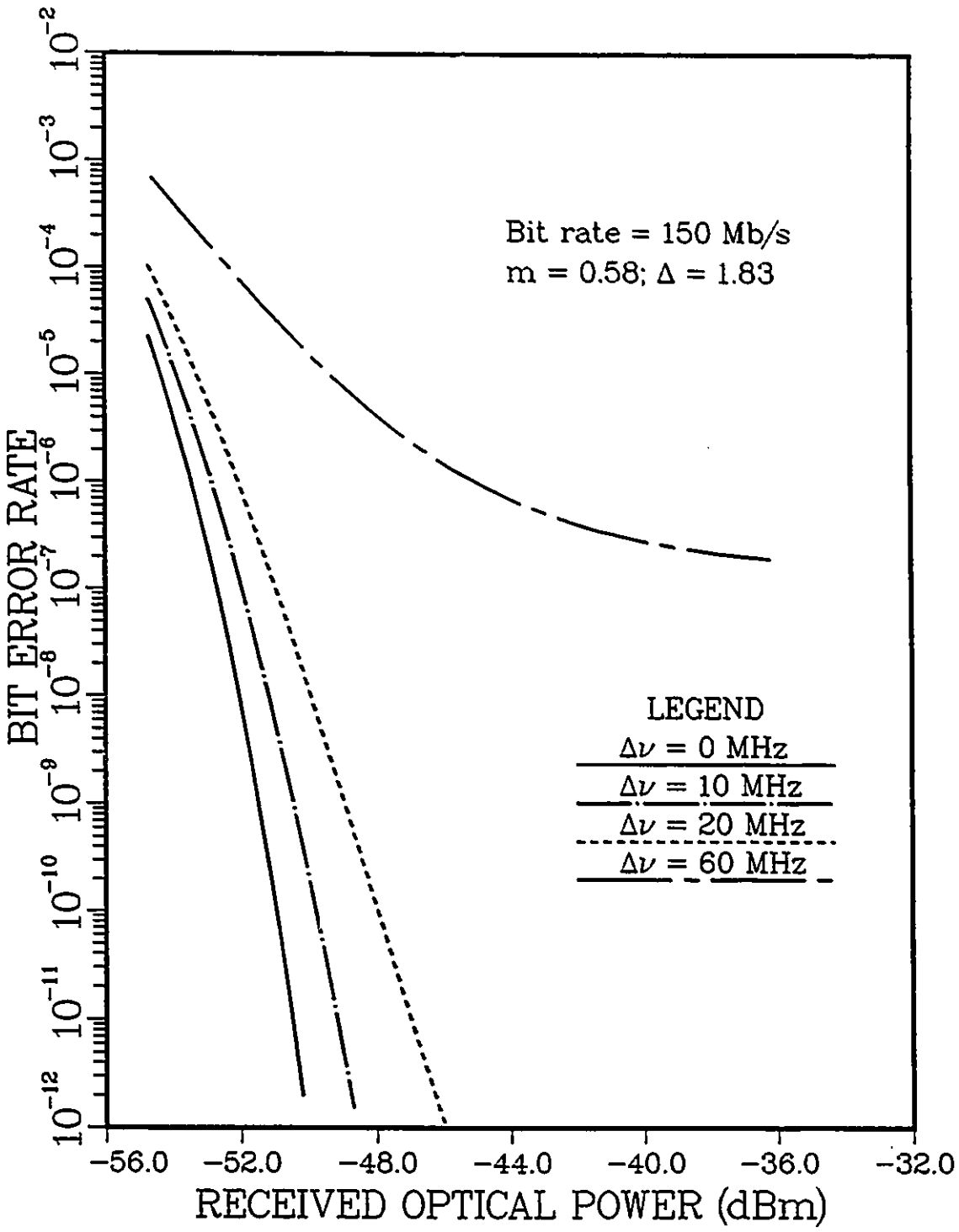

Figure 8.4: BER as a function of received optical power for a phase-diversity SCM/CD homodyne receiver. The normalized frequency deviation is $D = 1.83$.

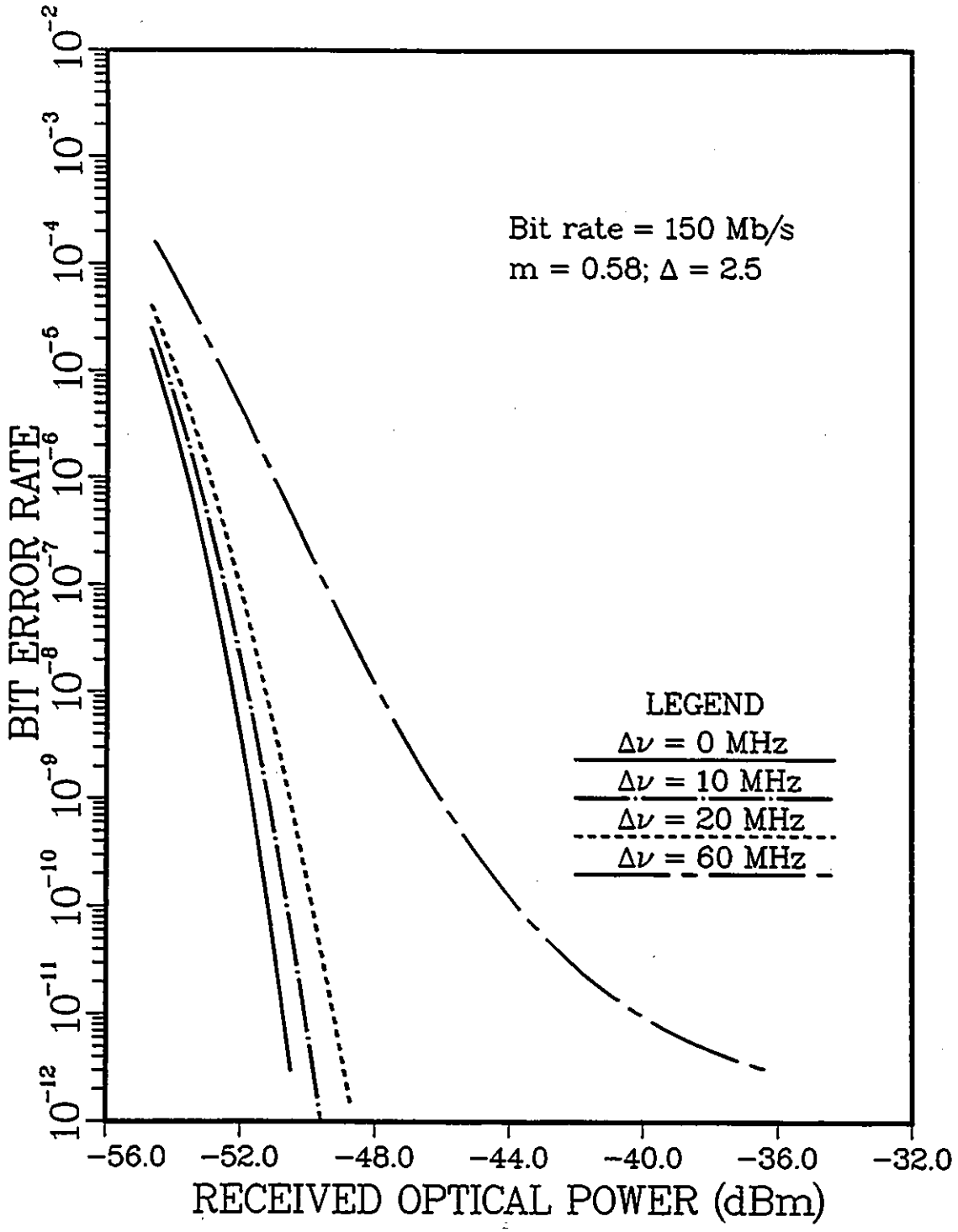

Figure 8.5: BER as a function of received optical power for a phase-diversity SCM/CD homodyne receiver. The normalized frequency deviation is $D = 2.5$.

Chapter 9

Conclusions and Suggestions for Future Work

In this thesis, we evaluated the usefulness of several alternatives for building fibre-optic LANs and MANs. We considered both distribution and multiple-access networks.

In the area of optical space switching, we identified in Chapter 4 the use of spatial light modulators (SLMs) as a promising approach for building a large-size (e.g., 1000×1000) photonic crossbar switch. Such a switch could be used as a network switching node, or for inter-processor interconnection in a large multi-processor computer system. For its practical implementation, progress is needed in device technology (the fabrication of the SLM), and in the way the fan-out and fan-in problems are solved.

In Chapters 5 and 6, we demonstrated that subcarrier-multiplexing techniques can be attractive solutions to many network problems. In Chapter 5, it was shown that the transmission of 64-QAM microwave subcarriers is a viable alternative for the distribution of large volumes of high-speed data and other services, e.g., HDTV, etc. We addressed the main system degradation factors — laser intensity noise and laser nonlinearities — and demonstrated the options of how to deal with these successfully:

by minimizing the reflections into the laser, and by using error-correction coding. The limited power budget of the systems can be improved by using optical amplifiers. One can expect that higher-level QAM fibre-optic transmission could be useful for the reasons discussed in Chapter 5. In fact, from private sources we know that NTT Labs in Japan have conducted a successful experimental transmission of a 256-QAM signal via optical fibre. However, we feel that a QAM transmission with number of levels any higher than this is unlikely to be of much use, because the gain in spectral efficiency increases only logarithmically with the number of levels, whereas the complexity of the system and the power budget degradation become prohibitive.

In Chapter 6, we discussed a novel photonic network architecture which uses subcarrier multiplexing and coherent optical detection. It was shown that this approach offers superior performance, compared to systems using direct optical detection. The SCM/CD approach is an intermediate step between DD systems and FDM coherent optical systems. We discussed several issues, namely the system topology, the optical modulation formats to be used, the potential number of users, etc. The future of this type of networks depends on the progress in integrated opto-electronics. Given the substantial research effort worldwide, we can be fairly optimistic.

In Chapter 7, we addressed the problem of laser phase noise in SCM/CD systems. It was shown that the RF modulation format is more critical for the system performance than the optical modulation format. Constant progress is made in laser device technology, and the phase noise is expected to become less of a problem in the future. For example, there are commercially available Nd:YAG lasers with linewidths of only a few kHz.

Finally, Chapter 8 introduced the receiver structure and analyzes the performance of an 8-port phase-diversity homodyne SCM/CD receiver. This particular receiver combines several desirable features: lower electronic bandwidth requirements (compared to heterodyne receivers); balanced operation; no need for optical phase locking; good immunity to laser phase noise.

A general suggestion for future work, which applies to most of the topics addressed in this thesis, is experimental work. This thesis has laid some conceptual and theoretical ground for fibre-optic network design. It would be interesting and worthwhile to prove the feasibility of these concepts experimentally. Particularly challenging would be the implementation of the SLM space switch.

Another important direction for future research is to consider the network control issues regarding multiple access (e.g., synchronization and call setup, etc.). The network control can turn out to be a serious bottleneck.

In conclusion, we hope that the work done in this thesis provides helpful insights into some important areas of fibre-optic network design.

Appendix A

Nonlinearities in Communication Systems

This appendix provides a brief discussion of nonlinearities in communication systems. The topic has been studied extensively [116,122,124,132]. The most commonly used mathematical model is of the polynomial type without memory [116]:

$$Y = C + A_1(X + A_2X^2 + A_3X^3) \tag{A.1}$$

where Y is the system output, X is the system input, and C, A_1, A_2, A_3 are constants. We ignore nonlinear terms of order higher than 3 as being insignificant.

Suppose that X is a set of equally-spaced RF carriers with unit amplitude:

$$X = \sum_{N=L}^{M} \cos(N\omega_0 t) \tag{A.2}$$

where ω_0 is the spacing between the channels. The second-order distortion terms are generated by the X^2 term in A.1:

$$X^2 = \frac{1}{2}\sum_{i=L}^{M}\sum_{j=L}^{M} \cos[(i+j)\omega_0 t] \tag{A.3}$$

Similarly, the X^3 term generates third-order distortion components:

$$X^3 = \frac{1}{4}\sum_{i=L}^{M}\sum_{j=L}^{M}\sum_{k=L}^{M} \cos[(i+j+k)\omega_0 t] \tag{A.4}$$

Term Type	Number of Components per Term	dB of Terms Above Harmonic	Number of Terms
Second Order			
2A	1	0	1, if N/2 is an integer
A+B	2	6	int(N+1/2)-L, 2L-1≤N≤L+M
A-B	2	6	M-L+1-N, 0≤N≤M-L+1
Third Order			
3A	1	0	1, if N/3 is an integer
2A+B	3	9.54	int[(N-L)/2] - int(N/3) + int[(N-1)/3]-L+1, 3L<N<2(L+M)
2A-B	3	9.54	int[(M-N)/2] + int[(N-L)/2], L≤N≤M
A-2B	3	9.54	int[(M-N)/2]-L+1, 0≤N≤M-2L, M>2L
A+B-C	6	15.56	int[(N-L)/2]int[(N-L-1)/2] + (N-L)(M-N) + int[(M-N)/2]int[(M-N-1)/2], L≤N≤M
A-B-C	6	15.56	int[(M-2L-N+1)/2]int[(M-2L-N)/2], 0<N<M-2L-1, M≥2L+1
A+B+C	6	15.56	int[(3M-N+3)/6] + int[(3M-N-1)^2/12], L+2M-1≤N≤3M-3

Table A.1: Intermodulation terms interfering with a carrier at frequency N, in a group of carriers with frequencies $L\omega_0, (L+1)\omega_0 \ldots M\omega_0$, where L, N, and M are integers. int[x] is the largest integer in x.

Formulas for calculating the number of distortion terms falling into the passband of each channel have been derived by Bennett [122]. This number depends on the frequency allocation plan, the total number of channels and the position of the particular channel within the channel group. Table A.1 (after[116]) provides the necessary information to calculate the number of distortion terms and their relative power.

At this point a definition of single-octave and of multiple-octave mode of operation will be given. If the carriers occupy a bandwidth between frequencies $L\omega_0$ and $2L\omega_0$, then the operation is single-octave (SO). Otherwise, it is multi-octave (MO).

In single-octave mode of operation (i.e., $M \leq 2L$), the second-order distortion terms fall outside of the spectral region occupied by the channel group. In this case, only third-order intermodulation products (IMPs) degrade the system performance.

It can be shown that the IMPs of the form A+B-C are the strongest, and are concentrated around the middle of the channel group. Therefore, the middle channels are the worst affected.

In multi-octave mode of operation, the second-order IMPs of the form A-B are the most damaging, and their number is the highest around the first channel of the group, which therefore is the worst.

The spectrum of the distortion terms is not the same as the original spectrum of the channels. In general, the spectrum of the IMPs is wider than the spectrum of the channels that produce it. Intuitively, this can be explained by the fact that a multiplication in the time domain results in a convolution in the frequency domain. Daly [116] gives an approximation of the IMPs spectral width when all channels have the same modulation format, bandwidth and amplitude, and are statistically independent. The bandwidth of the second-order IMPs is $\sqrt{2}$ times the channel bandwidth, and the third-order IMPs' bandwidth is $\sqrt{3}$ times the channel bandwidth.

For a detailed system analysis, it is necessary to estimate the fraction of the IMPs' power that passes through the bandpass filter of the particular channel of interest. Olshansky et al. [50] define a coefficient h which takes this into account. For the second-order IMPs, it is defined as:

$$h_2 = \frac{\int_{-\infty}^{+\infty} S_i(f) * S_j(f)|H_{BP}(f)|^2 df}{\int_{-\infty}^{+\infty} S_i(f) * S_j(f) df} \tag{A.5}$$

where $*$ denotes convolution, i and j are integers $(i, j = L, \ldots M)$, $S_i(f)$ is the power spectrum of the i-th channel, and $H_{BP}(f)$ is the frequency response of the bandpass filter. Similarly, for the third-order IMPs we have:

$$h_3 = \frac{\int_{-\infty}^{+\infty} S_i(f) * S_j(f) * S_k(f)|H_{BP}(f)|^2 df}{\int_{-\infty}^{+\infty} S_i(f) * S_j(f) * S_k(f) df} \tag{A.6}$$

Note that the coefficients defined above account for the spectral spreading of the IMPs, as well as for the position where the IMPs fall. For example, third-order

IMPs, whenever they affect a particular channel, fall exactly into the passband of the channel. On the other hand, with appropriate frequency allocation techniques, one can ensure that the second-order IMPs fall in the guard band between the channels.

Appendix B

Derivation of Signal Power and IMPs' Power for the OIM Case

The type of polynomial nonlinearity given by (6.15) has been studied in [116,122],[124, 132]. For the signal current of the j-th subcarrier at the output of the photodiode, we have:

$$i_s(t) = 2R\sqrt{P_m P_{LO}} \cos\left(\frac{\alpha\pi}{4}\right) m_{cI} \times \frac{1}{2}\cos[(\Omega_c - \Omega_{LO} \pm \omega_j)t + x_j(t)] \qquad \text{(B.1)}$$

The mean-square (MS) value is therefore:

$$< i_s^2 >= \frac{1}{2}R^2 P_m P_{LO} m_{cI}^2 \cos^2\left(\frac{\alpha\pi}{4}\right) \qquad \text{(B.2)}$$

The current due to the j-th second harmonic is:

$$i_{2h} = \frac{2}{2!}R^2\sqrt{P_m P_{LO}} \sin\left(\frac{\alpha\pi}{4}\right) m_{cI}^2 \times \frac{1}{4}\cos[2(\Omega_c - \Omega_{LO} \pm \omega_j)t] \qquad \text{(B.3)}$$

The amplitude of a second-order IMP of the type $f_i \pm f_j$ is twice the amplitude of the second harmonic [116]. Hence,

$$< i_{2d}^2 >= \frac{1}{8}R^2 P_m P_{LO} \sin^2\left(\frac{\alpha\pi}{4}\right) m_{cI}^4 \qquad \text{(B.4)}$$

Finally,

$$\sigma_{I2d}^2 = h_2 K_2 < i_{2d}^2 >= \frac{1}{8}h_2 K_2 R^2 P_m P_{LO} \sin^2\left(\frac{\alpha\pi}{4}\right) m_{cI}^4 \qquad \text{(B.5)}$$

The current due to the j-th third harmonic is:

$$i_{3h} = \frac{2}{3!}R^2\sqrt{P_m P_{LO}}\cos\left(\frac{\alpha\pi}{4}\right)m_{cI}^3 \times \frac{1}{8}\cos[3(\Omega_c - \Omega_{LO} \pm \omega_j)t] \qquad \text{(B.6)}$$

The amplitude of the third-order IMP of the dominant type $f_i + f_j - f_k$ is six times the amplitude of the third harmonic. Therefore:

$$< i_{3d}^2 >= \frac{1}{32}R^2 P_m P_{LO}\cos^2\left(\frac{\alpha\pi}{4}\right)m_{cI}^6 \qquad \text{(B.7)}$$

And:

$$\sigma_{I3d}^2 = h_3 K_3 < i_{3d}^2 >= \frac{1}{32}h_3 K_3 R^2 P_m P_{LO}\cos^2\left(\frac{\alpha\pi}{4}\right)m_{cI}^6 \qquad \text{(B.8)}$$

Bibliography

[1] P. Kaiser, J. Midwinter, and S. Shimada, "Status and future trends in terrestrial optical fiber systems in North America, Europe and Japan," *IEEE Commun. Mag.*, vol. 25, pp. 8–21, Oct. 1987.

[2] K. Kümmerle, J. O. Limb, and F. A. Tobagi, eds., *Advances in Local Area Networks.* IEEE Press, 1987.

[3] E. Savov, W. Steenaart, and A. Javed, "Photonic switching using spatial light modulators — a feasibility study," in *Proc. of GLOBECOM'88*, pp. 943–947, IEEE, Nov. 1988.

[4] M. Kavehrad and E. Savov, "Fiber-optic transmission of microwave 64-QAM signals," *IEEE J. Sel. Areas Commun.*, vol. 8, pp. 1320–1326, Sept. 1990.

[5] M. Kavehrad and E. Savov, "Fiber-optic transmission of microwave 64-QAM signals and applications," in *Proc. of Int. Conf. Commun.*, pp. 409–414, Apr. 1990.

[6] W. I. Way, "Fiber-optic transmission of microwave 8-phase PSK and 16-ary quadrature-amplitude-modulated signals at the 1.3-μm wavelength region," *IEEE J. Lightwave Technol.*, vol. 6, pp. 273–280, Feb. 1988.

[7] E. Savov, W. Steenaart, and M. Kavehrad, "Theoretical analysis of multiple-access photonic networks with subcarrier multiplexing and coherent optical

detection," in *Proc. of 15th Bienn. Symp. on Commun., Kingston, Canada*, pp. 252–255, Queen's Univ., June 1990.

[8] E. Savov, W. Steenaart, and M. Kavehrad, "Theoretical comparison of modulation methods for coherent subcarrier-multiplexed photonic systems," in *Proc. MILCOM'90, Monterey, CA.*, pp. 574–578, Sept. 1990.

[9] E. Savov, W. Steenaart, and M. Kavehrad, "Laser phase noise in coherent subcarrier-multiplexed optical systems,". presented at The IEEE First International Workshop on Photonic Networks, Components & Applications, Montebello, Canada, October, 1990.

[10] Various authors, "Special issue on photonic switching," *IEEE Commun. Mag.*, vol. 25, May 1987.

[11] OSA/IEEE, *Topical Meeting on Photonic Switching, Incline Village, Nevada*, Mar. 1987.

[12] P. W. Smith, "On the physical limits of digital optical switching and logic elements," *Bell Sys. Tech. Jour.*, vol. 61, pp. 1975–1993, Oct. 1982.

[13] Various authors, "Special issue on photonic switching," *IEEE J. Sel. Areas in Commun.*, vol. 6, Aug. 1988.

[14] J. A. Salehi and C. A. Brackett, "Fundamental principles of fiber optics code division multiple access (CO-CDMA)," in *Proc. of Int. Conf. on Communications*, pp. 1601–1609, IEEE, 1987.

[15] P. R. Prucnal and M. A. Santoro, "Spread-spectrum fiber-optic local area network using optical processing," *IEEE J. Lightwave Technol.*, vol. 4, pp. 547–554, May 1986.

[16] P. R. Prucnal, D. J. Blumenthal, and P. A. Perrier, "Photonic switch with optically self-routed bit switching," *IEEE Commun. Mag.*, vol. 25, pp. 50–55, May 1987.

[17] G. J. Foschini and G. Vannucci, "Using spread-spectrum in a high-capacity fiber-optic local network," *IEEE J. Lightwave Technol.*, vol. 6, pp. 370–379, Mar. 1988.

[18] I. P. Kaminow *et al.*, "FDMA-FSK star network with a tunable optical filter demultiplexer," *IEEE J. Lightwave Technol.*, vol. 6, pp. 1406–1414, Sept. 1988.

[19] N. Takato *et al.*, "128-channel polarization-insensitive frequency-selection switch using high-silica waveguides on Si," *IEEE Photonics Tech. Lett.*, vol. 2, pp. 441–443, June 1990.

[20] G. J. Foschini, "Sharing the optical band in local systems," *IEEE J. Lightwave Technol.*, vol. 6, pp. 974–986, July 1988.

[21] Various Authors, "Special issue on coherent communications," *IEEE J. Lightwave Technol.*, vol. 5, Apr. 1987.

[22] B. S. Glance *et al.*, "WDM coherent optical star network," *IEEE J. Lightwave Technol.*, vol. 6, pp. 67–72, Jan. 1988.

[23] B. S. Glance *et al.*, "Densely spaced FDM coherent star network with optical signals confined to equally spaced frequencies," *IEEE J. Lightwave Technol.*, vol. 6, pp. 1770–1782, Nov. 1988.

[24] W. J. Tomlinson and R. H. Stolen, "Nonlinear phenomena in optical fibers," *IEEE Commun. Mag.*, vol. 26, pp. 36–44, Apr. 1988.

[25] R. A. Spanke, "Architectures for large nonblocking optical space switches," *IEEE J. Quantum Electron.*, vol. 22, pp. 964–967, Jun. 1986.

[26] A. A. Sawchuk *et al.*, "Optical crossbar networks," *IEEE Computer Magazine*, pp. 50–60, Jun. 1987.

[27] R. Soref, "Electrooptic 4×4 matrix switch for multimode fiber-optic systems," *Appl. Optics*, vol. 21, pp. 1386–1393, June 1982.

[28] P. Healey, "Optical switching networks using multiplexed crosspoints," in *ECOC'88*, pp. 53–55, 1988.

[29] J. W. Goodman, A. R. Dias, and L. M. Woody, "Fully parallel, high-speed incoherent optical method for performing discrete Fourier transforms," *Optics Letters*, vol. 2, pp. 1–3, Jan. 1978.

[30] A. A. Sawchuk and T. C. Strand, "Digital optical computing," *IEEE Proceedings*, vol. 72, pp. 758–779, July 1984.

[31] H. S. Hinton, "Applications of the photonic switching technology for telecommunications switching," in *Proc. of Int. Conf. Commun.*, pp. 1559–1564, 1987.

[32] W. I. Way *et al.*, "90-channel FM video transmission to 2048 terminals using two inline traveling-wave laser amplifiers in a 1300 nm subcarrier multiplexed optical system," in *14th Eur. Conf. Opt. Communications*, pp. 37–40, IEE, Sept. 1988.

[33] N. A. Olsson and L. L. Buhl, "Single-laser high-selectivity bidirectional transmission system for local-area-network applications," *Electron. Lett.*, vol. 23, pp. 62–64, Jan. 1987.

[34] R. Olshansky, V. Lanzisera, and P. Hill, "Design and performance of wideband subcarrier multiplexed lightwave systems," in *14th Eur. Conf. Opt. Communications*, pp. 143–146, IEE, Sept. 1988.

[35] J. E. Bowers, "Optical transmission using PSK-modulated subcarriers at frequencies to 16 GHz," *Electron. Lett.*, vol. 22, pp. 1119–1121, Oct. 1986.

[36] P. Iannone and T. E. Darcie, "Multichannel intermodulation distortion in high-speed GaInAsP lasers," *Electron. Lett.*, vol. 23, pp. 1361–1362, Dec. 1987.

[37] T. E. Darcie, R. S. Tucker, and G. J. Sullivan, "Intermodulation and harmonic distortion in InGaAsP lasers," *Electron. Lett.*, vol. 21, pp. 665–666, Aug. 1985.

[38] T. E. Darcie *et al.*, "Lightwave system using microwave subcarrier multiplexing," *Electron. Lett.*, vol. 22, pp. 774–775, July 1986.

[39] T. E. Darcie, "Subcarrier multiplexing for multiple-access lightwave networks," *IEEE J. Lightwave Technol.*, vol. LT-5, pp. 1103–1110, Aug. 1987.

[40] T. Okoshi and K. Kikuchi, *Coherent Optical Fiber Communications.* KTK Scientific Publishers, 1988.

[41] R. Olshansky *et al.*, "InGaAsP buried heterostructure laser with 22 GHz bandwidth and high modulation efficiency," *Electron. Lett.*, vol. 23, pp. 839–841, July 1987.

[42] S. Y. Wang, S. H. Lin, and Y. M. Houng, "GaAs traveling-wave electrooptic waveguide modulator with bandwidth $>$ 20 GHz at 1.3 μm," in *Optical Fiber Conference*, p. 177, IEEE/OSA, 1987.

[43] R. C. Alferness, "Waveguide electrooptic modulators," *IEEE Trans. Microwave Theory Techniques.*, vol. 30, pp. 1121–1137, Aug. 1982.

[44] T. E. Darcie *et al.*, "Resonant p-i-n-FET receivers for lightwave subcarrier systems," *IEEE J. Lightwave Technol.*, vol. 6, pp. 582–589, Apr. 1988.

[45] B. T. Debney *et al.*, "Coherent analog fiber optic links," *Proc. SPIE*, vol. 995, pp. 99–105, 1988.

[46] A. C. van Bochove, J. P. Bekooij, and C. M. de Blok, "A coherent optical system for analogue multichannel video transmission," in *14th Eur. Conf. Opt. Communications*, pp. 541–544, IEE, Sept. 1988.

[47] R. Gross, R. Olshansky, and P. Hill, "Five-channel coherent heterodyne subcarrier multiplexed system," *IEEE Photonics Tech. Lett.*, vol. 1, pp. 179–181, July 1989.

[48] R. Gross and R. Olshansky, "Third-order intermodulation distortion in coherent subcarrier-multiplexed systems," *IEEE Photonics Tech. Lett.*, vol. 1, pp. 91–93, Apr. 1989.

[49] R. Gross, R. Olshansky, and P. Hill, "20 channel coherent FSK system using subcarrier multiplexing," *IEEE Photonics Tech. Lett.*, vol. 1, pp. 224–226, Aug. 1989.

[50] R. Gross and R. Olshansky, "Multichannel coherent FSK experiments using subcarrier multiplexing techniques," *IEEE J. Lightwave Technol.*, vol. 8, pp. 406–415, Mar. 1990.

[51] M. Ross, *Laser Receivers.* John Wiley & Sons Inc., 1966.

[52] A. W. Davis *et al.*, "Phase-diversity techniques for coherent optical receivers," *IEEE J. Lightwave Technol.*, vol. 5, pp. 561–572, Apr. 1987.

[53] J. Salz, "Coherent lightwave communications," *Bell Sys. Tech. Jour.*, vol. 64, pp. 2153–2209, Dec. 1985.

[54] E. E. Basch, ed., *Optical-Fiber Transmission.* Howard W. Sams & Co., 1987.

[55] Y. Yamamoto, "Receiver performance evaluation of various digital optical modulation-demodulation systems in the 0.5–10 μm wavelength region," *IEEE J. Quantum Electron.*, vol. QE-16, pp. 1251–1259, Nov. 1980.

[56] Y. Yamamoto and T. Kimura, "Coherent optical fiber transmission systems," *IEEE J. Quantum Electron.*, vol. QE-17, pp. 919–934, June 1981.

[57] T. Okoshi, "Heterodyne and coherent optical fiber communications: recent progress," *IEEE Trans. Microwave Theory Techniques.*, vol. MTT-30, pp. 1138–1149, Aug. 1982.

[58] T. Okoshi, "Recent progress in heterodyne/coherent optical-fiber communications," *IEEE J. Lightwave Technol.*, vol. LT-2, pp. 341–346, Aug. 1984.

[59] L. G. Kazovsky, "Balanced phase-locked loops for optical homodyne receivers: performance analysis, design considerations and laser linewidth requirements," *IEEE J. Lightwave Technol.*, vol. LT-4, pp. 182–195, Feb. 1986.

[60] R. A. Linke and A. H. Gnauck, "High capacity coherent lightwave systems," *IEEE J. Lightwave Technol.*, vol. 6, pp. 1750–1769, Nov. 1988.

[61] T. Kane and R. Byer, "Monolithic unidirectional single mode Nd:YAG ring laser," *Optics Letters*, vol. 10, pp. 65–67, 1985.

[62] G. Garret and G. Jacobsen, "The effect of laser linewidth on coherent optical receivers with nonsynchronous demodulation," *IEEE J. Lightwave Technol.*, vol. LT-5, pp. 551–572, Apr. 1987.

[63] I. Garrett *et al.*, "Weakly coherent optical systems using lasers with significant phase noise," *IEEE J. Lightwave Technol.*, vol. 6, pp. 1520–1526, Oct. 1988.

[64] L. G. Kazovsky *et al.*, "Wide-linewidth phase-diversity homodyne receivers," *IEEE J. Lightwave Technol.*, vol. 6, pp. 1527–1536, Oct. 1988.

[65] L. G. Kazovsky, "Phase- and polarization-diversity coherent optical techniques," *IEEE J. Lightwave Technol.*, vol. 7, pp. 279–292, Feb. 1989.

[66] I. M. Habbab and L. J. Greenstein, "Phase-insensitive zero-IF coherent optical detection using sinusoidal phase modulation instead of phase switching," in *14th Eur. Conf. Opt. Communications*, pp. PDP 65–68, IEE, Sept. 1988.

[67] M. Kavehrad and B. Glance, "A polarization-insensitive FSK optical heterodyne receiver," in *Proc. of Int. Conf. on Communications*, pp. 1230–1234, IEEE, 1988.

[68] I. M. Habbab and L. J. Cimini, Jr., "Polarization-switching technique for coherent optical communications," *IEEE J. Lightwave Technol.*, vol. 6, pp. 1537–1548, Oct. 1988.

[69] S. B. Alexander, "Design of wide-band optical heterodyne balanced mixer receivers," *IEEE J. Lightwave Technol.*, vol. LT-5, pp. 523–537, Apr. 1987.

[70] R. Gross, P. Meissner, and E. Patzak, "Theoretical investigation of local oscillator intensity noise in optical homodyne systems," *IEEE J. Lightwave Technol.*, vol. 6, pp. 521–530, Apr. 1988.

[71] L. G. Kazovsky *et al.*, "Impact of laser intensity noise on ASK two-port optical homodyne receivers," *Electron. Lett.*, vol. 23, pp. 871–873, Aug. 1987.

[72] L. G. Kazovsky and J. L. Gimlett, "Sensitivity penalty in multichannel coherent optical communications," *IEEE J. Lightwave Technol.*, vol. 6, pp. 1353–1365, Sept. 1988.

[73] Y. H. Cheng, T. Okoshi, and O. Ishida, "Performance analysis and experiment of a homodyne receiver insensitive to both polarization and phase fluctuations," *IEEE J. Lightwave Technol.*, vol. 7, pp. 368–374, Feb. 1989.

[74] J. Siuzdak and W. Van Etten, "BER evaluation for phase and polarization diversity homodyne receivers using noncoherent ASK and DPSK demodulation," *IEEE J. Lightwave Technol.*, vol. 7, pp. 584–599, Apr. 1989.

[75] L. G. Kazovsky, "Multichannel coherent optical communication systems," *IEEE J. Lightwave Technol.*, vol. LT-5, pp. 1095–1102, Aug. 1987.

[76] S. Betti, A. Fioretti, and C. Perazzini, "Numerical analysis of intermodulation interference in optical coherent multichannel systems," *IEEE J. Lightwave Technol.*, vol. LT-5, pp. 587–591, Apr. 1987.

[77] H. E. Lassen, P. B. Hansen, and K. E. Stubkjaer, "Crosstalk in 1.5-μm InGaAsP optical amplifiers," *IEEE J. Lightwave Technol.*, vol. 6, pp. 1559–1565, Oct. 1988.

[78] R. M. Jopson *et al.*, "Measurement of carrier-density mediated intermodulation distortion in an optical amplifier," *Electron. Lett.*, vol. 23, pp. 1394–1395, Dec. 1987.

[79] T. E. Darcie, R. M. Jopson, and R. W. Tkach, "Intermodulation distortion in optical amplifiers from carrier-density modulation," *Electron. Lett.*, vol. 23, pp. 1392–1394, Dec. 1987.

[80] B. S. Glance *et al.*, "Crosstalk degradation caused by optical amplification in a multichannel FSK heterodyne system," *IEEE J. Lightwave Technol.*, vol. 7, pp. 759–765, May 1989.

[81] E. Sunde, *Communication Systems Engineering Theory*, ch. 11. John Wiley & Sons, 1969.

[82] E. D. Hirleman and P. Dellenback, "Faraday effect light valve arrays for adaptive optical instruments," in *Proc. ICALEO*, 1987.

[83] C. Clos, "A study of non-blocking switching networks," *Bell Sys. Tech. Jour.*, pp. 406–424, Mar. 1953.

[84] J. Bellamy, *Digital Telephony.* John Wiley & Sons, 1982.

[85] M. J. O'Mahony, "Optical amplifiers for communications," in *Proc. OFC/IOOC*, 1987.

[86] J. Goodman *et al.*, "Optical interconnection for VLSI systems," *IEEE Proceedings*, vol. 72, pp. 850–866, July 1984.

[87] D. Shaefer and J. Strong, III, "TSE computers," *IEEE Proceedings*, vol. 65, pp. 129–138, Jan. 1977.

[88] B. K. Jenkins *et al.*, "Sequential optical logic implementation," *Appl. Optics*, vol. 23, pp. 3455–3464, Oct. 1984.

[89] B. K. Jenkins *et al.*, "Architectural implications of a digital optical processor," *Appl. Optics*, vol. 23, pp. 3465–3474, Oct. 1984.

[90] B. K. Jenkins, "Optical digital computing and interconnections," in *Proc. ISCAS'88*, pp. 1075–1078, 1988.

[91] R. J. Collier, C. B. Burckhardt, and L. H. Lin, *Optical Holography*, ch. 16, pp. 477–493. Academic Press, 1971.

[92] W. J. Hossak, P. McOwan, and R. E. Burge, "Computer generated optical fan-out element," *Optics Communications*, vol. 68, pp. 97–102, Sept. 1988.

[93] S. K. Case, P. R. Haugen, and O. J. L. kberg, "Multifacet holographic optical element for wave front transformations," *Appl. Optics*, vol. 20, pp. 2670–2675, Aug. 1981.

[94] Y. Fujii, N. Suzuki, and J. Minowa, "A 100 input/output-port star coupler composed of low-loss slab waveguide," in *Proc. of 4-th Int. Conf. on Integrated Optics and Optical Communications, Tokyo*, pp. 341–343, Jun. 1983.

[95] M. A. Duguay *et al.*, "Antiresonant reflecting optical waveguides in SiO_2–Si multi-layer structures," *Appl. Phys. Lett.*, vol. 49, pp. 13–18, 1986.

[96] T. Baba *et al.*, "Loss reduction of an ARROW waveguide in shorter wavelength and its stack configuration," *IEEE J. Lightwave Technol.*, vol. 6, pp. 1440–1445, Sept. 1988.

[97] *Application Notes.* Semetex Corp.

[98] "High-speed light valve is non-volatile," Lasers and Applications, Dec. 1986.

[99] S. H. Lin, T. F. Krile, and J. F. Walkup, "Two-dimensional optical Clos interconnection network and its uses," *Appl. Optics*, vol. 27, pp. 1734–1741, May 1988.

[100] D. J. Blumenthal and L. Thylen, "A parallel optical processor for control of optical crossbar switches," in *ECOC'88*, pp. 268–271, 1988.

[101] J. E. Midwinter, "Novel approach to the design of optically activated wideband switching matrices," *IEE Proceedings*, vol. 134, p. 261, 1987.

[102] R. Olshansky and V. A. Lanzisera, "60-channel FM video subcarrier multiplexed optical communication system," *Electon. Lett.*, vol. 23, pp. 1196–1198, Oct. 1987.

[103] W. I. Way *et al.*, "Applications of traveling-wave laser amplifiers in subcarrier multiplexed lightwave systems," in *Proc. of Int. Conf. Commun.*, pp. 987–995, IEEE, 1989.

[104] J. E. Bowers, *et al.*, "Direct fiber-optic transmission of entire microwave satellite antenna signals," *Electon. Lett.*, vol. 23, pp. 185–187, 1987.

[105] N. Kanno and K. Ito, "Fiber optic subcarrier multiplexing transport for broadband subscriber distribution network," in *Proc. of Int. Conf. Commun.*, pp. 996–1003, 1989.

[106] S. C. Liew and K. W. Cheung, "A broadband optical local network based on multiple wavelengths and multiple RF carriers," in *Proc. of Int. Conf. Commun.*, pp. 996–1003, 1989.

[107] M. Kavehrad, "Convolutional coding for high-speed microwave radio communications," *AT&T Technical Journal*, vol. 64, pp. 1625–1637, Sept. 1985.

[108] K. Sato, "Intensity noise of semiconductor laser diodes in fiber optic analog video transmission," *IEEE J. Quantum Electron.*, vol. 19, pp. 1380–1391, Sept. 1983.

[109] Y. Yamamoto, "AM and FM quantum noise in semiconductor lasers — part I: theoretical analysis," *IEEE J. Quantum Electron.*, vol. 19, pp. 34–46, Jan. 1983.

[110] Y. Yamamoto, S. Saito, and T. Mukai, "AM and FM quantum noise in semiconductor lasers — part II: comparison of theoretical and experimental results for AlGaAs lasers," *IEEE J. Quantum Electron.*, vol. 19, pp. 47–58, Jan. 1983.

[111] J. G. Proakis, *Digital Communications*, ch. 4. McGraw-Hill, 1983.

[112] N. Yoshikai, K. Katagiri, and T. Ito, "mB1C code and its performance in an optical communication system," *IEEE Trans. Commun.*, vol. 32, pp. 163–168, Feb. 1984.

[113] S. Kawanishi *et al.*, "DmB1M code and its performance in a very high-speed optical transmission system," *IEEE Trans. Commun.*, vol. 36, pp. 951–956, Aug. 1988.

[114] W. D. Grover, "Forward error correction in dispersion-limited lightwave systems," *IEEE J. Lightwave Technol.*, vol. 6, pp. 643–654, May 1988.

[115] M. Kavehrad, "Implementation of a self-orthogonal convolutional code used in satellite communications," *IEE, Trans. on Elec. Circuits and Systems*, vol. 3, pp. 134–138, May 1979.

[116] J. C. Daly, "Fiber optic intermodulation distortion," *IEEE Trans. Commun.*, vol. 8, pp. 1954–1958, Aug. 1982.

[117] W. E. Stephens and T. R. Joseph, "System characteristics of direct modulated and externally modulated RF fiber-optic links," *IEEE J. Lightwave Technol.*, vol. 5, pp. 380–387, Mar. 1987.

[118] G. E. Bodeep and T. E. Darcie, "Semiconductor lasers versus external modulators: a comparison of nonlinear distortion for lightwave subcarrier CATV applications," *IEEE Photonics Tech. Lett.*, vol. 1, pp. 401–403, Nov. 1989.

[119] B. Villeneuve, N. Cyr, and M. Tetu, "Precise optical heterodyne beat frequency from laser diodes locked to atomic resonances," *Electron. Lett.*, vol. 23, pp. 1082–1084, Sept. 1987.

[120] W. Yizun, "Coherent optical fibre system with Zeeman lasers," *Electron. Lett.*, vol. 23, pp. 49–50, Jan. 1987.

[121] P. F. Panter, *Modulation, Noise, and Spectral Analysis*. McGraw-Hill, 1965.

[122] W. R. Bennett, "Cross-modulation requirements on multichannel amplifiers below overload," *Bell Sys. Tech. Jour.*, vol. 19, pp. 587–610, 1940.

[123] A. Yariv, *Optical Electronics*, ch. 9. Holt, Rinehart and Winston, 1985.

[124] R. G. Westcott, "Investigation of multiple f.m./f.d.m. carriers through a satellite t.w.t. operating near to saturation," *Proc. IEE*, vol. 114, pp. 726–738, June 1967.

[125] K. Iwashita and T. Matsumoto, "Modulation and detection characteristics of optical continuous phase FSK transmission system," *IEEE J. Lightwave Technol.*, vol. 5, pp. 452–460, Apr. 1987.

[126] R. Gross, R. Olshansky, and M. Smidt, "Coherent FM-SCM system using DFB lasers and phase noise cancellation circuit," *IEEE Photonics Tech. Lett.*, vol. 2, pp. 66–68, Jan. 1990.

[127] M. J. Pettit *et al.*, "Optical FSK transmission system using a phase-diversity receiver," *Electon. Lett.*, vol. 23, pp. 1075–1076, Sept. 1987.

[128] T. G. Hodgkinson *et al.*, "In-phase and quadrature detection using 90° optical hybrid receiver: experiments and design considerations," *Proc. IEE*, vol. 135, pp. 260–267, June 1988.

[129] Hen-Wai Tsao *et al.*, "Performance analysis of polarization-insensitive phase diversity optical FSK receivers," *IEEE J. Lightwave Technol.*, vol. 8, pp. 385–395, Mar. 1990.

[130] D. Hoffmann *et al.*, "Integrated optical 90°-hybrid on $LiNbO_3$ for phase diversity receivers," in *14th Eur. Conf. Opt. Communications*, pp. PDP 33–36, IEE, Sept. 1988.

[131] D. Hoffmann *et al.*, "Integrated optics eight-port 90° hybrid on $LiNbO_3$," *IEEE J. Lightwave Technol.*, vol. 7, pp. 794–803, May 1989.

[132] M. Kavehrad, "Multiple FM/FDM carriers through nonlinear amplifiers," *IEEE Trans. Commun.*, vol. 29, pp. 751–756, May 1981.